

See discussions, stats, and author profiles for this publication at: <https://www.researchgate.net/publication/51100751>

Analyzing Nanomaterial Bioconjugates: A Review of Current and Emerging Purification and Characterization Techniques

ARTICLE in ANALYTICAL CHEMISTRY · JUNE 2011

Impact Factor: 5.64 · DOI: 10.1021/ac200853a · Source: PubMed

CITATIONS

114

READS

234

5 AUTHORS, INCLUDING:



[Jeffrey R Deschamps](#)

United States Naval Research Laboratory

309 PUBLICATIONS 4,969 CITATIONS

[SEE PROFILE](#)

Analyzing Nanomaterial Bioconjugates: A Review of Current and Emerging Purification and Characterization Techniques

Kim E. Sapsford,^{*,†} Katherine M. Tyner,[‡] Benita J. Dair,[§] Jeffrey R. Deschamps,^{||} and Igor L. Medintz^{*,||}

[†]Division of Biology, Office of Science and Engineering Laboratories, Center for Devices and Radiological Health, [‡]Division of Drug Safety Research, Office of Testing and Research, Office of Pharmaceutical Science Center for Drug Evaluation and Research, and [§]Division of Chemistry and Materials Science, Office of Science and Engineering Laboratories, Center for Devices and Radiological Health, U.S. Food and Drug Administration, 10903 New Hampshire Avenue, Silver Spring, Maryland 20993, United States

^{||}Center for Bio/Molecular Science and Engineering, Code 6900, U.S. Naval Research Laboratory, 4555 Overlook Avenue, S.W. Washington, DC 20375, United States

CONTENTS

Complexities of the Nanomaterial-Biological Conjugate	4454	Atomic Force Microscopy	4472
Nanomaterial-Bioconjugation Chemistries	4455	Near-Field Scanning Optical Microscopy	4472
Properties of Nanomaterial-Biological Hybrids	4456	Spectroscopic Techniques	4473
Why Is Purification and Characterization Important?	4457	UV—Visible Absorbance	4473
Purification	4458	Circular Dichroism	4474
Chromatography	4458	Fluorescence Spectroscopy	4474
Gravity Flow and Low-Pressure Liquid Chromatography	4458	Infrared Spectroscopy	4475
High-Performance Liquid Chromatography	4458	Nuclear Magnetic Resonance and Magnetic Resonance Imaging	4475
Field Flow Fractionation	4458	Mass Spectroscopy	4476
Electrophoresis	4459	Thermal Techniques	4476
Centrifugation and Analytical Ultracentrifugation	4461	Modeling	4476
Dialysis and Filtration	4462	Predictive Modeling	4479
Extraction	4463	Structural Estimates	4479
Characterization	4463	Protein Binding to Nanoparticles	4479
Separation Techniques	4463	Modeling of Quantum Dot Bioassemblies	4479
High-Performance Liquid Chromatography	4463	Emerging Technologies and Instrumentation	4481
Nanofluidic Size Exclusion	4463	CytoViva with Hyperspectral Imaging	4481
Field Flow Fractionation	4463	Xigo Acorn Area Analysis	4481
Electrophoresis	4463	Resonance Frequency Devices (Quartz Crystal Microbalance and Suspended Cantilevers)	4481
Analytical Ultracentrifugation	4464	Single Particle Tracking (Nanosight and Others)	4482
Electrospray Differential Mobility Analysis (ES-DMA)	4466	Coulter Counter Devices	4482
Scattering Techniques	4466	Impact of NM Characterization on Nanotoxicology	4482
Dynamic Light Scattering	4466	Summary	4483
Fluorescence Correlation Spectroscopy	4466	Author Information	4483
Resonance Light Scattering Correlation Spectroscopy	4468	Biographies	4484
Zeta (ζ) Potential	4468	Acknowledgment	4484
Raman Techniques	4470	References	4484
X-ray Diffraction	4470		
Small-Angle Scattering Techniques	4470		
Microscopy	4470		
Electron Microscopy	4472		

The growing maturity of nanotechnology has led to the establishment of more focused subdisciplines including especially that of bionanotechnology. This field can more easily

Special Issue: Fundamental and Applied Reviews in Analytical Chemistry

Published: May 05, 2011

be defined as the intersection of nanotechnology and biology and is loosely characterized by two somewhat converse foci: (i) exploiting nanomaterials (NMs) to investigate biological processes as exemplified by developing, for example, antibody functionalized magnetic nanoparticles for *in vivo* tumor imaging,¹ and in more simplistic terms, exploitation of a unique NM property in a biological setting and (ii) use of biological processes or systems to create, order, and investigate new nanoscale materials or devices. A primary example of the latter would be that of using DNA architecture and chemistry to control the placement of nanoparticles in the pursuit of creating molecular electronic devices at the sublithographic regime.² NM-biological hybrid materials are considered “value-added” in that they are capable of far more than each individual component alone. Each participant imbues the composite with a unique property or function that is lacking in the other. For example, in (i) above, the antibody provides the biorecognition and targeting while the nanoparticle may allow for *in vivo* electromagnetic contrast. The composite uniquely exploits each property to derive a novel, designer nanoscale entity. NM-bioconjugates have the potential to revolutionize many fundamental and applied aspects of science and are already having significant impact in developing biomedical therapeutics and diagnostics.^{1–6}

It is important to begin by pointing out that what exactly constitutes a NM is still quite contentious and depends upon the perspective of origin. The initial working definition was any material (biotic or abiotic, though not chemical) that was less than 100 nm in at least one dimension. Several national and international standards organizations have proposed acceptable nomenclature and terminology for use when describing nanoscale materials (see ASTM International E2456 and ISO technical specification documents 27687 and 80004). While most describe an upper size limit of approximately 100 nm in at least one dimension, there is currently limited scientific evidence to strictly support this value for all materials.⁷ This debate is not trivial as it has important legal and regulatory implications.⁷ What is not in dispute is that many of these materials display unique nanoscale size-dependent properties that are of interest to biology. These can include, for example, intrinsic properties such as the quantum confinement displayed by semiconductor quantum dots,⁸ the paramagnetism of iron oxide and other metal alloy nanoparticles,⁹ along with the conductivity and ballistic transport found in nanoscale carbon allotropes.¹⁰ Beyond photophysical and electronic properties, NMs, and nanoparticles in particular, have extremely high surface-to-volume (S/V) ratios (e.g., at <2 nm the S/V atomic ratio exceeds 50%), along with nontrivial surface areas.⁴ This can allow for the display of multiple biological entities on their surface which can cumulatively provide increased avidity in certain configurations. NMs can also act as a carrier for an insoluble agent such as a drug. Alternatively, the NM can display multiple *different* biomolecules, thus imbuing the composite with multifunctionality. Indeed, one of the current engineering goals is to create viable nanotheranostic agents where a NM would provide inherent fluorescent or magnetic contrast while displaying multiple targeting agents such as, for example, tumor-specific antibodies along with cell penetrating peptides and a chemotherapeutic agent. This nanomedicine concept is being pursued to overcome many of the issues associated with current systematically delivered medicines.¹¹

Some relevant discussions about the analytical challenges facing researchers who wish to apply bionanotechnology, both from a physicochemical/surface property characterization

stand-point along with an understanding of the structure/function and further interaction within biological systems are available in the literature.^{4,12–16} Prior to a review of the techniques available for purifying and characterizing NM-bioconjugates, a brief discussion of their structure, the chemistries used to assemble them, their physicochemical properties, and the driving impetus behind characterization is warranted.

Complexities of the Nanomaterial-Biological Conjugate. For the purposes of this review, the term nanomaterial (NM) will be used as an overarching term to describe materials, particles, or structures with a size dimension less than 1000 nm. Where appropriate, the terms nanoparticle (NP), nanotube (NT), and nanorod (NR) and the specific constituent type of material will be directly used in the text. We include NMs of all types and origin, be they metallic, semiconductor, alloys, oxides, etc. We further include multifunctional designer polymers and dendrimers, along with biotic NP-like materials such as DNA Origami, viral capsids, and large protein assemblies such as light-harvesting complexes. These NMs either display novel nanoscale properties or when combined with other materials provide novel property or function. We inclusively define biologicals as proteins, peptides, amino acids, nucleic acids, lipids, enzymatic cofactors, carbohydrates, drugs, and the like, and in certain circumstances, biocompatible molecules such as polyethylene glycol (PEG).

The complexities underlying the structure and function of such hybrid materials are more easily illustrated by using NPs as an example. Composite NM and NP-biologicals can most simply be described as multilayered structures, see Figure 1A. A given NP sample, for example, is usually polydisperse with some finite distribution of size. Further, its surfaces are not uniform but rather characterized by defects, edges, lattices, and vertices.⁴ For biological utility, many NPs consist of core or core-(shell)_n structures, where the outer shell(s) protect and insulate the core along with mediating solubility and linkages to biomolecules, see Figure 1. This concept is exemplified by the structure of biocompatible CdSe-ZnS core-shell semiconductor quantum dot (QDs), where the ZnS shell protects and passivates the core thus maintaining its optical properties while also preventing leaching.¹⁷ Most NPs are intrinsically hydrophobic and need to be made hydrophilic and biocompatible by attaching a coating of surface ligands which act to mediate solubility or, more commonly, colloidal stability. Ligand chemistry is complex and can range from small charged molecules to amphiphilic block copolymers or dendritic structures which completely enwrap the NP.⁵ Ideally, the ligands would also provide chemical “handles” for attaching biomolecules of interest. Biomolecules usually make up the outer layer of the composite structure, especially when their intended function is for recognition or targeting. The complexity of these structures is further exacerbated by the sheer number of different structural iterations that are possible. This is highlighted in Figure 1A where eight different NP-biological assembly configurations are schematically depicted. These range from the simplest, where the biological interacts with the NP core directly while providing solubility, for example, to where the biological is entrapped inside the NP or the NP decorates the biological. Figure 1B provides a slightly different, more-functional version of this composite structure. Here, the central NP is surrounded by a solubilizing PEG layer and then functionalized with a variety of representative biomolecules in three dimensions. In this example, the NP itself contributes to the desired utility with its intrinsic fluorescence.

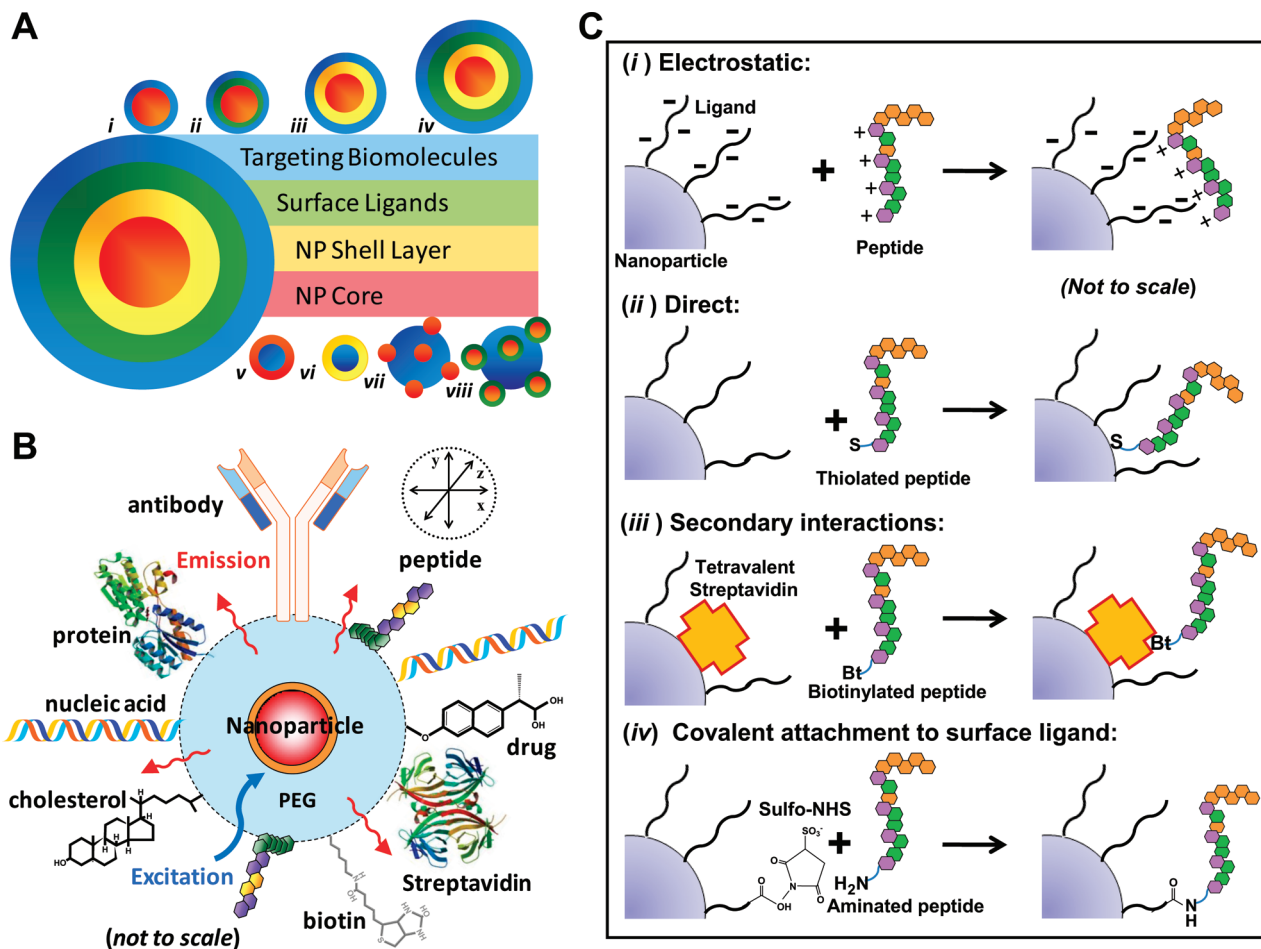


Figure 1. NM-bioconjugates: (A) Schematic of the various potential NP-bioconjugate components and configurations. Note: not to scale. (i) Biomolecule interacting with NP core, (ii) biomolecule interacting with a NP core via intermediate ligands, (iii) biomolecule interacting with NP shell layer that surrounds the NP core, (iv) biomolecule interacting with NP shell layer–NP core via intermediate ligands, (v) porous NP core containing entrapped biomolecules, (vi) porous or hollow NP core containing entrapped biomolecules surrounded by a NP shell layer, (vii) NP core (or NP core/NP shell structures) particles smaller in size than the much larger biomolecule, (viii) NP core (or NP core/NP shell structures) particles smaller in size than the much larger biomolecule attached via intermediate ligands. (B) Multifunctional NP assembly: A representative NP decorated with multiple disparate functional molecules (e.g., nucleic acids, proteins, drugs, peptides) is depicted. Although shown as a flat representation, the construct would display biologicals in three dimensions. Robust conjugation of biomolecules to the NP surface is critical for the development of such “value-added” constructs that can provide multiple functions within one active NP platform. (C) The four general schemes routinely used for the conjugation of peptides to NP materials: (i) electrostatic interaction, opposite charges on the surface of the NP and the peptide are used to mediate charge–charge-based NP-peptide assembly; (ii) direct interaction, certain peptide motifs can bind to/coordinate with the NP surface with high affinity, and examples include the interaction of free thiols with the surface of AuNPs and the high-affinity coordination of polyhistidine tracts with NPs (e.g., QDs) displaying Zn^{2+} -bearing surfaces; (iii) secondary interactions, this scheme utilizes specific ligand-receptor interactions and is exemplified by the biotin-streptavidin (SA) interactant pair. The incorporation of the biotin moiety at the peptide’s terminus can mediate direct assembly of the peptide with the NP. (iv) Covalent chemical attachment, these linkages utilize classical bioconjugation chemistry such as EDC-based coupling of amines to carboxyls or NHS- and maleimide-mediated conjugation to amines and thiols. The figure concept adapted with permission from ref 4 and IOP Publishing Ltd. Copyright 2008 IOP Publishing Ltd.

Nanomaterial-Bioconjugation Chemistries. The number of chemistries that have been applied to biofunctionalizing NMs is immense and far beyond the current discussion.¹ Despite this diversity, almost all can be grouped into three major categories: covalent chemistry, noncovalent interactions, and encapsulation. Figure 1C presents a schematic overview of the first two categories using the interactions of a peptide with a NP.⁴ For brevity, encapsulating biologicals into NMs is not discussed here. The initial choice of which approach to utilize is usually determined by a variety of factors such as the NM itself, along with its structure, size, and shape, the type of NM-surface ligand, and presence of available functional end groups, in combination

with the type of biomolecule, their size, available functional groups, chemical composition, and of course, what is ultimately required from the composites in practice. In the case of NPs, an excellent discussion of how NP curvature, size, shape, and other characteristics influence the subsequent bioconjugation chemistry is provided by Hamad-Schifferli.⁴

Covalent chemistries attach the biological directly to the NM surface or to an intermediary which is most commonly a surface-attached stabilizing ligand.^{1,5} Bioconjugation to NM surface ligands and other intermediaries, such as bifunctional cross-linkers, borrow heavily from standard bioconjugation chemistries; that is, chemistries developed to join/modify biomolecules

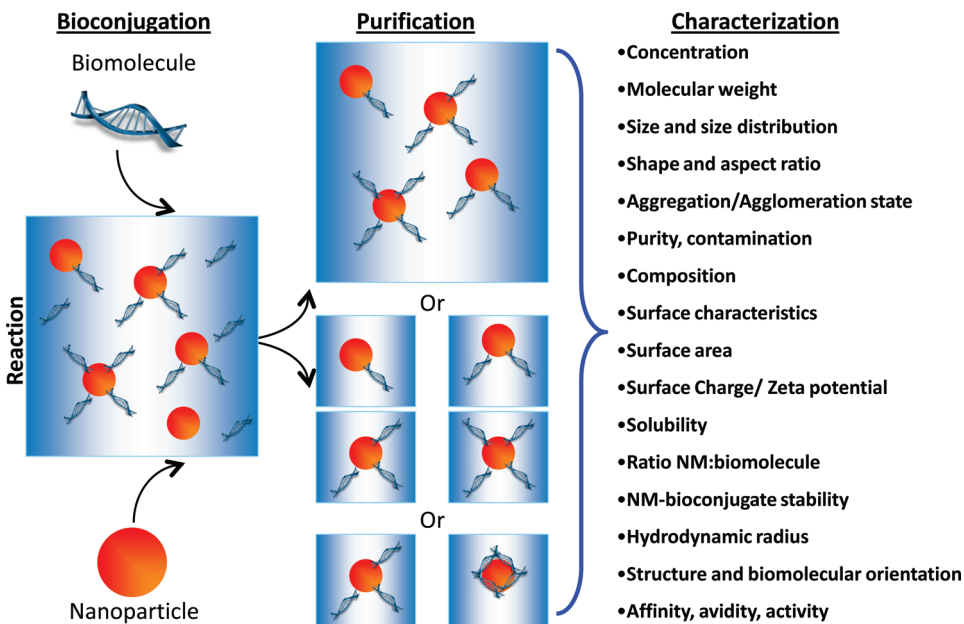


Figure 2. Schematic highlighting issues pertinent to the purification and characterization of NP-bioconjugates.

with dyes, haptens, and other linkers. Hermanson's *Bioconjugate Techniques* continues to be one of the best resources on this subject.¹⁸ Because of the exquisite specificity that is inherently afforded, recent research has focused heavily on adapting chemoselective or bioorthogonal chemistries such as the superfamily of "click" reactions to modifying NMs and NPs in particular.¹⁹

Noncovalent attachments can be subgrouped into those based on electrostatic interactions along with those based on biological recognition/binding, affinity interactions, or enzyme activity. Electrostatic interactions require that both materials display appropriate cognate surfaces to mediate attachment. Some biologicals such as DNA have inherently strong negative charges which can facilitate such an interaction. Biologically driven binding strategies are typified by biotin–avidin binding and again require the requisite display of each participant in the appropriate configurations. The ability to synthesize peptides and nucleic acids in a biotinylated form along with access to a myriad of reagents allowing site-specific biotinylation and the strong intrinsic affinity of this reaction ($K_a \sim 10^{15} M^{-1}$) have made this one of the most popular NM-bioconjugation approaches.¹⁸ Direct surface interactions are usually "dative" bonds as exemplified by gold-thiol chemisorption. Thiolated peptides, proteins, nucleic acids, etc are commonly attached to gold (or other noble metal) surfaces or NMs using this approach.²⁰ Another example would be metal affinity coordination between polyhistidine sequences and the ZnS on semiconductor nanocrystal surfaces.^{8,17} A variety of enzyme based approaches are also available where a NM surface is premodified with a target molecule and then exposed to a chimeric enzyme-protein fusion construct that binds the target. An example of this strategy would be that of glutathione-S transferase fusion proteins binding to glutathione-modified surfaces.²¹

Considering the nature of all these chemistries, it is critical to keep in mind that NM-bioconjugation typically occurs via a stochastic process resulting in a distribution of NMs functionalized with different numbers or populations of biomolecules, see Figure 2.²² Conjugates may consist of NMs both with and

without attached biomolecule or alternatively a narrow or broad distribution in the ratio or valence of attached biomolecule. Depending upon the assembly chemistry utilized, there may also be heterogeneity in the orientation of the attached biomolecules. This is especially true where the chemistry reacts with multiple groups such as when implementing carbodiimide (EDC) chemistry to form an amide bond between the ubiquitous carboxyls or amines present on proteins and the cognate target group present on a NM.¹⁸ These same types of reactions also have a high propensity for cross-linking and forming higher order structures and aggregates. Similar issues can be expected for biomolecules displaying multiple biotin groups when presented to NM-avidin conjugates, given the latter's multiple binding sites.

Properties of Nanomaterial-Biological Hybrids. With the characterization of NM-bioconjugates, a number of physicochemical metrics are of particular interest: including NM size and size distribution, shape and aspect ratio, aggregation/agglomeration state, purity, chemical composition, surface characteristics, ζ (zeta) potential (overall charge), surface area, stability, and solubility, see Figure 2.^{15,23,24} Bioconjugation, however, adds additional questions and metrics to this equation including (1) confirmation of and type of biomolecule attachment, (2) average ratio of NM/biomolecule and ratio distribution, (3) hydrodynamic radius, (4) structure and orientation of the biomolecule upon attachment, (5) separation distance between the biomolecule and the NM, (6) stability of the material during conjugation and of the resulting composite within the NM environment during the intended application, and (7) activity of the biomolecule upon attachment.⁴ In the context of attaching an antibody to a given NM (Figure 1B), for example, it would be important to know the ratio attached per NM along with the antibody orientation and thus the availability of the active binding sites. Depending upon the attachment chemistry used, the NM conjugates may also be cross-linked and contain aggregates of various sizes. These descriptive metrics become exponentially more complex when examining NMs functionalized with multiple (different) biological and chemical entities.

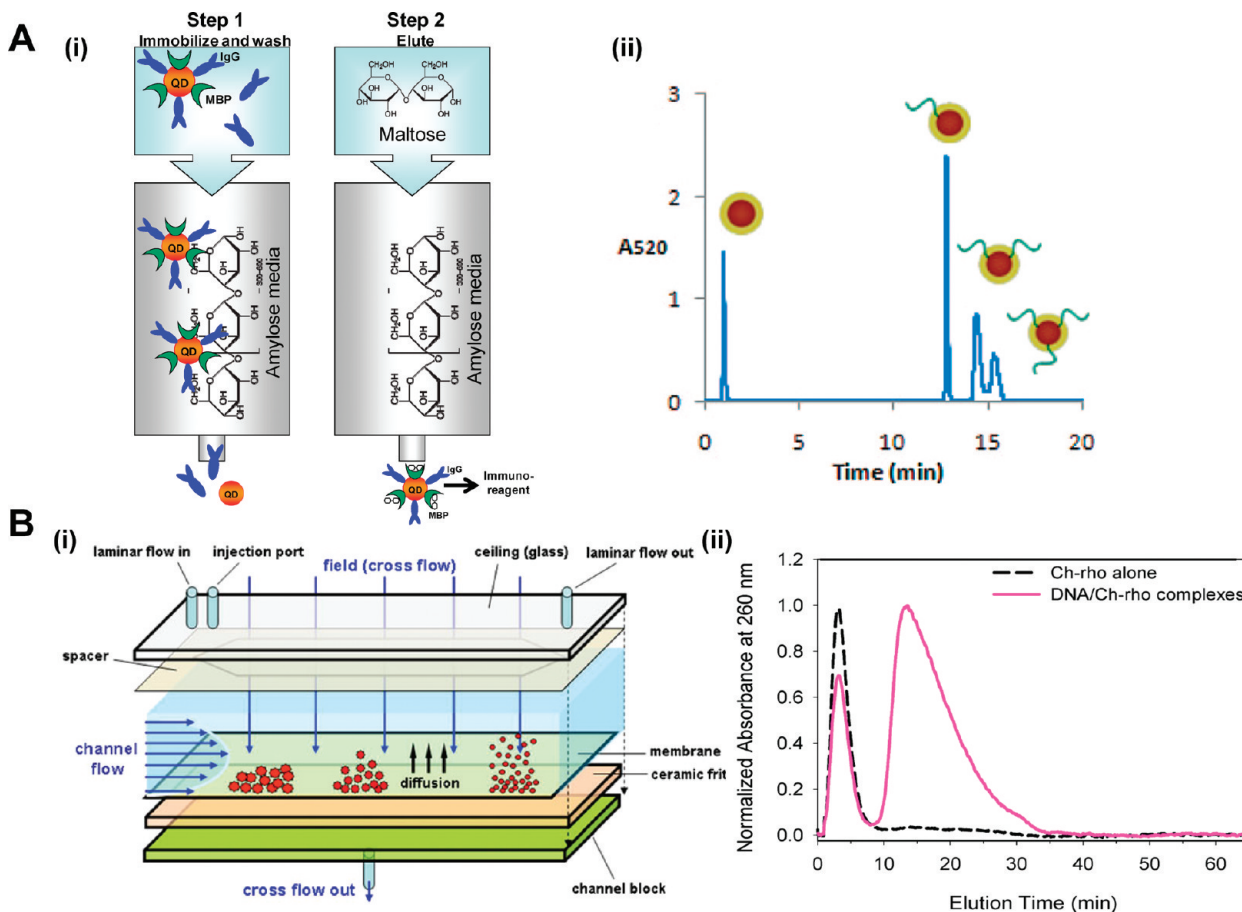


Figure 3. Chromatography and field flow fractionation. (A) Chromatography: (i) schematic demonstrating the affinity chromatography-based purification of QD-antibody bioconjugates from unbound antibody. The QDs are prelabeled with MBP prior to antibody exposure. The antibodies were biotinylated and bound to avidin electrostatically attached to the QDs. With the use of the affinity of MBP for the amylose column, the QD-antibody bioconjugate binds to the column while unbound antibody is washed away (step 1). The QD-antibody bioconjugate is eluted from the column via addition of a maltose containing mobile phase that competes with the amylose stationary phase for the MBP binding site causing displacement (step 2). The QD-antibody immunoreagent is then directly applied to the immunoassay.³⁶ (ii) HPLC purification of 70-base polyT DNA conjugated to 5 nm AuNPs. When the sample was purified by HPLC, multiple peaks were observed corresponding to AuNP with differing stoichiometries of the attached DNA. Figure reprinted from ref 42. Copyright 2008 American Chemical Society. (B) Field flow fractionation (FFF): (i) schematic diagram of an asymmetric-flow field flow fractionation (AF4) channel illustrating the modes of flow and principle of hydrodynamic separation. Reprinted with permission from ref 50. Copyright 2010 Springer Science+Business Media. (ii) AF4 fractograms of chitosan-rhodamine and DNA/chitosan-rhodamine monitored by UV-vis showing normalized absorbance at 260 nm as a function of the elution time. Reprinted from ref 51. Copyright 2010 American Chemical Society.

Why Is Purification and Characterization Important? Simply put, given just some of the relevant issues listed above, rigorous attention to purification and characterization methodologies during the design and manufacture of NM-biocomposites are essential to achieving reproducible and well-controlled performance in the intended application, see Figure 2. This concept was eloquently iterated by Royce Murray, the editor of this journal, in a recent perspective on this subject “As important as these applications are or may become, researchers sometimes charge into NP use with inadequate attention to what the NPs actually are. When used as chemical substances, or carriers thereof, NPs should not be deployed in ignorance of their composition and, ultimately, structure”.²⁵ Adequate characterization is also fundamental in the emerging field of nanotoxicology (discussed below).^{13,23,24,26,27} Furthermore, it will not be long before such comprehensive characterization of NM-biocomposites will be essential and even mandated in the research,

commerce, and regulatory sectors, to ensure reproducibility of synthesis, quality assurance, predictable behavior in intended use, along with safety and effectiveness.^{28,29} A somewhat simpler answer to the above question comes in the form of a pragmatic question straight from the bench researcher’s perspective, namely, “What have I made and how do I confirm this prior to the final application?”

There are already in place a variety of established analytical methods that have been successfully applied to the characterization of bare and modified NMs.^{4,30–34} These are well-developed techniques that primarily grew out of the colloidal chemistry field which, for all intents and purposes, has now “morphed” into the NP chemistry field. Beyond a cursory introduction, we do not review the characterization techniques themselves here but rather focus on their applicability in the current context. The aim is to provide an updated overview of current and emerging technologies that have particular utility in the characterization of

NM-bioconjugates.³⁰ In many cases, it will be apparent that established techniques are being applied and/or interpreted in new ways. Given the scope and breadth of this field, rather than being all inclusive, selected characterization examples are highlighted from the recent literature along with a critical discussion of the benefits and liabilities of each technique where warranted. We extend our apologies for the many omissions. As there are no reviews in this subject area that precede this one, we include references that extend beyond the last 2 years where pertinent. Since many of the techniques utilized here have found dual-use in both purification and characterization of NM-bioconjugates, we begin with an overview of the relevant methods of purification.

PURIFICATION

In an ideal world, following bioconjugation, purification would be capable of separating the NM-bioconjugate from both unconjugated-biomolecules and unmodified NMs while also having the ability to resolve discrete subpopulations of the NM-bioconjugates, see Figure 2.⁴ While certain NMs, such as those that are magnetic, provide inherent properties that make purification relatively simple (i.e., collection using a permanent magnet),³⁵ most rely on several commonly utilized methods to minimally separate the unbound biomolecule from the NM-bioconjugate.

Chromatography. These techniques separate based upon the differing affinities of the multiple sample components for the chosen chromatographic mobile- and/or stationary/solid-phase. The actual separation mechanism depends on the chromatographic method utility but, in all cases, care should be taken to limit nonspecific interactions with the stationary phase or denaturation due to solvents which can be problematic for sensitive or labile biomolecules.

Gravity Flow and Low-Pressure Liquid Chromatography. Ion-exchange, size exclusion, and affinity chromatography, run under either gravity or low-pressure conditions, are commonly applied to NM-bioconjugate purification and can even be extended to materials of quite large mass.^{36–40} Sapsford and co-workers, for example, used ion-exchange chromatography to separate dye-labeled cowpea mosaic viral particles (CPMV, MW 5.6×10^6 kDa) chemically functionalized with antibodies from unbound antibody (MW ~ 150 kDa) based upon their differing affinities for a Q-10 Sepharose column under a salt gradient.³⁷ Increasing the NaCl concentration altered protein–media interactions allowing the CPMV-antibody bioconjugate (elution at ~ 0.5 M NaCl) to be collected after the free antibody (elution at ~ 0.2 M NaCl). The colabeled dye/antibody viral nanoplatforms were subsequently applied in immunoassays and demonstrated improved limits of detection (LOD) compared to dye-labeled antibodies alone. Goldman et al. used an affinity chromatography technique to separate antibody-labeled QDs from the unbound antibody. For this procedure, QDs were noncovalently decorated with both maltose binding protein (MBP) and antibodies. MBP was recombinantly engineered to express a positively charged leucine-zipper domain which electrostatically interacted with the QDs-negatively charged surface ligands. The antibodies were biotinylated for attachment to avidin which was also electrostatically coupled to the QD surface. MBP's natural affinity for amylose media bound and immobilized the QD-protein complex in the column where unbound antibody could be easily washed away, see Figure 3A.³⁶ Antibody-QD conjugates were then eluted from the column via the addition of maltose-supplemented buffer and subsequently used for detection in four color

multiplex toxin immunoassays. In this example, the eluted conjugates were used directly; however, depending upon application, and excess salt or other eluent present such as maltose may need to be removed first. Affinity-based methods do have the additional drawback in that they require the NM to be labeled with an affinity tag (e.g., biotin, His-tag, MBP, peptide). This can increase the complexity of the resulting bioconjugate, along with the requisite synthesis and purification steps and may impact the intended application as the NM surface must now be partially allocated to accommodating and displaying another potentially interfering or complicating species with a different intended utility.

High-Performance Liquid Chromatography. High-performance liquid chromatography (HPLC)⁴¹ coupled with reverse-phase,²² ion-exchange,⁴² and size exclusion (SEC)^{34,41,43,44} stationary phases have been extensively used for purification of NM-bioconjugate from excess biomolecules. Optimized HPLC has demonstrated the ability to resolve discrete NM-bioconjugates each displaying a different NM-to-biomolecule ratio.^{22,42,45} Alivisatos's group elegantly demonstrated this ability using anion-exchange HPLC combined with increasing salt concentration in the mobile phase to elute and purify gold NPs modified with 0, 1, 2, or 3 DNA molecules for subsequent assembly into plasmonic structures, see Figure 3A.⁴² They also found that elution time was dependent on the length of the DNA sequence conjugated to the gold NP. Importantly, the high pressure and binding/elution from the column did not compromise the NP-bioconjugate structure or functional integrity. In contrast to most standard HPLC applications, elution with high concentrations of organics (i.e., acetonitrile) and inclusion of strong acids (i.e., trifluoroacetic acid) need to be carefully considered when purifying NM-protein conjugates given the possibility of denaturation.

Stravis and co-workers recently demonstrated a nanofluidic size exclusion technology capable of separating and characterizing the size of 100 and 210 nm diameter fluorescent NPs with strong potential for purification and size characterization of NM-bioconjugates.⁴⁶ The benefit of this approach would be that sample volumes can be significantly reduced, with the sample reservoir holding as little as 10 μL . Overall, chromatography techniques are growing in popularity for a number of interrelated reasons. These include relative cost, ease of use, wide range of commercially available instruments and column materials, and facile tailoring of a given procedure for a specific NM-bioconjugate system. Moreover, as these are well-established techniques, the requisite equipment may already be available in a particular facility.

Field Flow Fractionation. Field flow fractionation (FFF) encompasses a family of analytical techniques in which the sample is introduced into a pressure driven mobile phase contained within an open channel (no stationary phase) demonstrating a parabolic flow profile, and an alternate field is applied perpendicular to the direction of flow.⁴⁷ Typically applied fields include cross-flow (direct or asymmetric), centrifugal (sedimentation), electrical fields (charge), thermal/temperature gradients, magnetic, and dielectrophoretic fields. The principles of separation are dependent on the applied field but the technique has demonstrated the ability to purify NM-bioconjugates from both unmodified NM and free biomolecules, as recently reviewed.^{30,48,49} Preoptimization of the buffer type, ionic strength and membrane used is required to obtain the desired FFF separation and limit any nonspecific binding that can

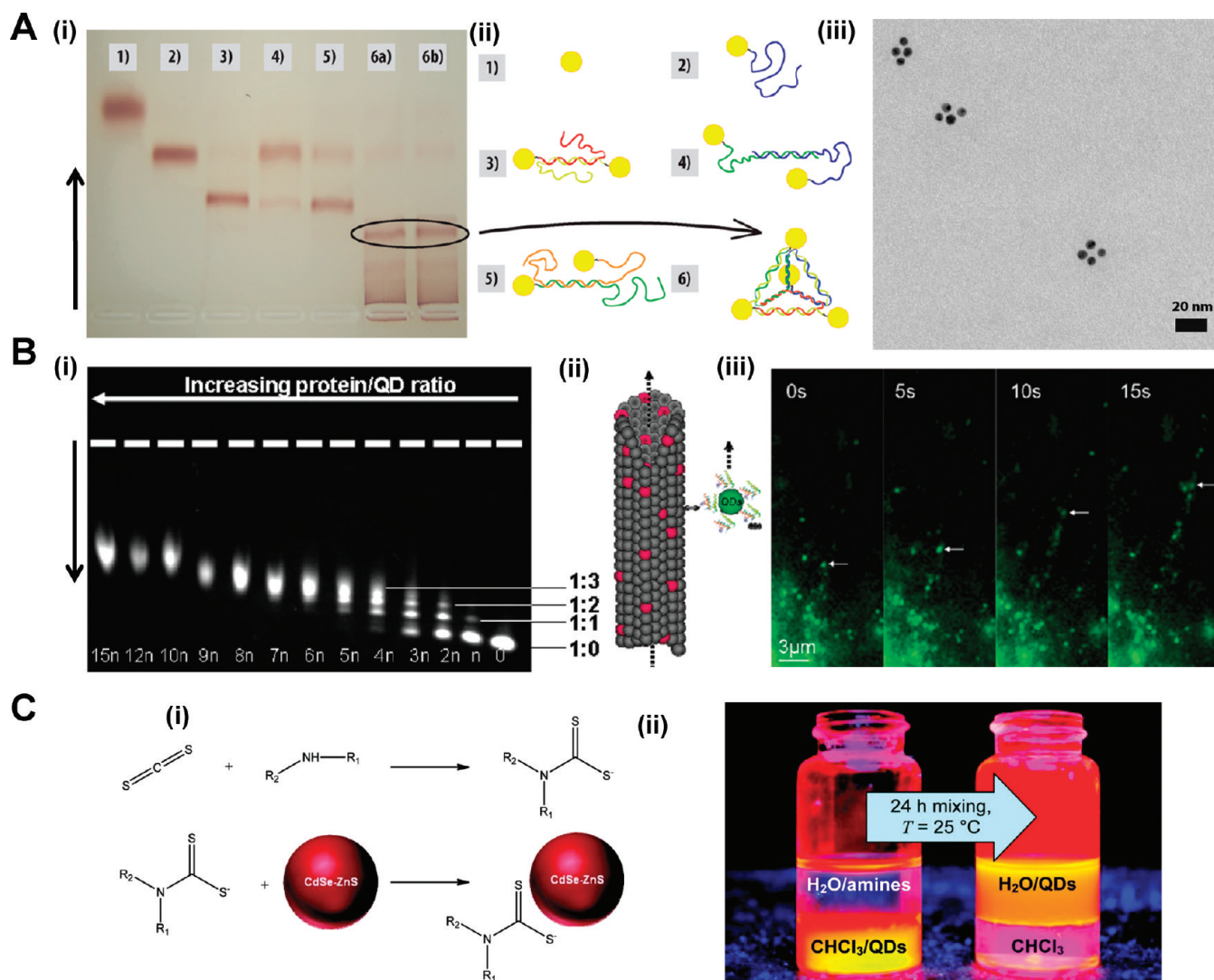


Figure 4. Gel electrophoresis and extraction techniques for purification. (A) (i) Gel electrophoresis purification of AuNP pyramidal structures, next to incomplete structures as standards. The direction of migration is bottom to top: (ii) (1) bare gold, (2) monoconjugate, (3–5) all possible two-strand products, (6a) pyramids formed by mixing all strands at once, and (6b) pyramids formed by mixing strands in pairs and then combining the two-strand products. No difference in yield was observed with this change in protocol. (iii) Typical TEM images of Au DNA-nanocrystal pyramids made from four strands of DNA. Images reprinted with permission from ref 62. Copyright 2009 American Chemical Society. (B) Separation of QD-ND/EB1 complexes by 0.5% agarose gel electrophoresis: (i) QD-ND loaded with Ni^{2+} was incubated with increasing concentrations of His-tag EB1 protein (n = ratio of EB1 to QD calculated from UV absorbance) for 1 h prior to loading and running the gel, (ii) model of QD/EB1 interacting with a microtubule, (iii) temporal image sequence (5 s/frame) of a single QD/EB1 moving on a microtubule (see arrow). Arrows in parts A (i) and B (i) indicate the direction of NP migration. Reprinted from ref 63. Copyright 2009 American Chemical Society. (C) Chemical extraction: (i) chemistry used by Zhang and co-workers to functionalize QDs with amino acids, (ii) transition of QDs from the organic (bottom) to aqueous phase (top) following the DTC-Lys reaction and ligand exchange. Reprinted from ref 83. Copyright 2010 American Chemical Society.

occur at the accumulation wall.⁵⁰ In a demonstrative example, Ma and co-workers used asymmetric flow-FFF to separate DNA/chitosan nanocomposites from chitosan, see Figure 3B.⁵¹ These structures were assembled to investigate their gene therapy potential, and the customized instrument allowed simultaneous UV-visible, multiangle light scattering (MALS) and dynamic light scattering (DLS) detection, which along with purification, provided insight into the amount of unbound polycation, hydrodynamic size, and size distribution. Commercial FFF instruments have recently become available which should aid in the wider adoption of this technology.

Electrophoresis. Slab/plate gel- and capillary-electrophoresis (CE) are the two principle types of electrophoretic techniques

commonly applied to the purification of NMs and NM-bioconjugates.^{52,53} Gel electrophoresis monitors the electrokinetic mobility of charged species in a gel matrix, typically agarose or polyacrylamide, when an electric field is applied across it. For both NMs and NM-bioconjugates, the overall size, shape, and charge density influences the direction and distance moved in the gel.^{52,53} On the small scale, these techniques are routinely used to separate and purify NM-bioconjugates and are also quite often used as a rapid and powerful tool for confirming biomolecular attachment to the NM scaffold through discrete changes in mobility, see Figure 4A,B.^{34,42,52–61} Separated NM-sample bands can also be extracted from the gels for subsequent application or further characterized using techniques such as

Table 1. Separation Techniques^a

technique/types	NM-bioconjugates analyzed	advantages	disadvantages	refs
chromatography (typical stationary phases include; reverse phase, ion-exchange and size exclusion.)	AuNP-DNA, AuNP-cytochrome ϵ , QD-antibody, QD-PEG	<ul style="list-style-type: none"> 1. used to purify NM-bioconjugates. 2. high resolving power, in some instances can resolve different NM-to-biomolecule ratios. 3. provide information on distributions. 4. can be used to investigate post production stability and impurities. 5. simple and cost-effective to use. 	<ul style="list-style-type: none"> 1. nonspecific interactions with the stationary phase. 2. requires optimization for the particular system under investigation. 	22,42,45,46
1. standard liquid chromatography 2. high-performance liquid chromatography (HPLC) 3. hydrodynamic chromatography field flow fractionation (FFF)	QD-DNA, polymer NP-peptides, polymer NP-drug	<ul style="list-style-type: none"> 1. sedimentary and flow can provide effective mass, hydrodynamic radius, density and volume. 2. provides size and size distribution. 3. used to purify NM-bioconjugates. 4. thermal FFF can separate based upon size and surface potential. 	<ul style="list-style-type: none"> 1. nonspecific interactions with the accumulation wall can be problematic. 2. requires optimization of the separation conditions for the particular system under investigation. 	48–51,84–86
1. sedimentary 2. electrical 3. flow 4. thermal 5. magnetic 6. dielectrophoretic electrophoresis	AuNP-DNA, QD-maltose binding protein (MBP), QD-BSA, silicon NP-streptavidin, iron oxide NP-protein/antibody, PEG polymer NP/protein, polymer NP-drug	<ul style="list-style-type: none"> 1. can separate and purify NM–bioconjugates. 2. can provide hydrodynamic radius, both relative and absolute, and ζ potential. 3. separated materials can be extracted and characterized by additional techniques. 4. separation can be dependent on NM shape. 5. simple and cost-effective to use. 	<ul style="list-style-type: none"> 1. for CE potential nonspecific interaction with the capillary wall can be problematic. 2. effective CE requires extensive optimization prior to analysis. 3. small scale use. 4. requires calibration with known size standards for absolute values. 	52–58,64,70,89,90
1. slab gel (including agarose, PAGE ^b -native and SDS-PAGE ^b -denatured 2. capillary (CE)				
centrifugation	layered double hydroxides (LDH)-enalaprilate, Au-streptavidin, Au-adenovirus, QD-BSA, QD-dihydrolipoic acid (DHLA), QD-PEG, silica NP-protein	<ul style="list-style-type: none"> 1. rapid, easily adapted to different materials, cheap and simple to use. 2. AUC: size, size distribution, and shape can be determined. 3. AUC: structural and conformational information about the conjugated biomolecule can be determined. 4. AUC: NM molecular weight can be measured. 5. AUC: self-association/aggregation and other interactions can be investigated. 6. AUC: purification and stoichiometry can be determined. 7. small sample size required and technique is nondestructive, hence sample can be extracted and further characterized using additional techniques. 	<ul style="list-style-type: none"> 1. AUC: expensive and not as intuitive as simple centrifugation. 2. can be difficult to recover separated materials. 3. not quantitative (except for AUC). 4. can cause additional self-association of the materials, which may cause misinterpretation of separation profiles. 	77,91–95

^a General information: Typically cost-effective and relatively simple to use. Routinely used to purify nanomaterial (NM)-bioconjugates. Can provide approximate hydrodynamic radius, purity of product, NM-to-biomolecule ratio, postproduction degradation, and impurities. ^b PAGE, polyacrylamide gel electrophoresis; SDS, sodium dodecyl sulfate.

AFM, mass spectrometry, etc.^{34,58,62} For example, Bücking and co-workers made CdSe/ZnS and InP/ZnS QDs water-soluble through various ligand exchange methods and then attached bovine serum albumin (BSA, used as a model protein) through noncovalent interactions to increase long-term stability. Agarose gel electrophoresis was used to separate the resulting BSA-QD conjugates from excess BSA present in the reaction mixture. The BSA-QD product was then extracted from agarose gel slices by soaking overnight in buffer.⁵⁸ Alivisatos's group used a similar strategy to purify unique pyramidal nanostructure assemblies prepared from various sizes of gold nanocrystals functionalized with complementary single stranded DNA, see Figure 4A.⁶² Here the DNA-nanocrystal pyramidal-bands were either cut out of the agarose gel and extracted into buffer or the gel was cut ahead of the band, filter paper inserted, and the gel run an additional 10 min to push the band onto the paper. Once purified, transmission electron microscopy (TEM) was performed to verify the nanostructures and characterize their novel chiral properties which arose from their tetrahedral symmetry, see Figure 4A.

In another elegant demonstration, Dif and co-workers synthesized QDs displaying mixed peptidic-PEGylated surfaces to bind polyhistidine-tagged (His)_n proteins.⁶³ Gel electrophoresis in 0.5% agarose was then applied to demonstrate successful QD binding of a recombinant (His)₆-tagged microtubular associated end binding protein-1 (EB1) followed by purification of the QD-conjugate displaying the desired 1:1 stoichiometry, see Figure 4B. Clearly as the ratio of EB1 to QD increases in the image, the corresponding QD-EB1 bioconjugate migration rate in the gel decreases in a proportional manner. Distinct and discrete bands were visible at the lower ratios which allowed the authors to purify the 1:1 conjugate. This was important as the gel confirms that the 1:1 assembly is only a minor species in that particular reaction mixture with most of the QD remaining unconjugated; if left unpurified, the brightness from these unconjugated QDs would significantly complicate the resulting experiment by interfering with the ability to track single QDs.

Such a low concentration of protein-conjugated QD in this reaction is to be expected due to the underlying Poissonian assembly kinetics when utilizing this type of assembly chemistry with the intention of creating these two particular conjugate assemblies, namely, those displaying one-protein and those displaying none.⁶⁴ Indeed, this gel result is also an excellent reminder of the stochastic nature of NP-bioconjugation and how reaction stoichiometry influences the resulting conjugate. Monovalent QD-EB1 bioconjugates were successfully used to monitor the interaction of EB1 with microtubules during mitotic spindle formation in *Xenopus* cell extracts, see Figure 4B. As evidenced in these representative examples, gel electrophoresis clearly has the ability to separate discrete ratios of NM-bioconjugates; however, this technique can be limited by the complex interplay of biomolecular size and chemistry, NM size, NM surface character, along with gel sieving and separation capacity. In other words, not every type of NM-bioconjugate will be amenable to monovalent resolution using this approach. To specifically address these types of resolution issues, Liu and Gao recently engineered a hybrid polyacrylamide-agarose gel system which demonstrated the capacity to separate monovalent antibody-functionalized QDs from a conjugation mixture.⁶⁵ Commercial QDs solubilized with an amphiphilic polymer and surface labeled with multiple SA moieties were exposed to antibodies that had been reduced and biotinylated on the hinge region sulfhydryl groups. The reactions were then separated in the

hybrid gel media and the monovalent QD-antibody conjugate extracted for subsequent use in Western blotting and cellular imaging where they demonstrated improved quantitative abilities.

In its first or "classical" iteration, CE measured the electrophoretic mobility of charged species in an open capillary (no solid matrix) filled with a liquid electrolyte under an electric field. Through a combination of sample component electrophoresis and electrolyte buffer electroosmotic flow (EOF), sample components are transported from the positive anode to the cathode while separating in a manner that is based on size-to-charge ratio.^{52,53} UV-visible and fluorescence spectroscopy are typically coupled with CE for detection.⁵² Extensive optimization of the technique is almost always required for effective CE, as outlined in a recent review by Surugau and Urban.⁵² The ability of CE to purify NM-bioconjugates from free NMs has been demonstrated for QD-BSA⁶⁶ and silicon-NP SA conjugates.⁶⁷ Variations on traditional CE include capillary gel electrophoresis, micellar and microemulsion electrokinetic chromatographies,⁶⁸ capillary isoelectric focusing, and capillary isotachophoresis, although the later have been less commonly applied to NMs.⁶⁹ Other electrophoretic methods with strong potential for application to NM purification include dielectrophoresis,^{52,70} isotachophoresis,⁵⁸ and isodielectric separation.⁷¹ One of the benefits of CE is its inherent high sensitivity, which allows for very small sample sizes/volumes to be used. This, however, suggests that as most commonly implemented, this technique may be more appropriate for analysis and characterization rather than bulk purification.

Centrifugation and Analytical Ultracentrifugation. Centrifugation is a relatively simple and cheap technique that can be used to purify functionalized NM-bioconjugates from unconjugated biomolecule. Depending on the density, size, and structure of the NM and biomolecules, application can sometimes be as straightforward as using a benchtop centrifuge to separate functionalized NMs from the reaction mixture and then either removing the soluble bioconjugate or, alternatively, resuspending the bioconjugate precipitate in the buffer of choice. For example, such a method has been used to purify layered double hydroxide NPs intercalated with the acetyl choline esterase (ACE) inhibitor enalaprilate from free drug.⁷² For smaller NMs, or those with a lower density, ultracentrifugation may also be useful for separation and purification. This is often used in gold NP-conjugate purification, for example, with gold-NP-SA conjugates,⁷³ and has also been applied to isolation of dye- or PEG-modified potato virus X.⁶¹ In other instances, glycerol, sucrose, salt (cesium chloride CsCl), or other gradient-based methods can be used to help separate out NM conjugates from unconjugated materials during ultracentrifugation. For example, Saini and co-workers genetically modified the hexon protein of adenovirus NPs with a (His)₆-affinity tag that allowed subsequent noncovalent coupling to 1.8 nm gold NPs (AuNPs) modified with nickel(II) nitrilotriacetic acid (Ni-NTA) to the virus surface.⁷⁴ A CsCl centrifuge gradient was then used to separate gold NPs conjugated with adenovirus from unconjugated AuNPs and adenovirus.⁷⁴ The resulting bioconjugates have the potential to be used in a variety of applications such as imaging, diagnosis, and as combined photothermal and gene therapy for cancer treatment. Interestingly, the authors demonstrated that adenovirus displaying an AuNP-labeling ratio of ~2000:1 had limited effect on the infectivity of the adenovirus toward HeLa cells; something that would not be expected *a priori*. As with many related techniques, optimization of the conditions is critical for effective separation.⁷⁵

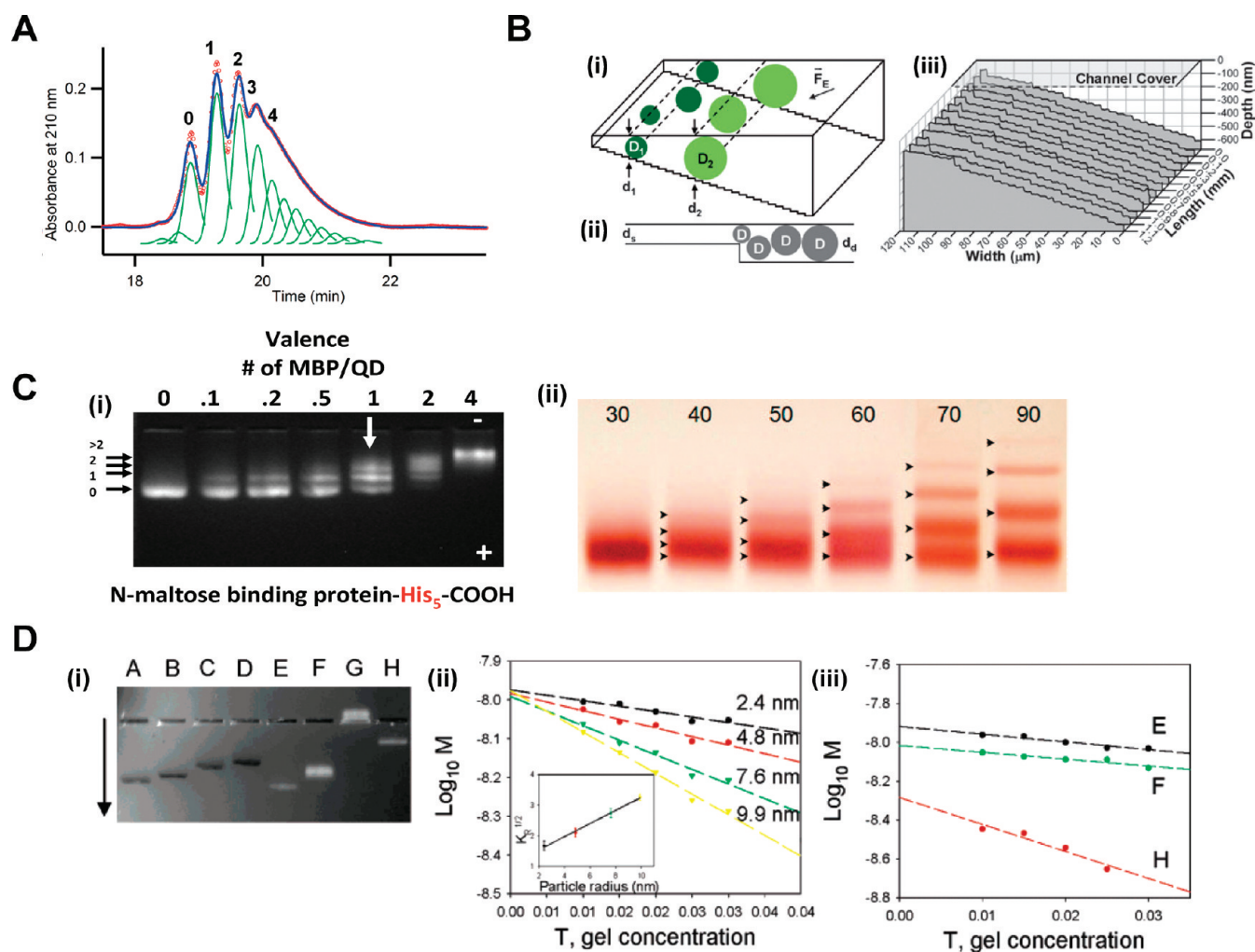


Figure 5. Chromatographic techniques and gel electrophoresis for characterization. (A) HPLC trace monitored at 210 nm of sample G (G5-Ac80-(NH₂)109-alkyne2.7) shown with red dots. Five different peaks (0–4) were observed in the sample's trace. Peak 0 had the same retention time as the parent dendrimer (G5-Ac80-(NH₂)32). Data were deconvoluted using peak fitting, individually fitted peaks are plotted in green, and the summation of the fitted peaks is plotted in blue. The fitting peak was developed to have the same shape as the parent dendrimer. Reprinted from ref 45. Copyright 2010 American Chemical Society. (B) Size exclusion nanofluidics: (i) schematic of the size separation and metrology of a mixture of NPs by 3D nanofluidic size exclusion, (ii) schematic of adjacent nanofluidic steps with excluded depths $d_s < d_d$ “binning” NPs of different sizes $d_s < D < d_d$ into a size subset. Schematics are not to scale. (iii) Etched channel surface as measured by scanning probe profilometry. Reprinted with permission from ref 46. Copyright 2010 The Royal Society of Chemistry. (C) Gel electrophoresis-characterization: (i) agarose gel characterization of maltose binding protein (MBP)-QD bioconjugates. Gel image clearly demonstrates the separation of QDs conjugates with different numbers of surface-assembled MBP. Reprinted from ref 64. Copyright 2006 American Chemical Society. (ii) Electrophoretic analysis of 5 nm AuNPs conjugated to polyT DNA 30–90 bases in length. Black arrowheads indicate visible bands as a guide to the eye. Reprinted from ref 42. Copyright 2008 American Chemical Society. (D) Ferguson analysis: (i) agarose gel picture showing BSP-coated 2.4, 4.8, 7.6, and 9.9 nm radius AuNPs (lanes A–D) visualized by absorption, and 540 nm QDs capped with DHLA (E), a 1:1 mixture of DHLA/DHLA-PEG600 (F), DHLA-PEG600 (G), and QD-20MBP-His₅ conjugates (H). QD bands were visualized by fluorescence. (ii) Electrophoretic mobility of gold particle standards as a function of gel concentration. For each size, the corresponding retardation coefficient, KR, is the slope of the linear fit. The inset shows $KR^{1/2}$ as a function of the particle radius for the gold particles. (iii) Electrophoretic mobility of QD samples vs gel concentration. Reprinted from ref 64. Copyright 2006 American Chemical Society.

Analytical ultracentrifugation (AUC) utilizes a special type of ultracentrifuge that consists of a high-speed centrifuge rotor with cell compartments and an optical system (usually UV) to measure concentration gradients of the sample during the separation process.^{76–78} The two principle modes used in AUC are sedimentation velocity and sedimentation equilibrium. While the technique can be applied to the purification of NM-bioconjugates, it is more commonly used for characterization of these composites and is discussed in more detail below.

Dialysis and Filtration. After chromatography, dialysis, filtration, and the centrifugation-assisted versions of these techniques

probably represent the most common methods applied to NM-bioconjugate purification. Dialysis and membrane filtration methods in particular are relatively cheap, commercially available, and simple to use. Both use some form of permeable or semipermeable membrane with a given size or molecular weight cutoff (MWCO) value to separate the biomolecule from the NM-bioconjugate. In the case of dialysis, the membrane containing the sample to be purified is immersed in a large excess volume of liquid and species of MW < membrane MWCO (typically the biomolecule) flow in the direction of high to low concentration.^{37,79} Filtration devices can be gravity driven, but

generally centrifugation is used to increase the speed and efficiency of the process.⁸⁰ For example, Vannoy assembled hen egg white lysozyme (HEWL)-QD conjugates using carbodiimide (EDC) chemistry and then utilized 100 kDa MWCO Amicon ultrafilter devices to selectively remove the unbound HEWL (MW ~ 15 kDa) along with excess reagents.⁸⁰ The propensity of the resulting conjugates to form fibrils suggested that they could be used as a tool to understand fibril self-assembly processes and the diseases associated with them. To date, ultrafiltration devices have shown some utility in purification of bare NMs but also have good potential for application to NM-bioconjugates.^{81,82}

Extraction. Chemical extraction and differential precipitation are other potentially efficient but largely underused purification techniques. In a relatively simple strategy that highlights the possibilities available, Zhang and co-workers recently used a biphasic cap exchange-extraction method to generate amino-acid functionalized QDs, see Figure 4C.⁸³ Water-soluble dithiocarbamates, created through the reaction of carbon disulfide with primary and secondary amine containing amino acids species, were dissolved in the aqueous layer of a biphasic reaction while QDs with native hydrophobic capping ligands were present in the organic chloroform layer. After overnight mixing of the reaction, the QDs had completely transitioned into the aqueous phase, demonstrating efficient cap exchange and extraction. As only QDs modified with surface biomolecules would transition into the aqueous phase, this extraction strategy could potentially be extended to purifying other QD or NP conjugates formed with larger peptides or appropriately modified biomolecules such as DNA, depending on their stability and tolerance to the reaction conditions. As an example of precipitation being used for purification purposes, Bücking and co-workers used selective precipitation of NP-bioconjugates by ammonium sulfate to purify BSA-coated InP/ZnS QDs.⁵⁸ After the supernatant containing unbound protein and reagents was removed from the precipitated NP-bioconjugates, they were redispersed in PBS buffer prior to characterization. Both extraction and precipitation methods typically rely on somewhat harsh conditions/solvents that can be detrimental to biomolecular stability and are therefore less commonly applied at the present time.

■ CHARACTERIZATION

The ultimate test of successful NM-bioconjugation is of course functionality in the desired application, and while the very nature of activity infers the presence and activity of the biomolecule on the NM surface, this does not reflect any specific details of the underlying NM-bioconjugate architecture. The latter may be essential to understanding any issues arising in subsequent behavior. A variety of well-developed techniques which already have been successfully applied to characterization of bare NMs are now being extended to examining NM-bioconjugates. These include separation-based, scattering, microscopy, spectroscopy, mass spectroscopy, and thermal techniques. A discussion of these techniques along with tables summarizing select applications and some relevant generalized details of each technique is detailed below.^{4,30–34}

Separation Techniques. In general, the separation techniques summarized in Table 1 are relatively cheap and widely available. As described above, some are already routinely used to purify NP-bioconjugates, and can also be quite effectively used for characterization purposes. Indeed they have been shown to be

particularly useful for confirming biomolecular attachment to the NM surface and providing information on approximate hydrodynamic radius, NM-to-biomolecule conjugation ratio and insight into post-production degradation (i.e., stability).

High-Performance Liquid Chromatography. As discussed above, chromatography techniques, and in particular HPLC coupled with anion exchange or reverse-phase columns, have demonstrated the exquisite ability to resolve NM-bioconjugates with different NM-to-biomolecule ratios, providing both the distribution and overall average ratio of NM-to-biomolecule per sample, see Figure 3A.^{22,42} In an especially challenging characterization example, Mullen and co-workers recently demonstrated the use of reverse-phase HPLC to investigate poly(amidoamine) (PAMAM) dendrimers modified with alkyne ligands which are important for subsequent conjugation using click chemistry.⁴⁵ Distinct peaks within each HPLC trace were observed, and deconvolution revealed the different dendrimer-ligand species allowing them to be quantified, see Figure 5A. From this analysis, the mean and distribution of dendrimer-ligand species within the sample were also determined, providing insight into the actual sample composition.

Nanofluidic Size Exclusion. Microfluidic and increasingly nanofluidic devices have much to offer researchers from improved synthesis to characterization as well as reduced sample volumes. Stravis and co-workers recently demonstrated a nanofluidic size exclusion device for on-chip NP size separation and characterization, see Figure 5B.⁴⁶ Currently the device is capable of separating particles in the 80–620 nm range with a step size resolution of 18 nm, although potential exists down to <10 nm. The authors used the device to characterize 100 and 210 nm fluorescent polystyrene particles and were able to determine size distribution profiles for each particle size. In the current context, this device has strong potential for purifying NM-bioconjugates from both biomolecules and unmodified NMs while independently characterizing the size and providing information on the NM-bioconjugate distribution.

Field Flow Fractionation. As discussed, FFF provides information on charge, size (peak height position), and size distribution (peak width).^{48,49} FFF has already been used by a number of researchers to provide size information on various unmodified NPs, including AuNPs,⁵⁰ polymer (polyorganosiloxane-based)⁵¹ NPs,⁸⁴ QDs/AuNPs,⁸⁵ bionanocomposites of DNA/chitosan,⁵¹ and AuNPs modified with PEG ligands.⁵⁰ As with many of the techniques discussed, precalibration with known “size” NM standards, such as Au or polystyrene NMs, is often desired. Size standard calibration is not always necessary, especially if the technique is combined with dynamic light scattering for detection,^{50,86} or in the case of flow and sedimentation FFF, if all geometric dimensions of the fractionation channel are accurately known.^{87,88} The latter allows you to convert retention times into size distribution profiles (see refs 87 and 88 for theory).

Electrophoresis. A number of electrophoretic methods have demonstrated wide utility in the characterization of NM-bioconjugates.^{52,53} For example, Gagnon and co-workers recently used dielectrophoresis to determine the effect that the surface coverage of single stranded DNA (ssDNA) immobilized onto silica NPs had on the ssDNA conformation and subsequent DNA hybridization efficiency.⁷⁰ Gel electrophoresis in particular is routinely used to confirm bioconjugation by visualizing the differing mobilities of NM-bioconjugates versus NMs.^{54–58,64,89} Under optimal conditions, gel electrophoresis has shown

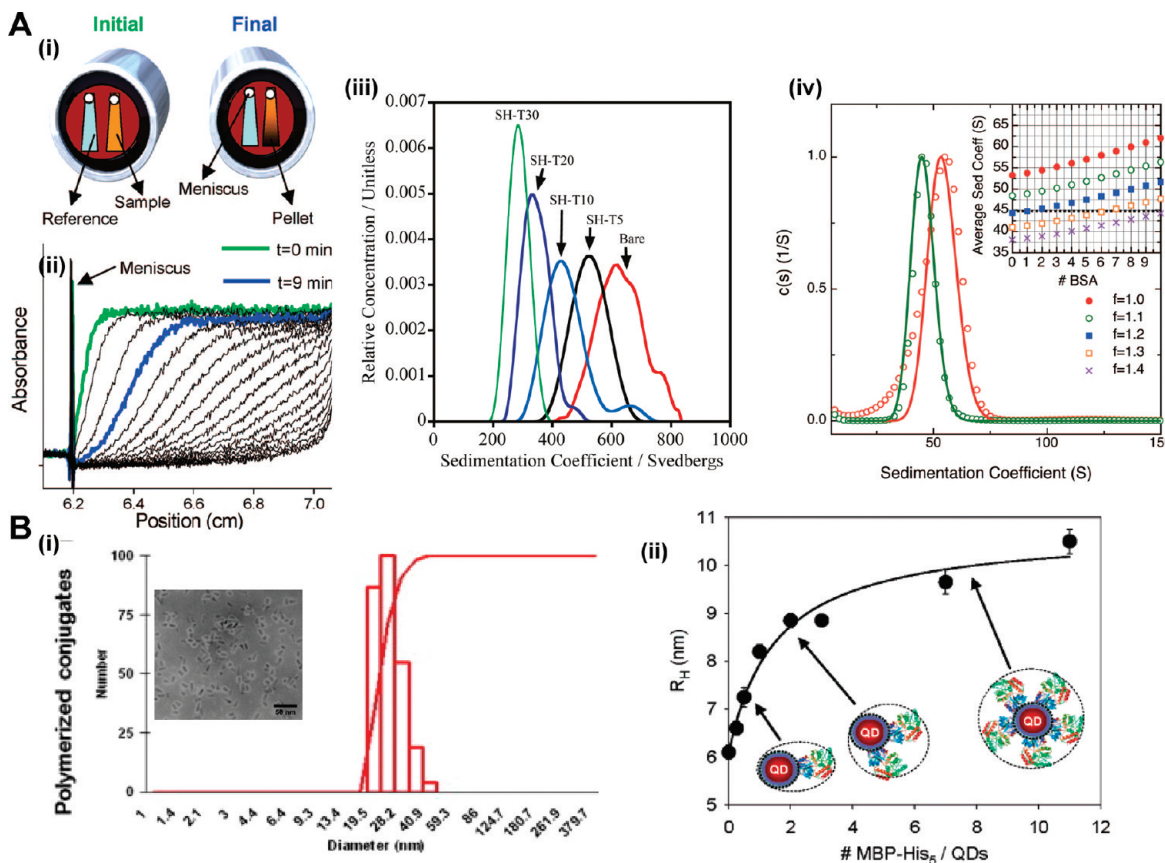


Figure 6. Analytical ultracentrifugation and dynamic light scattering for characterization. (A) (i) Ultracentrifugation causes the NPs to sediment and ultimately pellet in the bottom of the cell (nonuniform cell on right) relative to the reference. (ii) The instrument scans the absorbance from top-to-bottom of the sample and reference cells and absorbance is plotted versus cell position. The multiple curves represent absorbance scans at different time intervals during the AUC process. Reprinted from ref 76. Copyright 2008 American Chemical Society. (iii) Progression of the sedimentation coefficient distribution for bare 10 nm gold particles and 10 nm AuNPs modified with thymidine homo-oligomers decreasing from 30 bases (SH-T30) to 5 bases (SH-T5) in size. Reprinted from ref 95. Copyright 2010 American Chemical Society. (iv) Sedimentation coefficient distributions of 3.05 nm radius CdSe/ZnS particles capped with DHLA-PEG in the presence (green circles) and absence (red circles) of BSA. Solid lines represent the fits of the data. The inset shows the change in average sedimentation coefficient with increasing numbers of bound BSA for different frictional ratio values. Reprinted from ref 93. Copyright 2008 American Chemical Society. (B) Dynamic light scattering (DLS). (i) The DLS and corresponding TEM characterization of QD-luc8 NP-bioconjugates postpolymeric encapsulation. Polymeric encapsulation cross-linked two to three QD-luc8-NPs resulting in an increased hydrodynamic radius observed in DLS. Reprinted with permission from ref 102. Copyright 2008 Elsevier. (ii) Hydrodynamic radii of QD-MBP-His₅ bioconjugates as a function of the average number of proteins per QD, measured from eight different samples. Schematics represent a CdSe-ZnS core-shell QD conjugated to ratios of 1, 2, and saturated with proteins. Reprinted from ref 64. Copyright 2006 American Chemical Society.

exquisite resolution, being able to separate NMs biolabeled with one, two, or three biomolecules. This provides further information on the distribution of bioconjugation ratios obtained with a particular chemistry, see Figure 5C.^{55,64} The technique can also be used to elucidate conformational information about DNA immobilized onto AuNPs.⁵⁴

Ferguson analysis of gel electrophoretic data can be further used to infer the hydrodynamic diameter and ζ potential of NM-bioconjugates, as demonstrated for AuNP-DNA and QD-MBP bioconjugates.^{54,55,64} The analysis typically requires the user to run the sample in a series of agarose gels comprising a range of concentrations (i.e., 0.5–3.5%) and incorporate calibration against known size standards prior to final analysis (such as AuNPs), see Figure 5D. The mobility of the unknown sample in the gel series can be converted either to its retardation coefficient to yield the effective particle diameter or its ζ potential (see refs 64 and 55 for some discussion of the theory along with good examples of the application). When Ferguson analysis is used to

evaluate gel electrophoretic data for the hydrodynamic diameter and ζ potential, a spherical assumption of the NM shape is typically assumed; however, with appropriate modifications it is also suitable for the analysis of rod shaped NMs.⁹⁰

Analytical Ultracentrifugation. In addition to purifying NM-bioconjugates, AUC can also determine the size, size distribution, and shape of NMs as well as structural and conformational information about the conjugated biomolecules, see Figure 6A. AUC has been used for analyzing protein-based NMs such as those assembled from cross-linked human serum albumin (HSA) along with inorganic NMs such as silica NPs and QDs.^{77,91–94} Falabella and co-workers recently used AUC to systematically characterize single stranded DNA binding to 10 and 20 nm AuNPs as a function of surface loading and strand length, see Figure 6A.⁹⁵ Mulvaney's group elegantly demonstrated the potential power of this technique by characterizing QD size distributions, ligand densities and bioconjugation with the model protein BSA, all using AUC, see Figure 6A.⁹³ They found the

Table 2. Scattering Techniques^a

technique/types	NM-bioconjugates analyzed	advantages	disadvantages	refs
dynamic light scattering (DLS) (also known as photon correlation spectroscopy (PCS) or quasi elastic light scattering (QELS))	QD-Luciferase (8), QD-PEG, QD-MBP	<ul style="list-style-type: none"> 1. nondestructive. 2. hydrodynamic dimensions readily determined. 3. rapid, simple and relatively cheap. 4. measurements can be performed in any liquid media, solvent of interest. 5. sensitive. 	<ul style="list-style-type: none"> 1. typically assumes spherical shape. 2. resolution issues. 3. biased toward larger particles. 4. sample preparation is extremely important, solutions should be filtered prior to use. 5. limited ability to measure polydisperse samples 	64,97–103
fluorescence correlation spectroscopy (FCS)	silver NP-DNA	<ul style="list-style-type: none"> 1. hydrodynamic dimensions readily determined. 2. photophysical properties can be determined. 3. used to investigate binding interactions. 	<ul style="list-style-type: none"> 1. limited to fluorescent species. 	34,104–111
ζ potential	silica NP-streptavidin, AuNP-cytochrome c, QD-[various capping agents]	<ul style="list-style-type: none"> 1. measures particle stability and surface charge. 		30,64,113,114
Raman spectroscopy resonance Raman (RR), Surface enhanced Raman (SERS) and Surface enhanced resonance Raman (SERRS)	gold NP-hemoprotein, silver NP-hemoprotein	<ul style="list-style-type: none"> 1. provides complementary data to IR. 2. isotope composition can be determined. 3. biomolecular interactions can be investigated. 4. characteristic fingerprint spectrum obtained. 	<ul style="list-style-type: none"> 1. Raman signal is relatively weak compared to Rayleigh scattering. 2. limited application to date. 	115–120
X-ray diffraction (XRD)	magnesium aluminum layered double hydroxide nanomaterial-DNA, lipid NP-vitamin A	<ul style="list-style-type: none"> 1. polymorphic information determined. 2. size and structure of NM-bioconjugate can be determined, depending on the NM system. 3. stability information can be determined about the NM-bioconjugate. 		121–128
small angle X-ray scattering (SAXS)	AuNP-DNA, polymer NP-DNA, QD-proteins, lipid NP-DNA	<ul style="list-style-type: none"> 1. provides macromolecular size, shape, distances, and hence packing structures. 2. can provide aggregation information. 	<ul style="list-style-type: none"> 1. requires crystalline samples. 2. distinguishing the small angle scattering can be complex (<10°). 3. biological entities can be damaged by the X-rays. 4. sample preparation can be complex (thin films required). 5. data analysis complex and requires modeling to interpret. 	129–134
small angle neutron scattering (SANS)	BSA-polymer NPs, PEG-peptide NPs, acrylamide-doxorubicin NMs	<ul style="list-style-type: none"> 1. can determine size, shape and orientation of samples. 2. can be used to probe “soft” biological containing samples without damage. 3. isotopic sensitivity can be used to elucidate structures. 	<ul style="list-style-type: none"> 1. limited availability of neutron sources. 2. crystalline samples are required. 	128,135,136

^a General information: NM structure, morphology, hydrodynamic size, aggregation state, biomolecule conformation, and NM-bioconjugate stability can all be determined.

sedimentation rate to be highly sensitive to particle size (resolution <0.16 nm), composition, and surface chemistry and were able to model each individual contribution (assuming a spherical particle). Addition of BSA to the surface of the QDs resulted in a decrease in the measured sedimentation rate, with curve fitting suggesting one-to-two BSA per QD in the final bioconjugate. Benefits to the AUC method include small sample sizes, direct analysis of liquid-based dispersions without the need for special solvents such as those commonly found in gradient centrifugation, and amenability to a wide range of usable concentrations. Often times, AUC is used in parallel with other characterization techniques, such as DLS and TEM;^{93,95} however, as AUC is nondestructive to the sample it is possible to perform it and then sequentially apply a small portion to a more destructive technique such as TEM.⁹²

Electrospray Differential Mobility Analysis (ES-DMA). ES-DMA has previously been used to study a range of biomolecules and unmodified NMs but more recently has been extended to the characterization of NM-bioconjugates.⁹⁶ Electrospray aerosolizes the sample which then passes through a neutralizer (to set charge on the particles) into the DMA that separates positively charged particles based on their size-to-charge ratio where they are detected using a condensation particle counter. ES-DMA thus provides the user an overall size and size distribution measurement based on the trajectory and the number of particles and hence a concentration based on size. The technique was recently demonstrated by Pease and co-workers in conjunction with TEM for characterizing SA coated QDs and QD-functionalized with Lambda phage.⁹⁶

Scattering Techniques. These techniques exploit the scattering of radiation (e.g., light or energetic particles) through its interaction with a sample, see Table 2. Depending on the scattering technique applied, information about the NM structure, morphology, hydrodynamic size, and aggregation state as well as the biomolecular conformation and the NM-bioconjugate stability postproduction can be obtained.

Dynamic Light Scattering. Of all the scattering-techniques available, dynamic light scattering (DLS), also known as photon correlation spectroscopy (PCS), is probably the most commonly used for characterizing the hydrodynamic size of NM-bioconjugates, given that it is simple, noninvasive, nondestructive, and relatively cheap to apply (the instrument itself can be costly though).^{97–99} Fluctuations in the scattered light intensity, due to the Brownian motion of the particles, are used to determine the particle diffusion coefficient which is then related to its hydrodynamic radius via the Stokes–Einstein relationship (see ref 64 for an example of application).^{64,100} DLS has a broad working concentration and size range of $\sim 10^8\text{--}10^{12}$ particles/mL and 10–1 000 nm, respectively; however, its sixth power dependence on scattering versus particle size means that wide NM-bioconjugate size distributions can obscure the presence of smaller materials in the sample.¹⁰⁰ In application, Murdock used DLS to study the effect of physiologically relevant dosing media (cell culture media with or without serum) on a variety of unmodified NMs (such as copper, silver, silicon dioxide, carbon nanotubes).⁹⁹ This demonstrated that while many of the NMs tended toward agglomeration in water, in some cases this effect was reduced in serum containing cell culture presumably because the proteins present interact with the NM surface and mitigate agglomeration. Examples of direct NM-bioconjugate characterization include examination of gelatin and human IgG adsorption to AuNPs,¹⁰¹ luciferase (Luc8)-conjugated QDs,¹⁰² or

cytochrome P450 interactions with QDs,¹⁰³ see Figure 6B. Jans and co-workers used DLS to characterize the nonspecific binding of protein A to various size AuNPs and subsequently used it to quantitatively measure the binding of human IgG to protein A *in situ* on the NPs at different incubation times determining that at least two antibodies bound per protein A molecule on the AuNPs.⁹⁸ Pons and co-workers used DLS to characterize the hydrodynamic radius and stability of CdSe/ZnS QDs modified with various hydrophilic surface capping agents, including dihydroxylic acid (DHLA) and amphiphilic polymers along with self-assembled QD-MBP bioconjugates.⁶⁴ They found that the measured hydrodynamic size was strongly dependent on the core QD size and the nature of the capping agent, with the DHLA ligand producing much smaller-sized hydrophilic QDs than their polymer-coated or lipid encapsulated counterparts. The bidentate DHLA were also found to produce more stable QDs that were less prone to aggregation compared to monothiol terminated ligands. Bioconjugation of QDs with MBP was monitored via DLS with the hydrodynamic radius found to saturate at ratios exceeding 10 MBP-per-QD, see Figure 6B. DLS is known to have poor peak resolution and can only resolve particle populations (within the same sample) if they differ in size by at least a factor of 3; therefore, DLS would not be able to simultaneously resolve the different MBP-per-QD ratios illustrated in Figure 6B if they comprised a single sample.¹⁰⁰ That said, the same data shows that when analyzing separate purified samples (individually assembled and monodisperse) that clear differences in stoichiometry could be resolved between the different samples.⁶⁴

Fluorescence Correlation Spectroscopy. Fluorescence correlation spectroscopy (FCS) is similar to DLS in that it measures signal fluctuations due to diffusion, aggregation, interactions, etc and has already been successfully applied to accurately size the hydrodynamic radius of fluorescent NMs including QDs and fluorescent beads.^{34,104,105} With the use of confocal microscopy, a laser (in single or multiphoton excitation mode) interrogates a sample containing a small number of particles and the fluorescent fluctuations observed within a confined optical volume are fitted to an autocorrelation function that can then be used to determine diffusion coefficients, see Figure 7A. The diffusion coefficient is again correlated to the particle hydrodynamic radius via the Stokes–Einstein equation. Müller and co-workers investigated the use of dual-focus FCS to accurately size dye-doped latex particles without precalibration to account for instrument response functions, the latter are usually dependent on the particular instrument arrangement.¹⁰⁵ The dual-focus system used two laser beams to create two overlapping foci with a small measurable shift between the two foci in the sample. The resulting autocorrelation functions (ACF) for each foci and cross correlation function (CCF) between foci were used to determine the NP radius. The authors found excellent agreement between this and DLS for measuring different size particles. Cross correlation of data can also be performed with a single laser if the emitted light is measured in two different detection channels, as described by Roy and co-workers.¹⁰⁶ In terms of NM-bioconjugates, FCS has also been used to determine binding kinetics between 100 nm unilamellar vesicles and fluorescently labeled peptides.¹⁰⁷ The correlation times for the free peptide versus the peptide bound to the large unilamellar vesicles investigated in this format differed significantly, which allowed for accurate kinetic measurement even at low nanomolar peptide concentrations, see Figure 7A. This technique has even been extended to observing metal enhanced fluorescence (MEF)

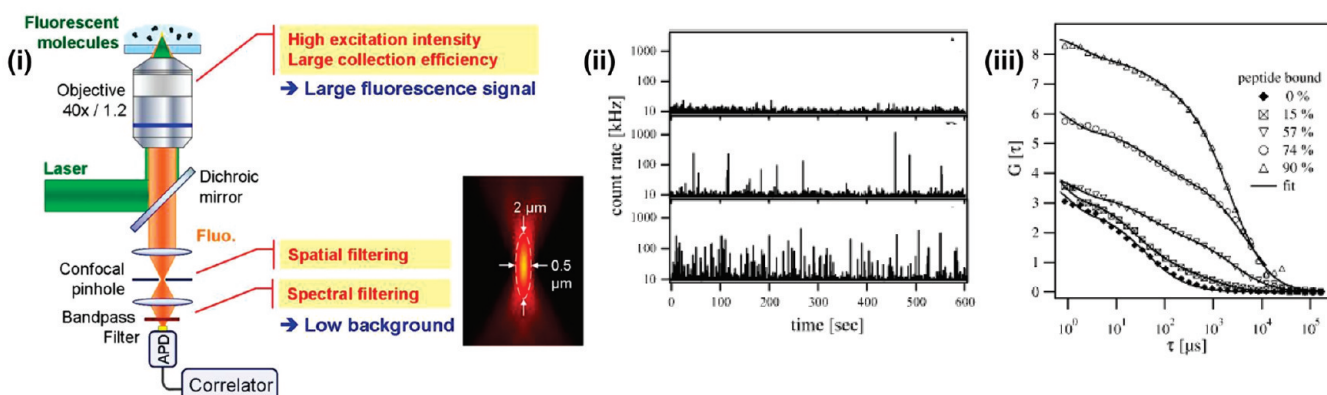
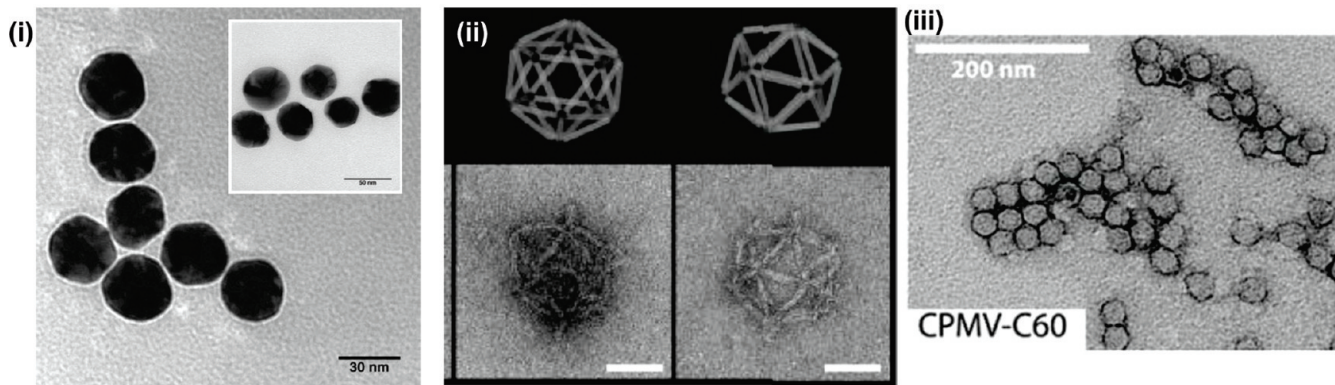
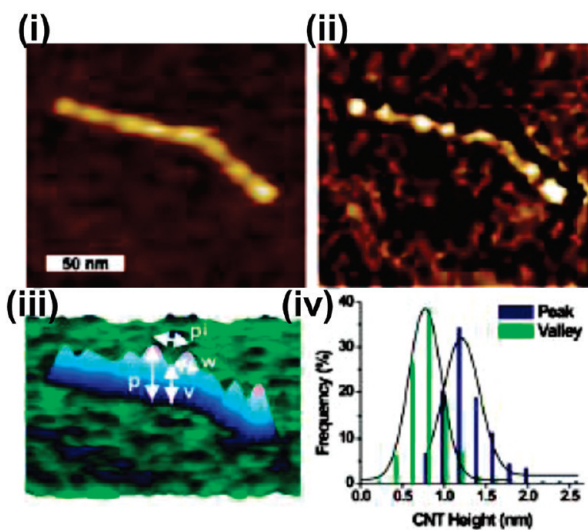
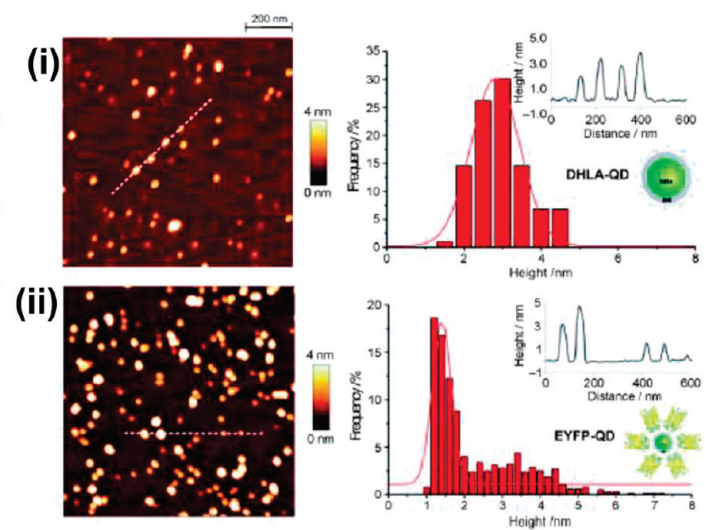
A**B****C****D**

Figure 7. Continued

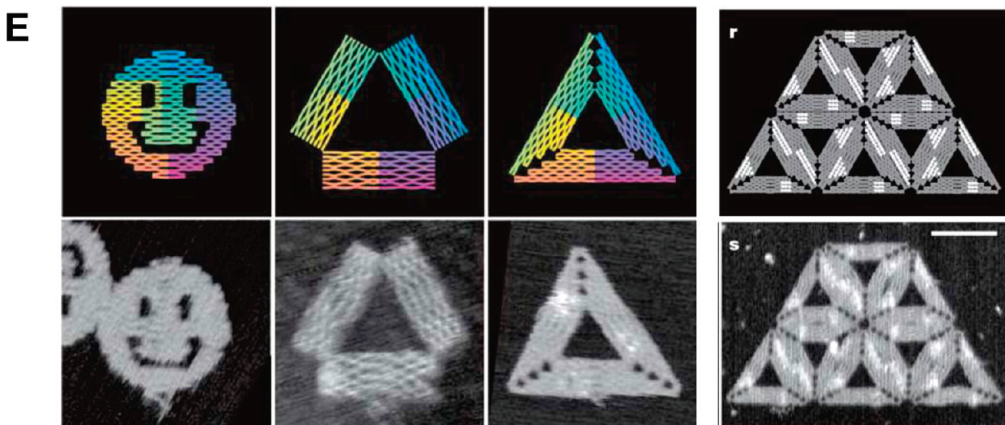


Figure 7. Optical and electron microscopy techniques: (A) (i) state-of-the-art fluorescence detection in solution based on a confocal microscope and fluorescence correlation analysis. The inset shows the size of the typical analysis volume. Reprinted with permission from ref 141. Copyright 2010 MDPI. (ii) Peptide binding vesicles. Time-resolved count rates from solutions containing 2 nM Alexa-labeled peptide only (top trace), Alexa-labeled peptide plus 0.2 μ M lipid vesicle (middle trace), and Alexa-labeled peptide plus 1 μ M lipid vesicle (bottom trace). (iii) The effect of vesicle (lipid) concentration on the autocorrelation curves obtained from a solution containing 2 nM peptide. Autocorrelation curves are shown from 0 to 4 μ M accessible lipid concentrations that correspond to 0–90% peptide bound. Reprinted with permission from ref 107. Copyright 2004 Elsevier. (B) Electron microscopy: (i) low-resolution TEM images of gold conjugates. Image shows a thin white “halo” layer surrounding the surface of the NPs indicating coating of the gold with protein. This “halo” effect is not present on the nonconjugated AuNP image, see insert. Reprinted with permission from ref 150. Copyright 2010 Elsevier. (ii) Uranyl formate staining of DNA Origami. Orthographic projection models and TEM data of two icosahedron particles. The scale bars on TEM images are 100 nm. Reprinted with permission from ref 152. Copyright 2009 Macmillan Publishers Ltd. (iii) Uranyl acetate staining of CPMV-C₆₀ fullerene conjugates for TEM imaging. Reprinted from ref 151. Copyright 2009 American Chemical Society. (C) Atomic force microscopy of carbon NTs wrapped with (GT)₃₀ oligonucleotide. (i) Height image (5 nm scale) and (ii) phase image (25° scale) of one representative carbon NT-DNA, along with (iii) a 3D representation (1.7 nm scale) indicating the peak height (p), valley height (v), peak width (w), and pitch (pi) measurements. (iv) Distributions of nanotube height measurements at peaks and valleys ($n = 300$ CNTs). Reprinted from ref 164. Copyright 2008 American Chemical Society. (D) AFM topographic data obtained for the measurement of (i) nonconjugated DHLA-QDs and (ii) EYFP-conjugated DHLA-QDs (ratio 10). The resulting histogram from particle cross section measurements is shown on the right. The inserts represent the corresponding cross section profiles of the dotted line in the AFM-height image. Reprinted with permission from ref 165. Copyright 2009 Wiley-VCH Verlag GmbH & Co. KGaA. (E) DNA Origami and AFM analysis. Folding circular genomic DNA from the virus M13mp18 into different shapes. Models are shown in the top row, with the resulting AFM images shown below. Reprinted with permission from ref 168. Copyright 2006 Macmillan Publishers Ltd.

resulting from Cy5-labeled DNA hybridizing to DNA-modified silver NPs by using the modified technique of fluorescence lifetime correlation spectroscopy.¹⁰⁸ This derivative approach measures intensity decay times, instead of intensity fluctuations, and found a 5-fold decrease in emission lifetime of the Cy5-DNA upon binding to its complement attached to 50 nm silver NPs. Hybridization also resulted in a 10-fold increase in Cy5 fluorescence intensity and increased its contribution to the autocorrelation function compared to free Cy5-DNA. These effects allowed the researchers to resolve different species within the sample mixture based on a combination of both intensities and lifetimes. A similar approach was used by Tang and co-workers to measure alpha fetal protein (AFP).¹⁰⁹ Here, silver NPs were functionalized with anti-AFP and AlexaFluor647-labeled AFP was used as the tracer antigen in a homogeneous competitive assay for AFP.

Popular derivatives of FCS include dual-color FCS, which allows the user to cross-correlate data from two different fluorescent channels simultaneously¹¹⁰ and Förster resonance energy transfer (FRET)-FCS, commonly called single-pair or particle (sp)FRET. Pons and co-workers used single-particle FRET measurements taken on a dual color FCS system to investigate the binding of acceptor-dye-labeled MBP to QDs (donor).¹¹¹ Donor and acceptor signals were separated using a dichroic filter, and results demonstrated that protein binding to QDs followed an expected Poisson distribution. Since FCS is, for all intents and purposes, a single molecule technique, an important factor often overlooked in performing this technique is getting the final sample concentration into the correct

dilution regime, with typical concentrations in the low to subnanomolar range.

Resonance Light Scattering Correlation Spectroscopy. RLSCS measures the resonant light scattering intensity fluctuations from NMs that posses a surface plasmon band (such as Au or silver NPs). Although limited to suitable NP materials, the technique has been used to study the bioconjugation of AuNPs with either BSA or thiol-modified DNA species, with the interaction resulting in increased diffusion times.¹¹²

Zeta (ζ) Potential. Measurement of the ζ potential of a NM in solution provides information on the net charge a NM-bioconjugate has and provides insight into NM-bioconjugate stability. The ζ potential is commonly determined by applying an electric field across a sample and measuring the velocity at which charged species move toward the electrode; this is proportional to the ζ potential.⁶⁴ The ζ potential can also be used to infer particle stability with a value of ± 30 mV often selected as an arbitrary delineation of stability. Values >30 mV indicate stability, while values <30 mV represent particles with a tendency toward agglomeration or instability.³⁰ Many factors can influence NM stability (and hence the ζ potential) including pH, concentration, ionic strength of the solution, temperature, radiation, and the nature of the surface ligands. ζ potential measurements have been used to study the stability and particle size of SA-functionalized silica NPs as a function of pH,¹¹³ the surface coverage of cytochrome c bioconjugated to AuNPs,¹¹⁴ and various QD capping agents.⁶⁴ In the latter AuNP example, Gomes and co-workers used ζ potential measurements to evaluate the surface

Table 3. Microscopy Techniques^a

technique/types	NM-bioconjugates analyzed	advantages	disadvantages	refs
atomic force microscopy (AFM)	AuNP-DNA, carbon nanotubes (CNT)-DNA, QD-streptavidin, titanium dioxide (TiO_2) NP-DNA, AuNP-cytochrome c	1. capable of 3D mapping of the sample surface. 2. can analyze individual NMs. 3. can be applied to nonconducting wet and soft samples on various substrates. 4. size and shape characterization of the NM and biomolecule can be determined. 5. biomolecular interactions can be characterized using functionalized tips.	1. sample under study must be immobilized onto a suitable surface and sample preparation can be complex. 2. only small areas can be mapped and the scan time can be slow. 3. analysis is, in general, limited to the NP exterior. 4. technique requires extensive optimization and interpretation.	114,149,164–169
transmission electron microscopy (TEM) cryogenic-TEM allows analysis of tissue samples	AuNP-hemoproteins, polyacrylic NP- adenoviruses, lipid micelles, vesicles and bilayers-transient nanostructures	1. can analyze individual NMs, can be used to determine NM size and shapes. 2. aspect ratios can be determined. 3. biomolecules can be somewhat visualized.	1. conducting or stained ultrathin sample required. 2. dry samples needed for analysis, nonphysiological. 3. ionizing radiation can cause sample damage. 4. small angle of view, only limited NPs can be analyzed at one time. 5. expensive equipment and technical expertise required to obtain meaningful data.	61,148–153
scanning electron microscopy (SEM) environmental SEM (ESEM)	polystyrene NP-protein	1. can analyze individual NM core, can be used to determine NM size and shapes. 2. can determine NM composition. 3. biomolecules can be imaged using ESEM.	1. conducting sample usually required. 2. dry samples needed for analysis, nonphysiological (unless running ESEM). 3. expensive equipment and technical expertise required to obtain meaningful data. 4. mainly used to characterize NP core. 5. ESEM reduces resolution.	154–160
light microscopy standard light microscopy and fluorescence confocal imaging	silver NP-DNA, luminescent NP-proteins	1. single-molecule based measurements are possible with fluorescent samples. 2. more widespread than many of the other microscopy based techniques.	1. somewhat limited by diffraction issues. 2. can require fluorescent samples.	139–146
near-field scanning optical microscopy (NSOM)	Au-NP-streptavidin-biotin		1. small surface area analyzed. 2. analysis limited to the surface of the NP. 3. currently a “specialist” technique.	170,171

^a In many cases, capable of single particle resolution. Techniques can be used to determine NM size and shape.

coverage of heart- and yeast-cytochrome *c* on 11.5 nm gold colloids following overnight incubation.¹¹⁴ They determined that the change in ζ potential depended on the [cytochrome *c*]/[AuNP] ratio in the sample mixture, and this was found to be saturated for both proteins at ratios of \sim 200:1 producing stable NP-bioconjugates with a final ζ potential ranging from -30 to -35 mV. As with DLS, the ζ potential is fairly easy to measure and oftentimes the two techniques are available on the same instrument.

Raman Techniques. Raman techniques commonly applied to characterization include Raman spectroscopy and surface enhanced Raman scattering (SERS). Raman spectroscopy measures the inelastic scattering of monochromatic radiation (UV, visible, or near IR) by a sample. The incident light becomes either Stokes or anti-Stokes shifted in wavelength resulting in sharp fingerprint Raman bands that are characteristic of the sample and complementary to infrared (IR) spectroscopy. Carbon nanotubes, for example, exhibit strong Raman scattering which has been found to be sensitive to isotope composition¹¹⁵ and biomolecular interactions.¹¹⁶ Yang and co-workers used Raman spectroscopy to investigate the noncovalent interaction between pyrene-labeled cellulose (Py-HPC) and multiwalled carbon nanotubes (MWCNTs).¹¹⁶ Pristine MWCNTs had characteristic Raman D (C–C) and G (C=C) bands at 1321 and 1565 cm^{-1} , respectively. Enhancement of the D band was observed upon binding Py-HPC, not only confirming bioconjugation but also the nature of the interaction, since D band enhancement is attributed to π – π stacking.

Metallic NPs and in particular silver NPs offer the unique possibility of localized surface enhanced Raman scattering (SERS)^{117,118} and have been used to study hemoprotein (heme-containing proteins such as hemoglobin, myoglobin, and cytochrome *c*) and lysozyme bioconjugation to Au and/or silver NPs along with aptamer conformational changes upon target binding.^{119,120} Zhang and co-workers looked at the interaction of lysozyme upon noncovalent interaction with 90 nm AuNPs, which induced protein aggregation resulting in the formation of extended protein-NP assemblies.¹²⁰ A blue shift in the amide I band combined with a red shift in the amide II band of the Raman spectra revealed conformational modifications in the gold-bound lysozyme. This was attributed to a shift from the α -helical structure to a more β -sheet or random coil conformation.

X-ray Diffraction. X-ray diffraction (XRD) is typically used to provide structural information about crystalline samples. It is also frequently used to characterize materials containing nanosized components embedded in an extended biological matrix, such as those found in tissue scaffolds and bone cements^{121,122} or nanobioconjugate layered materials such as nanobiohybrids,^{123,124} where analysis of *d*-spacing changes upon bioconjugation between layers of the nanomaterial can be used to assess reaction completion or investigate the biomolecular orientation.^{125,126} For example, Choy and co-workers prepared anionic clays comprising brucite-like cationic hydroxide nanolayers with exchangeable anions.¹²⁶ When the nitrate ions were replaced with DNA, the spacing between hydroxide layers was found to increase \sim 2 nm consistent with the DNA double helix laying parallel to the basal plane of the layers. In some cases, XRD is used to characterize the biomolecule after it has been associated with the NM, as seen in its use to assess the polymorph stability of solid-lipid NPs containing vitamin A.¹²⁷ XRD had also been used to assess the effect of PEG content on the self-assembly of peptide fibril nanostructures.¹²⁸

Small-Angle Scattering Techniques. Small-angle X-ray scattering (SAXS) and small-angle neutron scattering (SANS) have been applied to elucidating information on the structure, morphology, and characteristic intra-assembly spacings of a variety of polymer and biological based nanomaterials.^{129,130} The principle mechanistic difference between SAXS and SANS is that X-rays are scattered by the electrons while neutrons are scattered by the nucleus. This has a direct impact on what can be observed and the magnitude of the observation (e.g., in neutron scattering the scattering factor of carbon and hydrogen is of approximately equal magnitude but opposite sign while with X-rays there is about a six-fold difference between carbon and hydrogen). Both X-rays and neutrons can be used at a variety of wavelengths; importantly though radiation damage to the sample is a function of wavelength (i.e., energy) and exposure time. For biological samples, the X-ray radiation used is generally 1.54 Å but can range from about 0.2 to 4.0 Å. It should be noted that long-wavelength X-rays are absorbed strongly by air and thus are seldom used. Neutrons used to study biological materials are generally in the range of 2–10 Å (the full spectrum of neutron radiation is from about 1.0 to 20 Å).

SAXS has been used for analyzing various NM-bioconjugate systems including the packing and extended structures of DNA-modified AuNPs,¹³¹ elucidating the internal structure of heparin loaded chitosan NMs,¹³² and determining the structural changes that occur in various ordered mesoporous (nanoporous) materials upon adsorption and release of lysozyme.¹³³ Bhattacharyya compared two different ordered mesoporous materials, silica-based SBA-15 and organosilica-based MSE, during their adsorption and release of lysozyme.¹³³ SAXS analysis revealed that the more hydrophilic material SBA-15 produced lattice structure increases in size upon adsorption and also release of lysozyme, whereas the MSE lattice structure remained constant during these conditions resulting in a slightly different release profile. A recent study by McKenzie and coworkers demonstrated a microscale flow system for simultaneous *in situ* monitoring of SAXS and UV-visible spectra.¹³⁴ The system was used for the real-time size determination of mercaptoethoxyethoxyethanol-stabilized AuNPs (0.8–5 nm) and while no bioconjugates were investigated here the technique could quite readily be applied to the characterization of NM-bioconjugates. Several studies have used SANS in combination with DLS and static light scattering (SLS) to elucidate the structure and core morphology of NMbioconjugates.^{128,135,136} Serefoglou and coworkers, for example, used SANS to study complexes formed between the protein BSA and two anionic graft copolymers, revealing core-corona NPs whose core size increased with decreasing content of the neutral poly(*N,N*-dimethylacrylamide) side chains in the graft copolymers.¹³⁵ However, the SANS technique suffers from a lack of suitable neutron sources (synchrotrons) and is thus not widely utilized at this time.

Microscopy. These techniques are based on visualizing a sample using light, electrons, or a scanning probe, as summarized in Table 3.^{137–139} Traditional optical light microscopy (sometimes referred to as bright field microscopy), and its myriad of fluorescent derivatives were until recently, however, unable to resolve nanoscale features $<$ 200 nm due to diffraction limitations. As a result, they found limited application in the characterization of individual NM-bioconjugates, although they have been extensively used to track and image an almost countless number of fluorescent NM-bioconjugates in cellular and small animal studies. Recent developments involving ultrahigh-resolution

Table 4. Spectroscopic Techniques^a

technique/types	NM-bioconjugates analyzed	advantages	disadvantages	refs
UV-visible spectroscopy	has been used to characterize a large number of NM-bioconjugate types. Examples: AuNP-protein, AuNP-DNA, iron oxide NP-protein, QD-protein	<ul style="list-style-type: none"> 1. cost effective, available in most laboratories, simple and fast. 2. a number of NMs have intrinsic optical properties that can be used to determine concentration, size and sometimes shape. Changes in the spectra can be associated with aggregation state. 3. biomolecules also typically have some intrinsic optical properties that can be used to determine concentration. 4. can be used to characterize NM-biomolecule conjugation and average ratio. 	<ul style="list-style-type: none"> 1. requires fairly concentrated samples as sensitivity is low. 2. provides average information only no distribution information. 	4,114,119, 173–184
circular dichroism (CD)	AuNP-protein, silica NP-protein, iron oxide NP-protein, CNTs-protein, QD-protein	<ul style="list-style-type: none"> 1. provides biomolecule (protein and DNA most common) conformational and stability information. 2. nondestructive. 3. liquid samples can be prepared in physiological environment. 	<ul style="list-style-type: none"> 1. extensive characterization of the biomolecule prior to NP bioconjugation required to obtain meaningful results. 2. non UV-absorbing buffers required. 3. oxygen can be interferent in UV analysis. 	4,59,94, 114,179, 182,185–190
fluorescence spectroscopy	standard fluorescence, wavelength and time-resolved. Both direct and indirect techniques. fluorescence resonance energy transfer (FRET): special fluorescent format that requires a donor fluorophore and an acceptor species.	<ul style="list-style-type: none"> 1. sensitive. 2. fluorescence can be environmentally sensitive which can be used to provide biomolecule conformational information or confirm attachment to NM. 3. NM-biomolecule average coupling ratio, in some instances distribution information. 4. FRET format sensitive to molecular distances. 	<ul style="list-style-type: none"> 1. intrinsic or extrinsic fluorescence required which may necessitate labeling. 2. non UV-absorbing buffers required. 3. oxygen can be interferent in UV analysis. 	37,89,145, 146,182, 186,187, 191–209
infrared spectroscopy (IR)	diamond NP-biotin, AuNP-dextran/albumin, AuNP-hemoproteins, silver NP-hemoproteins, silicon NP-streptavidin, silica NP-β-lactoglobulin	<ul style="list-style-type: none"> 1. confirms NM-biomolecule attachment through the appearance of characteristic fingerprint IR bands. 2. can provide conformational information about the biomolecule upon NM bioconjugation. 3. H₂O is an interference, strong absorbance. 4. appropriate backgrounds are required. 	<ul style="list-style-type: none"> 1. sample preparation can be complicated. 2. optimization of the technique is often required. 3. H₂O is an interference, strong absorbance. 4. appropriate backgrounds are required. 	67,119, 179,172, 180,182, 186,210–213
nuclear magnetic resonance (NMR) ^b	lipid NP-PEG, AuNP-PEG, dendrimer NP-surfactant species	<ul style="list-style-type: none"> 1. nondestructive technique. 2. physical, chemical, structural, and environmental information available about the biomolecule. 	<ul style="list-style-type: none"> 1. only certain nuclei are NMR active. 2. relatively insensitive, requires high sample concentrations. 3. deuterated solvents required. 4. technique relatively expensive and requires expertise. 	45,64,172, 211,214

^a Includes a variety of techniques that can provide NM-biomolecule conjugation confirmation, conformational information about the immobilized biomolecule, NM size, and in some instances, shape, average NM-biomolecule ratio, stability, and concentration. ^b 2D NMR, 2-dimensional NMR; NOE NMR, nuclear Overhauser effect NMR; TROSY NMR, transverse relaxation optimized spectroscopy.

optical systems especially in fluorescent microscopy now provide the ability to resolve features less than 100 nm.^{139–142} In addition, single-molecule microscopic measurements of fluorescent species and especially QDs have become more commonly used to study various biological processes.¹⁴³ Other types of pertinent microscopic analyses that have been accomplished include monitoring Cy5-labeled DNA hybridizing to DNA-modified silver NPs,¹⁴⁴ stepwise photobleaching of fluorescently labeled (Alexa488) proteins attached to lanthanide-ion doped oxide luminescent NPs,¹⁴⁵ or dye-labeled ssDNA binding to silica NPs¹⁴⁶ along with various Förster resonance energy transfer (FRET) studies.¹⁴³ These are discussed further in the fluorescence and emerging technologies sections below.

Electron Microscopy. TEM and SEM readily obtain single particle resolution and are more frequently applied to characterizing the NM core along with core-shell size and/or structure. Both techniques rely on the wave nature of electrons to directly illuminate a sample in either transmission or reflectance modes, respectively, and generate an image.¹³⁷ The direct imaging capability of the TEM and SEM is particularly useful for NMs with nonspherical shapes allowing a direct measure of aspect ratio.^{119,147} While TEM is more commonly used to image the core NM itself, it is possible at low accelerating voltages to visualize biomolecules attached to a NM core as demonstrated for polylactide NM-adenoviruses constructs,¹⁴⁸ carbon NTs modified with horse radish peroxidase or antibodies,¹⁴⁹ and AuNPs modified with antibodies,¹⁵⁰ see Figure 7B. As Thobhani pointed out, this layer appears to be much smaller than expected from concurrent DLS analysis of the bioconjugated-NMs and is likely a result of the drying required for TEM analysis.¹⁵⁰ Imaging the biological components can be facilitated by staining the biomolecules with contrast agents such as uranyl acetate or uranyl formate as demonstrated for Potato virus X, fullerene-labeled CPMV NPs, and DNA-derived 3D nanoscale shapes (see Figure 7B) but, as with drying, staining may also alter the sizes of the NM-bioconjugate.^{61,151,152} Although dried samples are typically required for TEM analysis, researchers recently imaged liquid samples of fixed fibroblast cells stained with epidermal growth factor (EGF)-labeled AuNPs by scanning TEM using a specially designed microfluidic device.¹⁵³ Since SEM uses electrons to image a surface in reflectance mode, it is mainly used to image NM core materials^{154–156} but has the added advantage of a larger imaging field of view than the TEM.^{147,156} SEM has less resolving power for features <20 nm than TEM, although the technology is steadily improving even in this area. SEM is often combined with energy-dispersive X-ray spectroscopy (EDX) analysis to confirm elemental composition of the NM.^{157,158} Environmental SEM (ESEM) does allow sample imaging under low pressure, fairly high humidity, and without the requirement of a conducting overcoat but has found limited use to date for the study of NM-bioconjugates.^{159,160}

Atomic Force Microscopy. In contrast to TEM and SEM, atomic force microscopy (AFM) is a scanning probe technique that can divulge a range of information about the NM, the biomolecule, and the NM-biomolecule interaction on a single-particle basis. Although once considered a fairly specialized technique, recent advances in both instrumentation and software have not only expanded the technique's capabilities but have also made it more user-friendly. Unlike TEM and SEM, which are best performed with conducting or semiconducting samples under vacuum conditions, AFM can be applied to

nonconductive, wet, and soft samples, allowing for many different types of materials to be analyzed in physiological environments.^{138,161,162} Samples can be analyzed using various scanning modes including static (noncontact) and dynamic/tapping (contact and intermittent sample contact), which provide information about various sample parameters including morphological information about the NP (size and shape, etc), information about the biomolecule (adhesion, elasticity, Young's modulus, and stretching parameters), and interactions between the individual particles and biomolecules (protein folding-unfolding, biomolecular attachment to a NM surface, NM-NM agglomeration, etc.).^{162,163} AFM has been applied to studying the interactions between multiple NM platforms and biomolecules including QDs, and carbon NTs binding to DNA,^{164,165} as well as AuNPs, carbon NTs, and QDs functionalized with different proteins,^{114,149,165,166} see Figure 7C. The sensitivity and versatility of AFM has allowed researchers to map ligands attached to a surface in 3D³⁰ and interestingly, when this is combined with data clustering analysis, it can provide approximate NM-bioconjugate stoichiometry, see Figure 7D.¹⁶⁵ Thus, AFM could potentially allow for a 3D representation of ligands or biologicals attached to a NM surface, the determination of how strongly bound the ligands are to that surface, as well as the structure of the underlying NM core. AFM has also been particularly useful in characterizing DNA derived nanostructures, so-called DNA Origami, which is based on programmed self-assembly of specially designed branched DNA junctions and tiles, see Figure 7E.^{152,167–169}

Near-Field Scanning Optical Microscopy. Another surface probe microscopy technique, near-field scanning optical microscopy (NSOM also known as SNOM), breaks the optical resolution limit of light microscopy by placing the detection probe extremely close (at distances much smaller than the wavelength of light) to the surface to be analyzed. High-frequency spatial and spectral information is obtained by analyzing the evanescent fields close to the sample surface. NSOM has the advantage of combining optical and/or spectroscopic data with high-resolution surface topographical information. Contrast properties, such as phase contrast, polarization, fluorescence, staining, etc., that are available through traditional optical microscopy are also available with NSOM. These properties allow for a variety of chemical interactions (such as biomolecular binding, ion sensing, nearfield surface enhanced Raman spectroscopy, etc.) to be studied at high spatial resolutions. Such versatility and specificity can also allow for a variety of NM-bioconjugate properties to be studied. For example, interactions between AuNP-streptavidin (SA) bioconjugates and biotin-functionalized surfaces have been studied using this technique.¹⁷⁰ NSOM of the surface was performed with a 514 nm argon laser attached to the end of an optical bent-fiber probe and scattered light from the AuNP detected via an avalanche photodiode. AuNP-SA bioconjugates were clearly observed in biotin-modified regions of the surface confirming the specificity of the SA-biotin interaction. Other interactions between the biomolecules and NMs can also be studied including the ability to differentiate between specific versus nonspecific interactions. NSOM/QD-based dipole-emission fluorescence imaging has been used to study the nanostructure of antigens on *Yersinia pestis* vaccine particles comprising V immunogen fused with protein anchor (V-PA) loaded on a gram positive enhancer matrix (GEM).¹⁷¹ Here, Zeng and co-workers used a combination of biotin-labeled

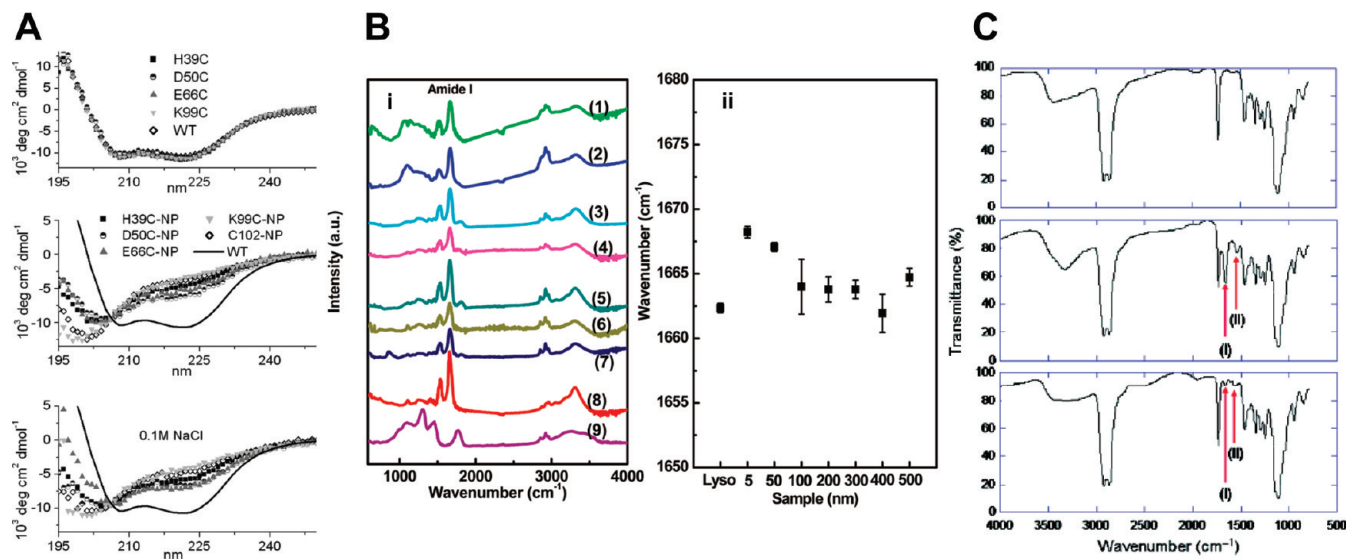


Figure 8. Spectroscopy: (A) CD spectra of unlabeled (top) and AuNP-labeled cytochrome c proteins (middle and bottom), with no salt (middle), with 0.1 M NaCl (bottom). Specific amino acids mutated to cysteine to allow subsequent NP labeling are indicated. Reprinted with permission from ref 59. Copyright 2009 PNAS. (B) (i) Infrared spectra of lysozyme attached to complex nanodiamonds (cNDs) of various sizes: (1) Lyso-5cND; (2) Lyso-50cND; (3) Lyso-100cND; (4) Lyso-200cND; (5) Lyso-300cND; (6) Lyso-400cND; (7) Lyso-500cND; (8) lysozyme; (9) 100cND. (ii) Amide I frequencies of the attached protein lysozyme as a function of cND size. Reprinted from ref 180. Copyright 2011 American Chemical Society. (C) FT-IR spectra of QDs with different surface ligands: (top) DHLA-PEG600; (middle) DHLA-PEG600/DHLA-PEG400-biotin (4:1 molar ratio); (bottom) DHLA-PEG600/DHLA-PEG400-COOH (19:1 molar ratio). (I) and (II) can be assigned as amide I and amide II bands, respectively. Reprinted from ref 213. Copyright 2007 American Chemical Society.

anti-c-Myc (which recognizes the c-Myc tag expressed on the V-PA fusion protein) and SA-conjugated QDs for immunostaining of the V-PA loaded GEM vaccine particles. They found that the V-PA tended to bind to the GEM surface in the form of nanoclusters, containing multiple (two or more) V-PA molecules, rather than single V-PA monomers, with \sim 3000 of these V-PA immunogen structures bound to a single GEM particle surface. Such high density of these immunogen structures is advantageous as the resulting V-PA-GEM vaccine particles are likely to elicit a robust immune response.

Spectroscopic Techniques. These techniques exploit the interaction of electromagnetic radiation with a sample material resulting in the wavelength dependent absorption, and in the case of fluorescence re-emission, of radiation, see also Table 4. Typically, a wavelength dependent spectrum is produced with characteristic absorption/emission peaks inherent to the sample.¹⁷² Spectroscopic techniques can provide average bulk analysis of the NM-bioconjugate including information concerning the confirmation of successful NM-biomolecule conjugation, the conformational state of the biomolecule once attached to the NM, the average NM-to-biomolecule ratio, and the stability of the resulting NM-bioconjugate.

UV–Visible Absorbance. The intrinsic UV–visible absorbance properties of many NMs can be used to monitor pertinent properties, such as concentration, size, and aggregation state. QDs for example have size-sensitive absorption profiles,¹⁷³ and optical absorption has been used to characterize composition, size, and purity of single-walled carbon NTs.¹⁷⁴ Metal NPs, in particular Au and silver, exhibit a strong absorption in the visible region known as the surface plasmon resonance (SPR) band (often shortened to the SP band). The SP band is dependent on a number of factors and is found to be sensitive to size, shape, composition (i.e., silver, Au, nanoshell structures), aggregation

state, and also refractive index changes within surface proximity.^{114,119,175,176} A number of researchers have looked at the effect of proteins binding to gold and silver NPs, finding small (\sim 5 nm) shifts in the UV–visible measured SP band as a result of protein binding and in some cases larger shifts due to subsequent aggregation.^{114,119,177,178} These changes alone can sometimes serve to confirm NM interactions or bioconjugation.

Both direct and in-direct analysis of UV–visible spectroscopy data can also provide information on the NM-bioconjugate. Direct characterization is possible when the biomolecule has a distinct UV–visible profile that remains discernible upon conjugation to the NM. Protein absorption bands at 280–290 nm and the soot bands (410 nm) of hemoproteins such as cytochrome c have been used to directly quantify the average amount of protein immobilized on a NM surface.^{4,179} Even if the NM displays a significant level of absorption, the presence of new peaks or increases in certain regions can confirm the presence of for example DNA (Abs \sim 260 nm). Proteins coeluting with NMs can also be viewed in gel electrophoresis using colorimetric stains, such as Coosamine Blue, which can then be quantified with appropriate instrumentation (such as a fiber optic spectrophotometer) to determine the average NM-to-biomolecule ratio. Alternatively, with the use of a more indirect method, the amount of protein present in solution before and after NM exposure can be quantified using either protein absorbance at 280–290 nm^{180–182} or a number of reactive colorimetric assays, including the Bradford reagent and bicinchoninic acid (BCA) assays,¹⁸³ as demonstrated for gold-coated magnetic particles modified with antibody fragments.¹⁸⁴ Many of these tests, although not specifically designed for NMs, can be applied to their analysis. However, as NMs have been demonstrated to interfere with certain chemical assays and tests, appropriate analysis of controls and the “naked” particles should be

undertaken prior to interpretation of the results. While allowing derivation of an average NM-to-biomolecule ratio, such analysis, however, does not give a NM-bioconjugate product distribution profile or information regarding biomolecular conformation once attached to the NM surface.

Circular Dichroism. Conventional circular dichroism (CD) measures the ability of optically active materials to differentially absorb circularly polarized light (usually UV) and is commonly applied to the conformational analysis of biomolecules such as proteins and nucleic acids.^{4,185} Far-UV (<250 nm) CD provides structural information concerning the proteins' secondary structure and has been successfully used to studying protein conformational changes that occur following both initial adsorption and later stable interactions with a variety of NM surfaces, including Au,^{59,114,179,186} silica,^{94,182} carbon NTs,¹⁸⁷ iron oxide,¹⁸⁸ and QDs.¹⁸⁹ Importantly, the observed conformational changes of proteins interacting specifically or nonspecifically with NM surfaces have been found to also depend on a number of other factors including pH,¹⁸⁶ surface density of the protein,¹⁸² additional ligands present on the NM surface, and temperature.⁴ Aubin-Tam used CD to monitor the global structure of cytochrome c as it was labeled with a 1.5 nm diameter AuNP at various mutational sites placed throughout its structure, see Figure 8A.⁵⁹ Losses in protein helicity were correlated with gross changes in structure, and these were further confirmed by modeling (see also below). A number of recent developments in CD technology offer some exciting prospects for extending this analysis.¹⁸⁵ For example, synchrotron radiation CD (SRCD) offers more detailed spectral information at wavelengths <190 nm due to its high light flux in this region, although the main disadvantage is limited availability. Vibrational CD (VCD) uses polarized light in the infrared (IR) region, looking predominately at variations in the amide I and amide II bands of proteins, although it does require replacement of H₂O with D₂O in solution-based measurements due to the strong absorption of water in this region.¹⁹⁰

Fluorescence Spectroscopy. This technique in both steady-state and time-resolved modes offers a powerful and sensitive technique for determining a number of the parameters associated with the immobilization of biomolecules to a NM surface including fluorophore local environment, biomolecule-NM coupling ratio, conformational state, and in some instances, intra-assembly molecular distances.¹⁹¹ Fluorescence techniques are of course limited to NM-bioconjugate components that have some form of either intrinsic or extrinsic fluorescence (or fluorescence quenching) capacity; however, given the variety of fluorescent NMs and the vast array of commercially available biomolecular-reactive fluorescent dyes, this should not be considered a limitation.^{191,192} Obviously if conjugation of a fluorophore to the NM is desired as part of the final application, then fluorescence is an excellent method to determine the average number of fluorophores per NM, as demonstrated for cellulose and viral NMs.^{37,89,193} This is especially useful when the NM and a dye have strong overlapping absorbance. A number of researchers have used the intrinsic fluorescence from tryptophan (Trp) residues, commonly found in protein sequences, to obtain information about local changes in tertiary structure upon NM binding.^{182,186,187,194} For example, Wu and co-workers looked at the interaction of β -lactoglobulin with silica NPs and found that the extent of protein unfolding, which produced an increase in the Trp fluorescence, was dependent on the number of proteins adsorbed to the NP surface.¹⁸² Lower

surface protein concentrations on the NP resulted in greater protein unfolding, presumably because the adsorbed protein had greater access to free NP surface with which to interact. Rather than relying on Trp emission, Reulen and co-workers used the intrinsic fluorescence of enhanced yellow fluorescent protein (eYFP) to monitor and confirm its conjugation to liposomal NMs.¹⁹⁵

Many biomolecules can be quite easily labeled with extrinsic fluorophores to aid in NM-bioconjugation characterization and optimization. For example, Hurst and co-workers used fluorescently labeled DNA to determine the effects of salt concentration, spacer composition, NM size, and sonication on the average DNA coverage per AuNP,¹⁹⁶ while Lockney et al. monitored fluorescently labeled peptide sequences binding to red clover necrotic mosaic virus.¹⁹⁷ Mittal and co-workers used biotin-avidin affinity to determine the average number of biotin-binding sites present on SA conjugated QDs, using a biotin-4-fluorescence (B4F) quenching assay.¹⁹⁸ B4F is a commercially available dye whose fluorescence is quenched upon binding to avidin proteins. While these methods provide information about the average biomolecular coverage on the NM surface, distribution information is again still lacking. In contrast, single-molecule studies combined with stepwise photobleaching are increasingly being used to obtain ratio distributions.^{145,146} Delpot and co-workers functionalized 250 nm silica NPs with an ATTO 647N labeled DNA 15-mer followed by immobilizing the NP-bioconjugates onto a cover glass for analysis with confocal microscopy.¹⁴⁶ After a NP was located in the confocal image, the 633 nm laser was focused on the NP and the fluorescently labeled DNA stochastically photobleached. Approximately 100 NPs were analyzed by looking at the number of energy levels in the stepwise decrease of the fluorescence intensity as a function of time for a particular NP. This was then correlated to a direct measure of the number of fluorescent DNA on the NP surface.

Flow cytometry is occasionally used to characterize biomolecules binding to NMs.^{199,200} Nakamura and co-workers looked at the binding of green fluorescent protein (GFP) and fluorescein-labeled DNA to epoxy-organosilica,¹⁹⁹ while the group of Zhong looked at poly(lactic-*co*-glycolic acid) (PLGA) NPs conjugated to fluorescein labeled Fab' fragments of anti-HER2 antibody via EDC/NHS coupling chemistry.²⁰⁰ In both cases, biomolecule binding resulted in the appearance of a fluorescence signal, confirming the interaction.

FRET is a specific fluorescence phenomenon that occurs between donor and acceptor molecules and is highly dependent on a number of factors, most important of which are the extent of donor/acceptor spectral overlap and the separation distance between the two. A number of extensive reviews concerning FRET can be found in the literature.^{191,201} The underlying process has been likened to a molecular ruler with separation sensitivities for donor/acceptor distances proportional to r^6 and which usually fall in the 1–10 nm range. Medintz and co-workers demonstrated the unique abilities of semiconductor QDs as donors in a variety of FRET formats²⁰² and have used the technique to establish the orientation of MBP immobilized to a QD (see Figure 9C)²⁰³ and to demonstrate that underlying bioconjugate chemistry can strongly influence the architecture of QD-DNA conjugates, see below.²⁰⁴ FRET has also been used to monitor the binding of fluorescently labeled proteins or peptides to the surface of QDs but is more commonly used as a signal transduction mechanism in functional biosensing assays.^{205,206} Morgner and co-workers used the FRET combination of

Table 5. Mass Spectroscopy and Thermal Techniques

technique/types	NM-bioconjugates analyzed	advantages	disadvantages	refs
mass spectroscopy electrospray ionization (ESI), inductively coupled plasma (ICP) and matrix assisted laser desorption ionization (MALDI)	viral NP-biotin, AuNP-hemoprotein, silver NP-hemoprotein, TiO ₂ NP-dopamine	1. characterization based on mass-to-charge ratio. 2. readily measures mass increase due to NM-biomolecule bioconjugation.	1. requires expensive equipment and expertise. 2. limited application to date for studying NM-bioconjugates.	119,215–218
thermal gravitational analysis (TGA)	magnetic NP-PEG, AuNP-dendrons, AuNP-paclitaxel (therapeutic drug), AuNP-PEG/cyclodextrin ligands	1. provides relative organic versus inorganic composition of the NM-biomolecule conjugate. 2. can provide relative amount of the biomolecule. 3. provides thermal stability of the NM-biomolecule conjugate.	1. inherently destructive to sample. 2. only provides bulk information about the amount of ligand.	158,219–221
calorimetry differential scanning calorimetry (DSC) and isothermal titration calorimetry (ITC)	polymer NP-proteins, lipid NP-insulin, polymer NP-paclitaxel, zinc NP-BSA, AuNP-CTAB ligands	1. provides bulk information about the NM-biomolecule conjugate, such as melting temperature, crystallization and glass transition information, decomposition and stability information.	1. only bulk sample information provided. 2. requires an appropriate reference. 3. somewhat limited application to date.	222–226
thermophoresis	QD-PEG	1. provides size and surface potential of the NM-biomolecule conjugate. 2. can provide effective diameter.	1. sample requires optical properties to aid in visualization. 2. somewhat limited application to date.	34,227,228

luminescent terbium complexes (donor) and QDs (acceptor) to infer information about the shape and size of QD biotin-SA bioconjugates.²⁰⁷ A number of researchers have used AuNP acceptors as quenchers in energy transfer studies with fluorescent donor species, and the resulting putative surface energy transfer (SET) process observed has been shown to have a nontraditional r^4 distance dependency, allowing in essence the ability to extend the reach of the molecular ruler.^{208,209} For example, Sen and co-workers recently used Trp-Au SET to probe conformational changes that occur when BSA binds AuNPs.²⁰⁹ Results demonstrated a significant quenching of the BSA Trp (donor) fluorescence upon protein binding to the AuNP (acceptor) surface under different pH conditions. With the use of SET theory, distances between the donor and acceptor were estimated and related to the conformation of the BSA adsorbed to the AuNP surface.

Infrared Spectroscopy. This technique measures the absorption of IR radiation by a sample resulting from the vibrational stretching and bending modes within the molecule.^{172,210} In particular, Fourier Transform (FT)-IR is frequently used to demonstrate NM bioconjugation through the appearance of characteristic spectral bands. For example, FT-IR has been used to characterize lysozyme binding to diamond NPs,¹⁸⁰ albumin and peptides to AuNPs,^{186,211} hemoproteins adsorbed on Au and silver NPs,^{119,179} SA bound to silicon NPs,⁶⁷ β -lactoglobulin adsorbed on silica NPs,¹⁸² along with papain and chitosan bound to magnetic NPs.²¹² In the case of globular proteins, careful interpretation of the stretching and bending vibrations in the amide regions, particularly the amide I band ($1\,600$ – $1\,700\text{ cm}^{-1}$), can provide secondary structural information and hence the conformational state of the bound protein, see Figure 8B.^{180,182,186} Perevedentseva and co-workers investigated lysozyme adsorbing to different sized nanodiamonds and found that a slight blue shift in the amide I band was observed only for the 5–50 nm nanodiamonds and not for the larger particles.¹⁸⁰ The observed blue shift suggested the adsorbed lysozyme was undergoing a conformational change from a predominately α -helix structure to that of a β -sheet or random coil conformation which significantly reduced the enzyme activity. Susumu et al. used FT-IR to verify the presence of particular combinations of different ligands that had been cap exchanged onto the QD surface. They were able to determine that the QDs were displaying the desired biotin moiety along with other molecules by unique amide band contribution, see Figure 8C.²¹³

Nuclear Magnetic Resonance and Magnetic Resonance Imaging. Nuclear magnetic resonance (NMR) spectroscopy and magnetic resonance imaging (MRI) measure the intrinsic magnetic moment of certain nuclei, typically either hydrogen (^1H) or carbon (^{13}C), in the presence of an applied magnetic field.¹⁷² NMR spectroscopy can provide physical, chemical, structural, or environmental information about the species under study as well as information concerning the dynamic interactions of many biological molecules, including proteins and nucleic acids. NMR spectroscopy has been used to characterize human carbonic anhydrase (HCA) I conformational changes that occur upon interaction with silica,²¹⁴ alkyne ligation of dendrimers,⁴⁵ thiol-modified peptides binding AuNPs,²¹¹ as well as QD cap exchange reactions.⁶⁴ For example, Pons and co-workers were able to confirm the highly efficient cap exchange of trioctylphosphine/trioctylphosphine oxide (TOP/TOPO) ligands with DHLA ligands on QDs, through the appearance or loss of ^1H NMR peaks characteristic of the ligands.⁶⁴ They were also able to

confirm the nature of the interaction of the DHLA with the QD surface through the disappearance of two disparate thiol resonances characteristic of the reduced dithiol moiety, which is present in the DHLA-only control spectrum but not in the DHLA-capped QDs. This confirmed dithiol affinity and binding of DHLA for the QD surface. Lundqvist and co-workers performed detailed NMR analysis of the human carbonic anhydrase I enzyme before and after interaction with ~9 nm silica NPs.²¹⁴ They found that desorption of the protein from the NP surface resulted in proteins regaining near-native conformations, with the most profound differences between native and desorbed enzyme being found in the β -strands typically located in the center of the protein structure.

Mass Spectroscopy. Mass spectroscopy (MS) comprises the family of technologies that analyze samples based on their mass-to-charge ratio, Table 5. MS has been used to characterize NM-bioconjugates and has found particular utility in the analysis of protein based NMs, such as viral NPs, where mass increases in the viral coat proteins due to the addition of biotin or fluorophore species were successfully monitored using matrix-assisted laser desorption/ionization (MALDI)-time-of-flight (TOF)-MS.^{215,216} Through the measured mass increase, the average stoichiometry of the additional species added per virus NP could readily be determined. MALDI-TOF MS has also been used to qualitatively demonstrate hemoprotein binding to gold and silver NPs.¹¹⁹ Inductively coupled plasma (ICP) MS was used to determine TiO₂ NP binding to a dopamine ligand that was subsequently used to complex a gadolinium MRI contrast agent.²¹⁷ Interestingly, QDs and a variety of other NP materials have recently found utility as matrixes for surface-assisted laser desorption/ionization-MS (SALDI-MS) analysis of proteins and peptides.²¹⁸ Their unique properties allow for sample enrichment and help overcome high background signals in the low-mass regions. Overall, the application of MS techniques has been fairly limited for NM-bioconjugate characterization, and this may in part be due to the relative cost of the instrumentation, the required level of expertise needed to run analyses, the destruction of the sample during analysis, and the fact that the requisite instruments are usually configured for other analyses, with the latter also used quite frequently in an automated fashion.

Thermal Techniques. As highlighted in Table 5, these techniques can aid in determining the amount of conjugated biomolecule as well as both the NM and the biomolecule's thermal stability. As with many of the techniques described above, sample preparation is the key to successful analysis, where sample weight, composition, and running conditions (heating rates, etc.) can all influence the quality of the data obtained. Typically, for techniques like differential scanning calorimetry (DSC), 1–10 mg of sample is required for analysis (depending on composition); however, newer instruments can now use low microgram amounts. Thermal gravimetric analysis (TGA) is a method that utilizes a high-precision balance to determine changes in the weight of a bulk sample relative to changes in temperature and has been used to characterize a variety of NMs functionalized with biomolecules, including AuNPs functionalized with dendrons, hydroxyapatite grown on Au-fibrin NMs, as well as the amount of paclitaxel bound to a NM drug delivery system.^{158,219,220} Further calculations can reveal information about the average number of ligands attached per NM and the extent of surface functionalization. For example, TGA has been utilized in conjunction with NMR to approximate the number of PEG and cyclodextrin ligands on AuNPs.²²¹

DSC and isothermal titration calorimetry (ITC) are other thermally based methods that can provide bulk information about the NM-bioconjugate. DSC is used to study various material transitions including melting, crystallization, glass transition, and decomposition. Subsequent analysis can indicate the state of the NM-bioconjugate including the stability of the biomolecule and structural information on both the NP and biomolecule including underlying crystallinity and how the different components are interacting with each other. Researchers have also used DSC to help elucidate the structure and stability of surface coatings of NM-bioconjugates as well as the state of their therapeutic payloads. For example, DSC has been used to probe the stability of lipid bilayers when the bilayers were embedded with silver NPs.²²² Sant and co-workers also used DSC to help elucidate the location of PEG ligands in a poly-(D,L)-lactide NP.²²³ DSC recrystallization analysis has further been applied to determine the stability of solid, lipid NP-insulin complexes²²⁴ and how the individual components of a Zn-NP BSA NM-bioconjugate system interacted with each other.²²⁵ ITC provides further potential to investigate the stoichiometry, affinity, and enthalpy of the NM-biomolecule interaction, as demonstrated by Cedervall and co-workers studying the corona layering mechanism for various polymeric NMs (based on the copolymer *N*-iso-propylacrylamide-*co*-*N*-*tert*-butylacrylamide) and binding proteins (either human plasma or single proteins such as HSA or fibrinogen). Overall, as an analytical technique this still remains vastly underutilized.²²⁶

Thermophoresis or thermodiffusion involves localized heating of a sample and monitoring the resulting motion of the particles due to the temperature gradient.^{34,227,228} Sperling and co-workers compared thermophoresis to various other analytical techniques for their ability to determine the size of various PEG-functionalized QDs.³⁴ They found that the reported particle diameters were highly dependent upon the particular technique applied along with the underlying physical principles and assumptions used to determine particle size. In particular, they found that while thermophoresis and FCS both measure diffusion of dispersed particles to determine effective diameters, the values obtained from both techniques differed significantly. The difference was speculated to be due to the difference in particle concentrations used. FCS is a single particle technique requiring dilute particle concentrations, while thermophoresis is an ensemble method requiring higher particle concentrations to ensure robust signals. Thermophoresis and its use for the analysis of colloidal suspensions have been recently reviewed in ref 228.

■ MODELING

Although not typically considered a "classical" characterization technique, modeling can provide important insight about the structure and function of NM-bioconjugates. The overall goal of any modeling effort is to gain insight into the properties or behavior of a system that cannot be directly observed. For molecular modeling of NM-bioconjugates, available techniques again borrow heavily from protein, peptide, and small molecule research and are usually based on either theoretical principles alone, include empirical or semiempirical parameters, or alternatively extend to dynamic simulation.

Methods that are derived directly from theoretical principles and do not include any (semi)empirical parameters are *ab initio* methods. The simplest uses classical mechanics to describe the physical basis behind the models and is referred to as molecular

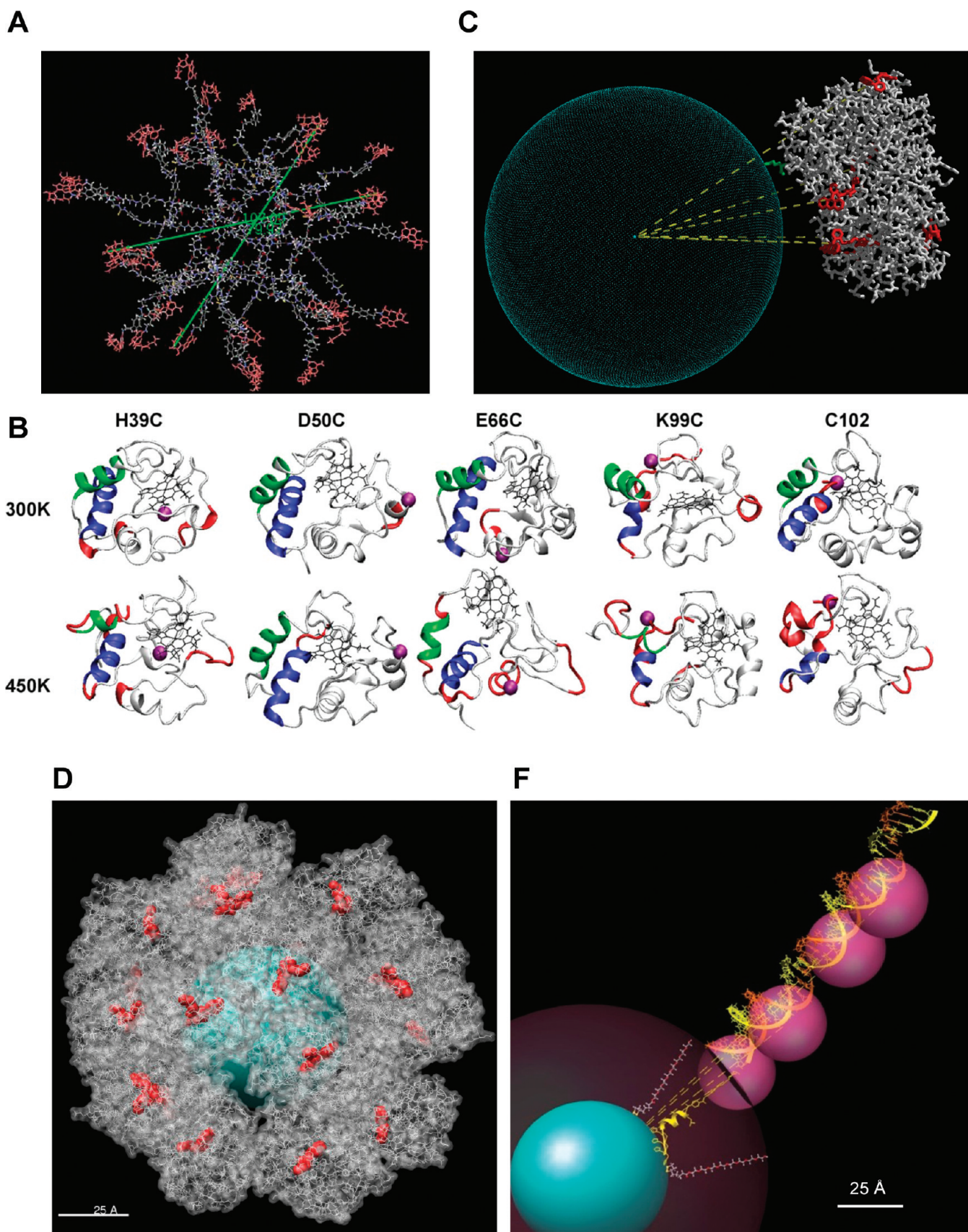


Figure 9. Continued

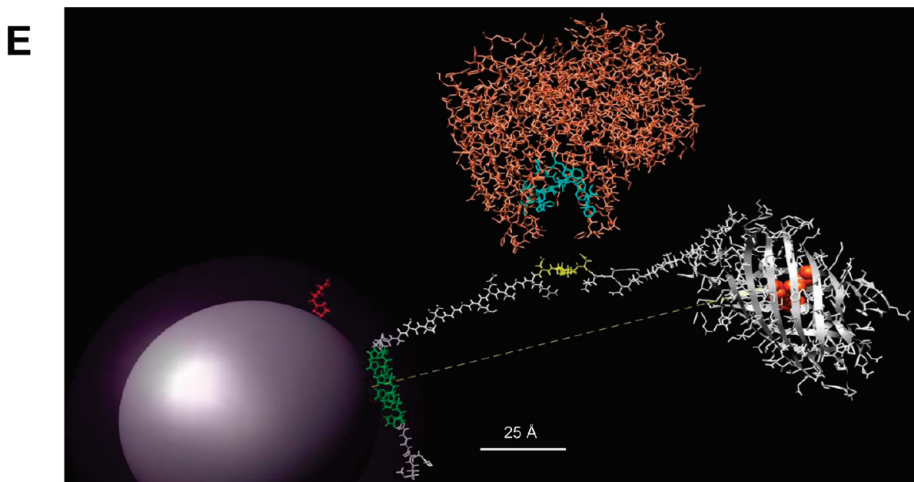


Figure 9. Modeling NM-bioconjugates: (A) energy-minimized structure of a G3-PAMAM dendrimer conjugate having 32 covalently bound DITC-APEC groups. Terminal adenosine moieties are highlighted in pink for visibility. Overall diameters, $\sim 80\text{--}110\text{ \AA}$, were measured (shown in green) between ligands approximately diagonal to each other through the central core. Reprinted with permission from ref 235. Copyright 2009 Springer Science + Business Media. (B) Snapshots of yeast cytochrome c protein structure at the end of an 8 ns MD simulations at 300 and 450 K. Green/blue, N-/C-terminal helices; red, loss of 50%-helicity from the wild-type structure; purple sphere, the AuNP attachment site. Reprinted with permission from ref 59. Copyright 2009 National Academy of Sciences. (C) Side view showing the refined MBP-QD orientational structure with all six dye-label structures shown in red. Distances from the QD center to each dye position on the protein were determined using FRET, and the refined distances are shown with the yellow dashed lines. With the use of this refinement, $\sim 45\text{ \AA}$ is estimated as the radius of the spheroid (or the distance from the nearest MBP atom of Lys-370, green, in the PDB 1LLS structure to the QD center). This residue in green is the location of the terminal (His)₅ sequence which attaches the protein to the QD. Reprinted with permission from ref 203. Copyright 2004 National Academy of Sciences. (D) Model used to estimate the maximum load of mCherry onto a QD surface. For clarity, the fluorescent groups in each protein molecule are shown in red as space-filling models. On the basis of the putative protein contact area and QD surface area, a maximum loading of 18 mCherry per QD was estimated. In the image shown, 11 of the 18 protein molecules can be seen. (E) Model of self-assembled QD-mCherry conjugate used to monitor caspase-3 activity. The QD is shown as a sphere with a radius of 30 \AA with its DHLA coating as a translucent shell 11.7 \AA thick. A single molecule of DHLA is shown in red. The QD His₆-binding region of the linker peptide is shown in green; the caspase-3 cleavage site is shown in yellow. The β -barrel conformation of mCherry is depicted as a ribbon while the chromophore is shown as an orange space-filling model within the barrel. Caspase-3 is shown in a stick representation with its active site highlighted in cyan. From this image it is clear that many conformations within the linker peptide with either an extended or bent structure could result in the cleavage site being accessible. (F) Modeling of QD-DNA structures showing a (His)₆-peptide-DNA construct bound to 530 nm QDs. The QD is shown as the central blue sphere with a radius of 28 \AA . The DHLA-PEG ligand is indicated by the crimson halo with an estimated extension of 30 \AA . DHLA-PEG ligands in energy-minimized conformation are shown within the crimson sphere. The His₆-portion of the peptide is shown with a yellow ribbon joining it to the DNA. Individual DNA strands within the dsDNA structure are shown in orange and yellow. The rotational extension of the dye molecules are shown by the magenta spheres. An orientation with the DNA and sequential dye placement sites extending linearly outward from the QD surface is shown.

mechanics. Here, molecular systems are treated as individual atoms and typically describe them as a point charge with an associated mass while the interactions between atoms are described by springlike processes; this simplification allows larger assemblies to be considered. *Ab initio* methods in which electrons are explicitly considered are termed quantum-chemical methods and solve the molecular Schrödinger equation. More complex versions considering electronic structure fall under Hartree–Fock schemes. Semiempirical methods (sometimes based on the Hartree–Fock scheme) that make approximations and which incorporate parameters from empirical data are important for modeling large systems where other approaches are too computationally intensive. Energy minimization is often incorporated as lower energy states typically represent more stable configurations and are more likely to represent a large fraction of the molecules in a given environment. Energy minimization is also useful for obtaining a static picture for comparison to similar systems.

In molecular dynamics simulations, the system configuration is computed over time resulting in atomic trajectories in both space and time. This provides information on dynamic processes and can include temperature effects. In cases where only a limited

number of changes to a template structure need to be made, a technique sometimes referred to as “comparative modeling” can be effective. This method, for example, builds a three-dimensional model for a protein of unknown structure (target) based on one or more related, known protein structures (templates).^{229–232} Comparative modeling relies on the similarity of target with known template structures. This approach to protein structure prediction in particular is possible because a small change in sequence usually results in only a small change in its 3D structure. It is further facilitated by the fact that protein folds defining the 3D structure are more highly conserved within a protein family than their primary sequence.²³³

Important points to consider about NM-bioconjugate modeling approaches are that even the most complex and computationally intensive modeling methods do not produce an exact solution; they are all approximations. Further as complexity increases, more accurate predictions of molecular properties may be obtained but with a greater computational cost. We briefly survey some examples where different modeling strategies have potential or already have proven useful to NM-bioconjugate characterization.

Predictive Modeling. Although not fully extended to NM-bioconjugates *per se*, predictive modeling can clearly aid in the characterization and processing of these materials. This was demonstrated by Saunders and co-workers who applied a total interaction energy model to accurately predict the size/size distribution of size-selectively precipitated NPs.²³⁴ Selective precipitation of QDs, AuNPs, and other NMs is an important part of their initial processing following synthesis into a more defined sample. In this example, NP precipitation was modeled as a simple two-body interaction which accounted for all relevant interaction energies. The model had only one manipulated variable, which is the amount of antisolvent added to the system. The model was then successfully applied to the size-selective fractionation of dodecanethiol-stabilized AuNPs dispersed in hexane by CO₂ addition/precipitation. An initial sample displaying a 4.56 ± 1.24 nm size (100%) was selectively precipitated into 3 fractions consisting of 6.01 ± 1.39 nm size (3.6%), 6.20 ± 1.18 nm size (9.2%), and 4.33 ± 1.12 nm size (87.2%). Importantly, these size values are all within 5% of those originally predicted. This model obviously depends heavily on *a priori* knowledge of the physical properties of the NP ligand in relation to the solvent conditions. An important future test will be whether this model can be extended to a NP dispersed in buffer and stabilized by a biological such as PEG, DNA, or a peptide. This may allow for selection of specifically functionalized materials away from reactants or for sorting by ratios of displayed molecules.

Structural Estimates. Modeling is also useful for estimating somewhat “simpler” parameters such as NP size. Jacobson’s group relied on energy minimization to estimate the overall size of a functionalized generation 3 polyamidoamine (G3 PAMAM) dendrimer.²³⁵ In this example, the author’s functionalized the dendrimer with a chemically reactive nucleoside A_{2A} adenosine receptor agonist (DITC-APEC) as part of an effort to develop multivalent ligands with enhanced pharmacological effects as compared to monomeric drugs. The drug was fully incorporated and displayed on the 32 ligand sites at the dendrimers periphery with the chemistry utilized. The energy-minimized structure of the construct, generated using HyperChem 7.5.2 Amber force field, suggested an overall diameter of ~80–110 Å with an ellipsoid shape, see Figure 9A. The author’s were gratified to find that the DITC-APEC-loaded dendrimers extended the diameter over previously reported derivatives by ~20 Å. It was envisioned that this could potentially increase the conformational flexibility of the appended ligands to achieve optimal geometry for efficient binding to the adenosine receptor.

Protein Binding to Nanoparticles. A variety of modeling strategies have recently helped either elucidate or improve how different proteins attach to NP materials. Mukherjee and co-workers used statistical optimization to improve how alkaline α-amylase immobilized onto supermagnetic iron oxide NPs.²³⁶ Plackett–Burman factorial design and response surface methodology were utilized to screen the influence of different parameters such as pH, NP concentration, and the response of the enzyme to the binding process. The authors utilized coefficients of determination and analysis of variance to validate the proposed model along with confirming the size of the NPs by X-ray diffraction and applying FT-IR spectroscopy to confirm enzyme-NP immobilization. Importantly, they found a significant 26-fold increase in specific activity, improved thermal and storage stability, along with extended reusability of α-amylase after optimized binding to the NPs in comparison to that of free

enzyme. These results have important commercial implications as this enzyme has significant industrial applications in the paper and brewing industries.

Hamad-Schifferli’s group elegantly demonstrated how to combine recombinant protein engineering, modeling, and other types of NP-protein characterization in order to understand how attachment site along with NP material and ligand all influenced subsequent protein structure.⁵⁹ As a model system, they utilized cytochrome c derived from *Saccharomyces cerevisiae* (Baker’s yeast) as its structure has been well studied both experimentally and computationally. They subsequently conjugated 1.5 nm diameter negatively charged AuNPs to the protein by introducing site-specific cysteine-thiols into its structure; this allowed for formation of thiol-Au surface linkages. The protein surface sites utilized for cysteine insertion and hence NP-modification were widely varied around the cytochrome c structure and also included areas around the N- and C-termini. Effects of protein-NP labeling were probed with circular dichroism which provided information on changes in the proteins helicity. They found that protein unfolding was the most severe when the NP labeled near the termini as this affected its core folding motif. NP attachment in the vicinity of charged residues also induced greater structural damage and was ascribed to salt-dependent electrostatic interactions with the negatively charged NP-surface ligand. Molecular dynamic simulations were then used to both confirm and elucidate the local and global structural perturbations in each mutant protein upon NP binding, see Figure 9B. Overall this study highlights and again reinforces the importance of judiciously choosing a labeling site as part of designing an efficient NP-protein bioconjugate.

Modeling of Quantum Dot Bioassemblies. Modeling of larger assemblies, such as proteins and small molecules assembled on the surface of a semiconductor QD, requires an amalgamation of various approaches; it can more easily be considered a hybrid derivative of comparative modeling. To the greatest extent possible crystallographic structures are used; obtained from either the Protein Data Bank (PDB, www.rcsb.org/pdb) or the Cambridge Structural Database (CSD, www.ccdc.cam.ac.uk). For small molecules or molecular linkers whose structure is not known, the tools in software such as Chem3D are used to produce energy minimized models. These structures are combined with experimental results to build models of the molecular assemblies. Conformational parameters of these assemblies are adjusted to produce a final model which is in close agreement with the experimental results. Uncertainties in the model can be teased out by examining alternate conformations that place functional groups in extremes of closest approach and furthest separation.

The ability to model these assemblies and have confidence in the results is derived from initial work with MBP. These were based on the crystal structure of MBP along with FRET measurements made from constructs that placed a fluorescent group in several discrete known locations around the protein surface to study the QD-MBP complex.²⁰³ Each of these differentially labeled MBPs was then separately assembled on the QD allowing monitoring of each FRET interaction. The separation between the QD and fluorophore was estimated from FRET measurements and the data set of pairwise separations used to orient the protein on the QD surface. From a separate set of experiments, it was known that a polyhistidine terminus (His₅) on the MBP was required for binding to the QD surface. The validity of orientation was confirmed by the proximity of this

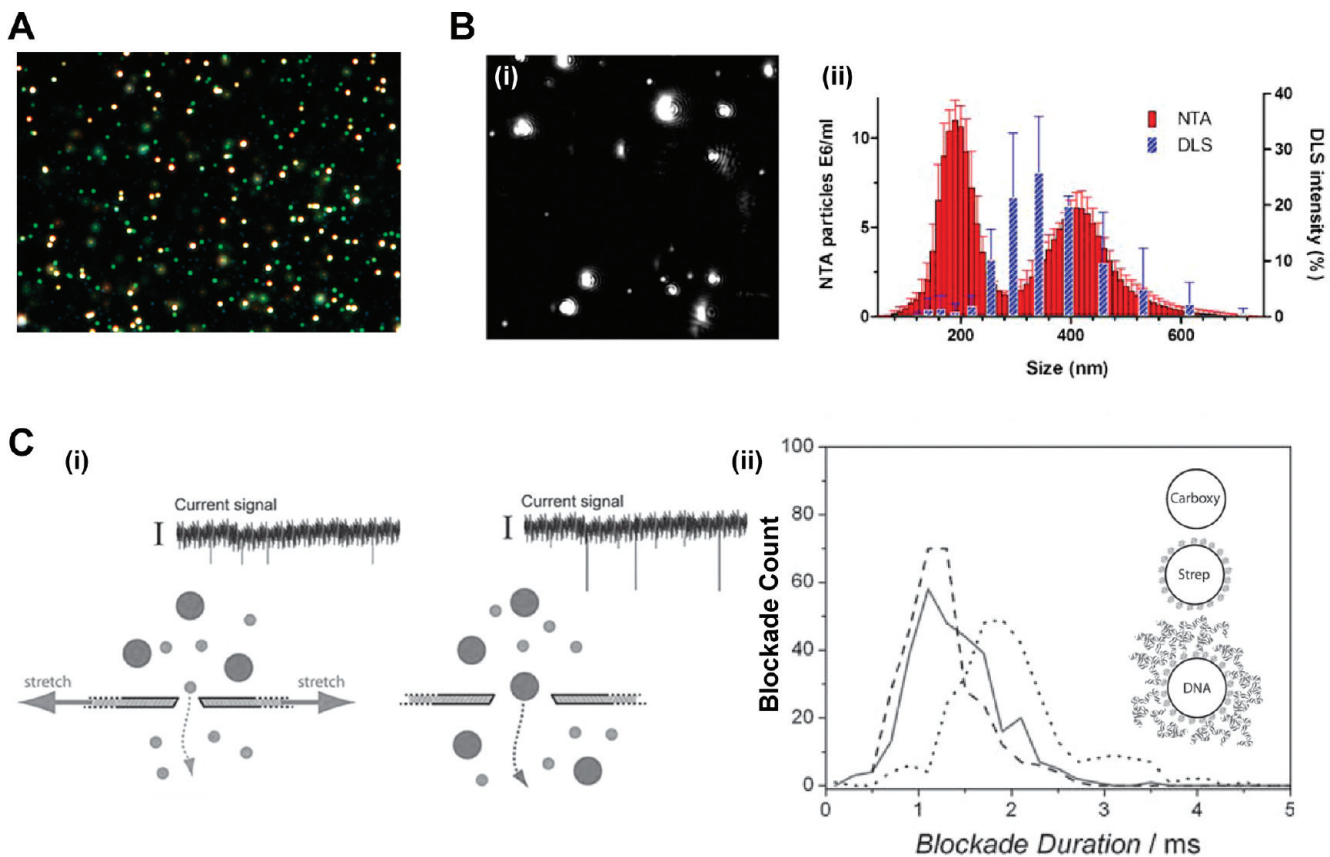


Figure 10. Emerging technologies. (A) Image of soluble 60 nm AuNPs captured with the CytoViva using 100 \times magnification. (B) Nanoparticle tracking analysis (NTA) by Nanosight: (i) NTA video frame and (ii) size distribution measurements taken with NTA and DLS of a mixture of 200 and 400 nm polystyrene beads (2:1 number ratio). Reprinted with permission from ref 100. Copyright 2010 Springer Science+Business Media. (C) Scanning ion occlusion sensing by Izon: (i) schematic of the tunable membrane pore that is key to the technology, (ii) detection of various NM-bioconjugates. Blockade duration collected for carboxylated silica particles (light gray, solid curves), SA particles (gray, dashed curves), and λ -DNA particles (black, dotted curves) at background current levels of 90 nA. Reprinted with permission from ref 250. Copyright 2010 Wiley-VCH Verlag GmbH & Co. KGaA.

sequence to the QD surface, see Figure 9C. Thus other model structures could be constructed using the His_n tail to orient further proteins on QDs. Interestingly, this work reflects MBP's strong role in prototyping NM-bioconjugates. This, in turn, originates from the excellent understanding of MBP's structure and function, similar to cytochrome c, above the ability to site specifically modify and label it as desired, along with it retaining functionality once tethered to a surface or NM.²³⁷ Once a putative orientation of a protein on the QD surface is produced, other parameters can be measured from a model. It is also important to consider when using FRET data that ensemble FRET measurements often reflect an average which can be dominated by those structures having the donor and acceptor in closest proximity.

One example of applying this type of modeling to QD biocomplexes was aimed at determining how many proteins and peptides can maximally load onto these nanocrystal materials as a function of size.²³⁸ This understanding has important implications for the design of high avidity and efficient sensing QD constructs. For this, models were constructed for QDs displaying surfaces of the solubilizing dihydrolipoic acid (DHLA) ligand, a His_n-appended <20 residue peptide, myoglobin, mCherry, and MBP. The contact area or surface footprint of

each molecule on the QD was estimated from these models and used to calculate maximum loadings (Figure 9D). In general, excellent agreement was obtained between the estimated and experimentally determined protein loadings (i.e., MBP 10/12, mCherry 18/20, myoglobin 24/30 for each model/experimental result, respectively). The latter values were determined from gel separation of increasing ratios of each dye-labeled molecule exposed to the QDs. It was only in the case of the His_n-peptide that any large difference between experimental and estimated values was found. Modeling suggested that a maximum of 140 peptides could assemble on the QDs and yet experiments consistently yielded average values of only 50 \pm 10. The difference was ascribed to the presence occupied by the DHLA ligand on the QD surface; there were no more available His_n binding sites on the surface. Modeling had estimated that from 157 to 268 DHLA molecules could attach to the QD surface depending upon conformation and, interestingly, other data had approximated a value of 140. Overall, this modeling suggested that the limiting factor for protein assembly on QDs was primarily their own size and how they sterically hinder each other when assembling on the QD surface, and in contrast, for the far-smaller His_n-peptide it was the number of available binding sites on the QD.²³⁸

In a slightly different configuration, a model of a fluorescent protein self-assembled to a QD surface by an extended His_n-linker was constructed to assess whether an enzymatic cleavage site could be inserted into the linker portion while still allowing a target protease access to this sequence.²³⁹ The point of this exercise was to evaluate whether this QD-sensor designed to monitor the activity of the apoptotic effector enzyme caspase-3 would not be sterically hindered *in silico* before recombinantly modifying the His_n-linker. With the use of the three-dimensional coordinates for mCherry (PDB entry 2H5Q), the enzyme caspase-3 (PDB entry 3EDQ) and a model peptide with strong homology to the linker, a construct was assembled, see Figure 9E. The model peptide which served as a linker between the QD and mCherry was subsequently energy minimized and assembled using the structure building tools available in Chimera. A large subsequence of this linker peptide had been frequently used in the production and purification of a number of recombinant proteins, and a search of the PDB found this same sequence at the N-terminus of many recombinant proteins which had been crystallized. Critically, no coordinates were available for this portion implying that this sequence does not have a well-defined 3D structure but is rather present in a random-coil conformation (i.e., many conformations of this peptide are possible). As a starting point for model building of this linking peptide, constraints were applied to produce an extended conformation allowing estimation of the maximum separation between the QD and the mCherry fluorophore when assembled to the nanocrystal surface. Torsion angles were then adjusted so that the His₆ region was in contact with the QD surface while the rest of the peptide was extended away from this surface. Torsion angles of the DEVD cleavage sequence region were also adjusted to match those of a tetrapeptide inhibitor bound to the active site of caspase-3. Overall, the model strongly suggested accessibility to the cleavage site and following the subsequent protein engineering, a FRET-based sensing ability was indeed experimentally confirmed.

In a last example, FRET was utilized in combination with modeling to investigate how attachment chemistry can affect subsequent QD-DNA conjugate conformation.²⁰⁴ Figure 9F shows a structural model of one of the three constructs used in the study, a (His)₆-peptide-modified DNA self-assembled onto a 530 nm PEGylated QD. The 40 basepair DNA “backbone” sequence was designed to be hybridized with a series of four complementary sequences which allow placement of the acceptor dye at a series of increasing 10 base pair increments spaced further away from the QD donor. In order to estimate QD acceptor distances, the “scope” of the acceptor dye on its linker was considered in the modeling and is depicted in the figure as a magenta sphere centered on the attachment point with a radius of 14.6 Å. With adjustment of the tilt of the DNA molecule relative to the QD surface, a good correlation could be obtained between measured QD-acceptor distances and those calculated from the model. This same strategy was applied to assemblies using SA rather than a peptide to attach DNA to a QD. In that case, the experimental data in conjunction with the modeling strongly suggested that the derived FRET distances were an average of all possible acceptor positions and reflected the heterogeneous nature of how the SA was originally attached to the QD.²⁰⁴

■ EMERGING TECHNOLOGIES AND INSTRUMENTATION

As the field of bionanotechnology continues to mature, new techniques and the requisite instrumentation to measure unique aspects of NP-bioconjugates in particular have emerged. It is expected that these instruments and their capabilities will continue to rapidly evolve over time. Some notable techniques and/or the instrumentation used to perform them are reviewed below.

CytoViva with Hyperspectral Imaging. As mentioned in the Microscopy section, recent advances in optical microscopy have allowed for sub-100 nm resolution with certain types of optical microscopy systems. One such system, produced by CytoViva, uses a proprietary darkfield-based optical illumination technology that provides improved contrast and signal-to-noise ratio over traditional optical systems, resulting in sub-100 nm resolution, see Figure 10A. Such resolution can allow tracking of NM-bioconjugates in cells.²⁴⁰ When used in conjunction with the dual mode fluorescence module, the user can simultaneously image both the fluorescent and nonfluorescent portions of the sample, without the need to switch excitation sources and emission filters and acquire separate images that are later merged. With the addition of a second piece of technology produced by the company, the Hyperspectral Imaging System, researchers can not only track the NM-bioconjugates in cells but by utilizing the spectral library capabilities of the instrument are able to positively identify the NM in the cell as well as determine if the NM and biomolecule are still associated. The hyperspectral imager comprises a concentric imaging spectrophotometer capable of providing spectral analysis of the sample from 400 to 1000 nm. Typically the user creates a spectral library of NMs of interest and, through a customized software analysis program, spectral outputs from an unknown sample are compared to the library to aid in identification.

Xigo Acorn Area Analysis. Surface area is an important parameter for monitoring NP reactivity. Traditionally, the surface area of NMs is determined through the method developed by Brunauer, Emmet, and Teller (BET). This involves the adsorption of gas molecules on the surface of the particles and therefore requires that the NM sample be dried. Since drying many NM systems can cause aggregation, the surface area determined by BET may be lower than the true value of the NMs in solution. The Acorn Area, developed by Xigo Nanotools, uses NMR to measure the wetted surface area of NMs in solution. The technique is based on the principle that liquid in contact with a particle surface has a markedly shorter NMR relaxation time relative to the bulk liquid. This technique allows the possibility of determining surface area pre- and post-NP-bioconjugation in relevant biological solutions.²⁴¹

Resonance Frequency Devices (Quartz Crystal Microbalance and Suspended Cantilevers). The use of quartz crystal microbalances (QCM) for NM-bioconjugate analysis has become more prevalent in the literature recently, especially as commercial sources for these instruments are expanded. QCM monitors mass per unit area via the frequency of a quartz crystal resonator.²⁴² The high sensitivity of this method allows QCM to be used for investigating the interactions between biomolecules and NMs. For example, QCM allowed monitoring of an antibody-labeled CoFe₂O₄/SiO₂ NP-functionalized surface during an immuno-assay for carcinoembryonic antigen.²⁴³ Binding kinetics and the binding specificity of antihuman vascular cell adhesion molecule 1 (VCAM-1) functionalized iron oxide NPs

to VCAM-1 modified QCM substrates have also been determined and found to be dependent on the number of antibodies immobilized on the NP surface.²⁴⁴ Burg and co-workers demonstrated the use of a suspended cantilever comprising a microfluidic channel to weigh single AuNPs that changed the resonance frequency of the cantilever as they transited through the device.²⁴⁵ The technique provided femtogram resolution, and the resulting histogram of particle mass could be converted to size when the density of the material was known.

Single Particle Tracking (Nanosight and Others). Nanoparticle tracking analysis (NTA), marketed by laser-illuminated optical microscopy to track the light scattering from NMs that are 10 (30)–1000 nm (lower limit depending on reference) and moving under Brownian motion. Unlike traditional scattering methods such as DLS, each scattering source (i.e., NM) is tracked separately, allowing for individual measurements of particle size (determined using the Stokes–Einstein equation) during population analysis. In addition, particle concentration (which can be quite challenging to determine when a strong absorbance or molar extinction coefficient values are not available) may be measured with this technique. NTA has also been used to cross-validate DLS data as well as to determine the relative thickness of protein opsonized layers on AuNPs.²⁴⁶ A critical evaluation of NTA versus DLS using polystyrene beads was recently performed by Filipe and co-workers.¹⁰⁰ The study highlighted the main advantage of NTA as its unbiased peak resolution of polydisperse samples which was not possible with DLS, see Figure 10B. The NTA technique currently is more complex to set up and time-consuming to perform but is not influenced by small amounts of large particles (such as dust) which is problematic for DLS. The NanoSight system is also capable of working under fluorescence mode, and the company recently announced the release of ζ potential analysis capabilities.

Single particle tracking based on fluorescence measurements rather than scattering has also been demonstrated for sizing fluorescent NMs. Obviously, the particles in this case must be intrinsically fluorescent or extrinsically labeled, and the size limitation is governed by the optical resolution of the microscope system. Nevertheless, Braeckmans was able to measure 100/200 nm fluorescent nanospheres and liposomes in undiluted whole blood, something not typically possible with DLS or scattering-based NTA.²⁴⁷ This study used a custom built laser widefield epi-fluorescence microscope system in combination with custom image analysis software to track individual NPs. Subsequent size calculations were determined using a maximum entropy deconvolution method (MEM).

Coulter Counter Devices. Coulter counter devices detect changes in electrical conductance of a small aperture as a sample is passed through, referred to as the Coulter principle. Its use for characterization of NMs has until recently been limited by the ability to generate nanosized apertures sensitive to NMs. However, Fraikin and co-workers recently achieved this using microfluidics.²⁴⁸ The microfluidic channel comprised a primary nanoconstriction (for particle detection) and fluidic restriction region (which provides a balancing electrical resistance) with a sensing electrode located between the two. Particles entering the nanoconstriction via fluid pressure altered the ionic electrical current that, in turn, changed the electrical potential of the fluid in contact with the sensing electrode. Following calibration with known dilutions of different sized polystyrene NPs, the size and concentration of T7 bacteriophage was successfully characterized. In addition analysis of polydisperse samples containing 51,

75, and 117 nm diameter polystyrene beads demonstrated the excellent resolving capabilities of the technology.

Scanning ion occlusion sensing (SIOS) makes use of the Coulter principle, and IZON of Christchurch, New Zealand, have developed a relatively low-cost commercial instrument based on a tunable nanopore technology that uses SIOS to characterize nanoscale particles, see Figure 10C.^{249,250} Electrophoretic force is applied to the nanoscale particle solution causing the particles to pass through a single, tunable membrane pore, which results in a measurable blockade of the ionic current. Users can vary numerous parameters (pressure, electrophoretic force, and nanopore size) to determine the particle concentration, electrophoretic mobility, particle size (single particle resolution), and aggregation state/kinetics using a wide range of pH and electrolyte buffers. The system relies on calibration with appropriate nanoscale standards, has a lower limit of detection of 40 nm, and as with DLS, typically assumes a spherical geometry. That said, the IZON SIOS system has already shown the ability to resolve polydisperse solutions and can distinguish between DNA modified polystyrene particles and unmodified particles.^{249,250}

■ IMPACT OF NM CHARACTERIZATION ON NANOTOXICOLOGY

Concerns over potential health issues arising from exposure to nanocontaining materials has resulted in the emerging field of nanotoxicology, which inherently relies on a large characterization component.^{24,27,251} Related to this, a number of groups are already characterizing the NM-protein corona that results when NMs are introduced into biological environments.^{226,252} The relative importance of characterization to this field was reinforced by a recent editorial in the ACS journal *Chemical Research in Toxicology*, which recommended that nanotoxicology submissions include five important features in the manuscript, one of which was “The chemical and physical characteristics of the particles should be well-defined”.²⁵³ There are already in place numerous toxicity tests available to the researcher, and the applicability of these tests to the study of NMs and NM-bioconjugates are the subject of a number of excellent reviews.^{254–256}

There are several key points to consider about this field in relation to characterization. First, results from toxicity tests may not be meaningful unless the model system under study is well understood; i.e., both the NM and the biological must be well characterized. Second, results may not have validity if the materials used are contaminated with synthetic byproduct or other biologicals picked up during processing or storage. Confounding this, recent studies have demonstrated that certain sterilization techniques can be detrimental to the NM, affecting the stability and physicochemical properties, hence adequate characterization may also be essential at this intermediary step as well.^{257,258} Samples may also need to be characterized both before and after bioconjugation. A further complication arises as quite often NPs and other NMs will interfere with the working or interpretation of an *in vitro* toxicity assay.

Recently, Grainger and Castner highlighted the importance of surface contamination and how this can influence toxicity studies.¹² In particular, microbial endotoxins are often overlooked, but given their known ability to trigger inflammatory responses, characterization of NMs for the presence of endotoxin is especially important when targeting *in vivo* applications.²⁵⁹ Endotoxins are lipopolysaccharides found in the outer

membrane of Gram-negative bacteria that are ubiquitous in the environment.²⁵⁹ Contamination of NMs with endotoxins during manufacture and handling prior to final application is a real concern for researchers trying to assess their toxic effects, especially the inflammatory responses generated by their NMs.^{260,261} This was eloquently highlighted by Vallhov who demonstrated that endotoxin contamination of their AuNPs was actually the cause of the cytokine production observed in exposed immature dendritic cells.²⁶⁰ Upon reduction of the endotoxin to below "acceptable" limits, the AuNPs generated only minor up-regulation of cytokines. Traditional limulus amebocyte lysate (LAL) assays can be used to determine endotoxin levels; however, as demonstrated recently by Dobrovolskaia, NPs can interfere with these assays and so carefully selected controls should be included in the studies.^{256,262} Clearly, to be valid and broadly accepted, NM-bioconjugate toxicity assessments will require carefully designed assays that are scrupulously implemented and appropriately interpreted. Rigorous characterization of the NM-bioconjugate will be the starting point and foundation for such studies.

SUMMARY

For NM-bioconjugates to make the leap from an exciting area of research to reliable products, biomedical materials, and enabling technologies, a number of important questions must be addressed in which adequate purification and characterization will play a fundamental role. These questions include (1) reproducibility of NM-bioconjugate production, (2) activity of biomolecules attached to NM, (3) long-term stability of the NM-bioconjugate, (4) level of control over chemical and biomodification of the NM surface, (5) purity and potential for contamination of NM-bioconjugate, (6) along with stability through sterilization and depyrogenation. As highlighted here, a number of current and emerging analytical techniques are available to address these concerns to some extent.

Purification of the NM-bioconjugate is a key issue, and most of the techniques discussed here are at least capable of minimally removing unbound biomolecules, although some (e.g., HPLC and electrophoresis) have the intrinsic resolving capability to distinguish different populations of NM-bioconjugates. Unfortunately many of these techniques are still only utilized in small scale purification and emphasis on scaling up the process will be required to transition into the commercial sector. Purification would likewise benefit from improved bioconjugation chemistries that limit NM aggregation and reduce the polydispersity of the products. Purity concerns also arise from the *in situ* and *ex situ* environment in which the NM-bioconjugate is synthesized or used, especially given the endotoxin contamination discussed above. These concerns can be somewhat alleviated through careful control of the reagents and environment used during the synthesis, purification, storage, and subsequent use of the final NM-bioconjugate.

Final characterization of the purified NM-bioconjugates will ultimately require a combination of techniques to fully address all physicochemical characteristics, in addition to the bioconjugation metrics of interest. Not all the techniques discussed here are applicable to all types of NMs or their subsequent NM-bioconjugates. In addition many of the techniques require some form of sample manipulation prior to analysis, such as drying or suspension in ultrapure liquids. This manipulation may result in non-physiological states and perturbed NM-bioconjugate properties,

and hence interpretation should be erred on the side of caution. The key issues to these technologies being incorporated into routine laboratory practice by researchers will be relative cost, ease of use, resolution capabilities, sample preparation requirements, ease of data interpretation, versatility, bulk versus single particle analysis, etc. Some techniques such as chromatography and electrophoresis are already routinely used, are relatively cheap, are widely available, can readily confirm biomolecular attachment to the NM surface, and provide either/both purification and characterization information on the bioconjugate product. DLS and ζ potential characterization of NM-bioconjugates are again relatively cheap and simple to perform providing hydrodynamic radius, aggregation state, and surface potential information. SEM and TEM are mainly used for characterization of the NM itself (not so much the biomolecule to date) and are relatively more expensive, equipment and maintenance-wise; however, they characterize the size and shape of the NM on an individual particle basis. AFM in contrast can divulge a range of information about both the NM and the biomolecule again on a single-particle basis. Many of the spectroscopic techniques (which range in cost) provide bulk analysis of the NM-bioconjugate, with NMR and IR spectroscopy demonstrating the ability to characterize biomolecular conformational states on the NM. High-resolution microscopy and a number of the emerging technologies discussed provide exciting alternatives for characterizing particular metrics of interest. It is anticipated that many of the requisite instruments for these analyses will soon start to populate core facilities and national user centers. Another area that will benefit NM-characterization as a whole is the development and availability of standard reference materials for calibrating many of the techniques described here. The U.S. National Institute of Standards and Technology (NIST, www.nist.gov/nanotechnology-portal.cfm) continues to develop a variety of NM standard reference materials, including gold, silica, polystyrene NPs, and single-walled carbon nanotubes (SWCNTs), that provide both size and shape variation. However, given the drive to develop multifunctional NMs, standards that reflect ligand chemistry and/or bioconjugation will also soon need to be developed.

Both the techniques and instruments described here are continually evolving to meet the demands of nanoscale characterization and while bulk analysis will continue to play a significant role, additional focus is now being placed on techniques capable of purifying and characterizing individual NP-bioconjugate populations. Such single particle techniques do, however, need to ensure enough discrete samples are analyzed to obtain statistically relevant data that reflect the underlying properties of the ensemble sample population. Importantly, judicious interpretation of all results in the correct context should be another primary concern. For example, spectroscopy may suggest a particular NM-biological interaction in solution; however, this may not necessarily translate into a strong binding event that can survive chromatographic separation to yield a viable bioconjugate for a given application. In summary, many of the technologies described here will play a pivotal role in the development of novel and increasingly complex NP-bioconjugates and these, in turn, will be indispensable to the future of bionanotechnology.

AUTHOR INFORMATION

Corresponding Author

*E-mail: Kim.Sapsford@fda.hhs.gov (K.E.S.); Igor.Medintz@nrl.navy.mil (I.L.M.).

BIOGRAPHIES

Dr. Kim E. Sapsford studied chemistry at the University of East Anglia (UEA, Norwich, U.K.) and in 2001 received her Ph.D. in analytical chemistry developing optical biosensors. In 2001, she moved to the Center for Bio/Molecular Science and Engineering at the U.S. Naval Research Laboratory, where she worked (until 2007) on creating fluorescent-based biosensors using the Array Biosensor technology developed by Dr. Frances Ligler. Currently she is a Staff Fellow at the U.S. Food and Drug Administration (FDA) in the Office of Science and Engineering Laboratories (OSEL), Division of Biology (DB). Her work involves assessing biotechnology concerning public health safety in particular future biosensing technologies.

Dr. Katherine M. Tyner studied chemistry at Carleton College (Minnesota). In 2004, she received her Ph.D. in materials chemistry from Cornell University (New York) under Professor Emmanuel Giannelis where she studied nanoparticles for gene and drug delivery applications. In 2004, she moved to the University of Michigan, where she completed a postdoctoral fellowship in nanoparticle sensors under the direction of Professors Raoul Kopelman and Martin Philbert. Currently, Katherine is a chemist at the U.S. Food and Drug Administration (FDA) in the Center for Drug Evaluation and Research (CDER), Office of Testing and Research (OTR), Division of Drug Safety Research (DDSR). Her work involves assessing nanotechnology as it relates to the safety and efficacy of therapeutics.

Dr. Benita J. Dair is a research materials engineer with a B.S. from Cornell and Ph.D. from MIT. She has experience in materials characterization, including electron microscopy, light scattering, and imaging techniques. She joined FDA's Center for Devices and Radiological Health (CDRH), Office of Science and Engineering laboratories (OSEL) in 2004 and currently serves as the Deputy Director of the Division of Chemistry and Materials Science (DCMS). Her interests in nanomaterials are characterization of their properties and assessing their interactions with biological systems to ensure safety and efficacy of medical devices incorporating nanotechnologies.

Dr. Jeffrey R. Deschamps has worked at the Naval Research Laboratory since 1985 on structural studies, structure function relationships of biological molecules, and biosensors. Prior to his position at NRL, Dr. Deschamps was a postdoctoral fellow in the Department of Pharmacology at the Johns Hopkins School of Medicine. He is the author of over 190 publications in diverse areas such as energetic materials, peptide and protein structure, and biosensor design and evaluation. He was elected to the American Crystallographic Association's "Data, Standards, and Computing Committee". His training and experience in biochemistry, structural studies, and molecular modeling puts him in a unique position to model inorganic-biomolecular composites. His recent work with others at NRL on nanomaterials has resulted in widely cited new methods for characterizing these complex assemblies.

Dr. Igor L. Medintz studied chemistry and forensic science at John Jay College of Criminal Justice, City University of New York (CUNY). In 1998, he received his Ph.D. in molecular biology under Prof. Corinne Michels of Queens College (also CUNY). He carried out postdoctoral research under Prof. Richard A. Mathies (UC Berkeley) on the development of FRET-based genetic assays using microfabricated devices. Since 2004 he has been employed as a Research Biologist at the Center for Bio/Molecular Science and Engineering of the U.S. Naval Research Laboratory in Washington D.C. His current research involves developing chemistries to controllably bridge the

biological–nanomaterial interface with a focus on the design of new biosensing hybrids that incorporate energy transfer.

ACKNOWLEDGMENT

I.L.M. and K.E.S thank F. Ligler at NRL for initial encouragement. I.L.M. acknowledges the NRL-NSI, ONR, DTRA, and DARPA for financial support. K.E.S would like to thank Dr. T. Umbreit and Dr. B. Casey (FDA) for their helpful comments during the preparation of this manuscript. This paper reflects the current thinking and experience of the authors. No official support or endorsement by the U.S. Food and Drug Administration is intended or should be inferred.

REFERENCES

- (1) Rana, S.; Yeh, Y.-C.; Rotello, V. M. *Curr. Opin. Chem. Biol.* **2010**, *14*, 828–834.
- (2) Willner, I.; Willner, B. *Nano Lett.* **2010**, *10*, 3805–3815.
- (3) Agasti, S. S.; Rana, S.; Park, M.-H.; Kim, C. K.; You, C.-C.; Rotello, V. M. *Adv. Drug Delivery Rev.* **2010**, *62*, 316–328.
- (4) Aubin-Tam, M.-E.; Hamad-Schifferli, K. *Biomed. Mater.* **2008**, *3*, 034001.
- (5) Thanh, N. T. K.; Green, L. A. W. *Nano Today* **2010**, *5*, 213–230.
- (6) Kim, B. Y. S.; Rutka, J. T.; Chan, W. C. W. N. *Engl. J. Med.* **2010**, *363*, 2434–2443.
- (7) EU Scientific Committee on Emerging and Newly Identified Health Risks (SCENIHR). *Report: Scientific basis for the definition of the term "Nanomaterial"*, 2010, http://ec.europa.eu/health/scientific_committees/emerging/docs/scenihro030.pdf (accessed March 24, 2011).
- (8) Rosenthal, S. J.; Chang, J. C.; Kovtun, O.; McBride, J. R.; Tomlinson, I. D. *Chem. Biol.* **2011**, *18*, 10–24.
- (9) Figuerola, A.; Di Corato, R.; Manna, L.; Pellegrino, T. *Pharmacol. Res.* **2010**, *62*, 126–143.
- (10) Schnorr, J. M.; Swager, T. M. *Chem. Mater.* **2011**, *23*, 646–657.
- (11) Subbiah, R.; Veerapandian, M.; Yun, K. S. *Curr. Med. Chem.* **2010**, *17*, 4559–4577.
- (12) Grainger, D. W.; Castner, D. G. *Adv. Mater.* **2008**, *20*, 867–877.
- (13) Gil, P. R.; Oberdorster, G.; Elder, A.; Puntes, V. Z.; Parak, W. L. *ACS Nano* **2010**, *10*, 5527–5531.
- (14) Baer, D. R.; Gaspar, D. J.; Nachimuthu, P.; Techane, S. D.; Casner, D. G. *Anal. Bioanal. Chem.* **2010**, *396*, 983–1002.
- (15) Gaumet, M.; Vargas, A.; Gurny, R.; Delie, F. *Eur. J. Pharm. Biopharm.* **2008**, *69*, 1–9.
- (16) Kranz, C.; Eaton, D. C.; Mizaikoff, B. *Anal. Bioanal. Chem.* **2011**, *399*, 2309–2311.
- (17) Medintz, I. L.; Uyeda, H. T.; Goldman, E. R.; Mattoussi, H. *Nat. Mater.* **2005**, *4*, 435–446.
- (18) Hermanson, G. T. *Bioconjugate Techniques*, 2nd ed.; Academic Press: Amsterdam, The Netherlands, 2008.
- (19) Perrier, T.; Saulnier, P.; Benoît, J.-P. *Chem.—Eur. J.* **2010**, *16*, 11516–11529.
- (20) Nguyen, D. T.; Kim, D.-J.; Kim, K.-S. *Micron* **2011**, *42*, 207–227.
- (21) Praig, V. G.; Hall, E. A. H. *Anal. Chim. Acta* **2003**, *500*, 323–336.
- (22) Mullen, D. G.; Desai, A. M.; Waddell, J. N.; Cheng, X.; Kelly, C. V.; McNerny, D. Q.; Majoros, I. J.; Baker, J. R.; Sander, L. M.; Orr, B. G.; Banaszak Holl, M. M. *Bioconjugate Chem.* **2008**, *19*, 1748–1752.
- (23) Powers, K. W.; Palazuelos, M.; Moudgil, B. M.; Roberts, S. M. *Nanotoxicology* **2007**, *1*, 42–51.
- (24) Warheit, D. B. *Nano Lett.* **2010**, *10*, 4777–4782.
- (25) Murray, R. *Anal. Chem.* **2009**, *81*, 1723.
- (26) Boverhof, D. R.; David, R. M. *Anal. Bioanal. Chem.* **2010**, *396*, 953–961.
- (27) Krug, H. F.; Wick, P. *Angew. Chem., Int. Ed.* **2011**, *50*, 2–21.
- (28) McNeil, S. E. *Characterization of Nanoparticles Intended for Drug Delivery; Methods in Molecular Biology*, Vol. 697; Humana Press: Totowa, NJ, 2010.

- (29) Tyner, K. M.; Nakissa, S. *Methods Mol. Biol.* **2011**, *697*, 17–31.
- (30) Dair, B. J.; Tyner, K.; Sapsford, K. E. *Methods in Bioengineering: Nanoscale Bioengineering and Nanomedicine*; Artech House: Boston, MA, 2009.
- (31) Liu, H.; Webster, T. J. *Biomaterials* **2007**, *28*, 354–369.
- (32) Hassellöv, M.; Readman, J. W.; Ranville, J. F.; Tiede, K. *Ecotoxicology* **2008**, *17*, 344–361.
- (33) Li, L.; Mu, Q.; Zhang, B.; Yan, B. *Analyst* **2010**, *135*, 1519–1530.
- (34) Sperling, R. A.; Liedl, T.; Duhr, S.; Kudera, S.; Zanella, M.; Lin, C.-A. J.; Chang, W. H.; Braun, D.; Parak, W. J. *J. Phys. Chem. C* **2007**, *111*, 11552–11559.
- (35) Medley, C. D.; Bamrungsap, S.; Tan, W.; Smith, J. E. *Anal. Chem.* **2011**, *83*, 727–734.
- (36) Goldman, E. R.; Anderson, G. P.; Tran, P. T.; Matoussi, H.; Charles, P. T.; Mauro, J. M. *Anal. Chem.* **2002**, *74*, 841–847.
- (37) Sapsford, K. E.; Soto, C. M.; Blum, A. S.; Chatterji, A.; Lin, T.; Johnson, J. E.; Ligler, F. S.; Ratna, B. R. *Biosen. Bioelectron.* **2006**, *21*, 1668–1673.
- (38) Hoshino, Y.; Haberaecker, W. W., III; Kodama, T.; Zeng, Z.; Okahata, Y.; Shea, K. J. *J. Am. Chem. Soc.* **2010**, *132*, 13648–13650.
- (39) Trapiella-Alfonso, L.; Montoro Bustos, A. R.; Encinar, J. R.; Costa-Fernández, J. M.; Pereiro, R.; Sanz-Medel, A. *Nanoscale* **2011**, *3*, 954–957.
- (40) Eck, W.; Craig, G.; Sigdel, A.; Ritter, G.; Old, L. L.; Tang, L.; Brennan, M. F.; Allen, P. J.; Mason, M. D. *ACS Nano* **2008**, *2*, 2263–2772.
- (41) Otto, D. P.; Vosloo, B. C. M.; de Villiers, M. M. *J. Liq. Chromatogr. Relat. Technol.* **2007**, *30*, 2489–2514.
- (42) Claridge, S. A.; Liang, H. W.; Basu, S. R.; Fréchet, J. M. J.; Alivisatos, A. P. *Nano Lett.* **2008**, *8*, 1202–1206.
- (43) Wu, C.; Schneider, T.; Zeigler, M.; Yu, J.; Schiro, P. G.; Burnham, D. R.; McNeill, J. D.; Chiu, D. T. *J. Am. Chem. Soc.* **2010**, *132*, 15410–15417.
- (44) Kuo, Y.-C.; Wang, Q.; Ruengruglikit, C.; Yu, H.; Huang, Q. *J. Phys. Chem. C* **2008**, *112*, 4818–4824.
- (45) Mullen, D. G.; Fang, M.; Desai, A.; Baker, J. R.; Orr, B. G.; Banaszak Holl, M. M. *ACS Nano* **2010**, *4*, 657–670.
- (46) Stavis, S. M.; Geist, J.; Gaitan, M. *Lab Chip* **2010**, *10*, 2618–2621.
- (47) Schimpf, M.; Caldwell, K. D.; Giddings, J. C., Eds. *Field Flow Fractionation Handbook*; Wiley Interscience: New York, 2000.
- (48) Williams, S. K. R.; Runyon, J. R.; Ashames, A. A. *Anal. Chem.* **2011**, *83*, 634–642.
- (49) Roda, B.; Zattoni, A.; Reschiglian, P.; Moon, M. H.; Mirasoli, M.; Michelini, E.; Roda, A. *Anal. Chim. Acta* **2009**, *635*, 132–143.
- (50) Cho, T. J.; Hackley, V. A. *Anal. Bioanal. Chem.* **2010**, *398*, 2003–2018.
- (51) Ma, P. L.; Buschmann, M. D.; Winnik, F. M. *Biomacromolecules* **2010**, *11*, 549–554.
- (52) Surugau, N.; Urban, P. L. *J. Sep. Sci.* **2009**, *32*, 1889–1906.
- (53) Pyell, U. *Electrophoresis* **2010**, *31*, 814–831.
- (54) Pellegrino, T.; Sperling, R. A.; Alivisatoes, A. P.; Parak, W. J. *J. Biomed. Biotechnol.* **2007**, 26796.
- (55) Park, S.; Hamad-Schifferli, K. *J. Phys. Chem. C* **2008**, *112*, 7611–7616.
- (56) Berti, L.; D'Agostino, P. S.; Boeneman, K.; Medintz, I. L. *Nano Res.* **2009**, *2*, 121–129.
- (57) Doane, T. L.; Cheng, Y.; Babar, A.; Hill, R. J.; Burda, C. *J. Am. Chem. Soc.* **2010**, *132*, 15624–15631.
- (58) Bücking, W.; Massadeh, S.; Merkulov, A.; Xu, S.; Nann, T. *Anal. Bioanal. Chem.* **2010**, *396*, 1087–1094.
- (59) Aubin-Tam, M.-E.; Hwang, W.; Hamad-Schifferli, K. *Proc. Natl. Acad. Sci. U.S.A.* **2009**, *106*, 4095–4100.
- (60) Quarta, A.; Ragusa, A.; Deka, S.; Tortiglione, C.; Tino, A.; Cingolani, R.; Pellegrino, T. *Langmuir* **2009**, *25*, 12614–12622.
- (61) Steinmetz, N. F.; Mertens, M. E.; Taurog, R. E.; Johnson, J. E.; Commandeur, U.; Fischer, R.; Manchester, M. *Nano Lett.* **2010**, *10*, 305–312.
- (62) Mastroianni, A. J.; Claridge, S. A.; Alivisatos, A. P. *J. Am. Chem. Soc.* **2009**, *131*, 8455–8459.
- (63) Dif, A.; Boulmedais, F.; Pinot, M.; Roullier, V.; Baudy-Floc'h, M.; Coquelle, F. M.; Clarke, S.; Neveu, P.; Vignaux, F.; Le Borgne, R.; Dahan, M.; Gueroui, Z.; Marchi-Artzner, V. *J. Am. Chem. Soc.* **2009**, *131*, 14738–14746.
- (64) Pons, T.; Uyeda, H. T.; Medintz, I. L.; Mattoucci, H. *J. Phys. Chem. B* **2006**, *110*, 20308–20316.
- (65) Liu, H. Y.; Gao, X. *Bioconjugate Chem.* **2011**, *22*, 510–517.
- (66) Huang, X.; Weng, J.; Sang, F.; Song, X.; Cao, C.; Ren, J. *J. Chromatogr. A* **2006**, *1113*, 251–254.
- (67) Choi, J.; Wang, N. S.; Reipa, V. *Bioconjugate Chem.* **2008**, *19*, 680–685.
- (68) Helle, A.; Hirsjärvi, S.; Peltonen, L.; Hirvonen, J.; Wiedmer, S. K. *J. Chromatogr. A* **2008**, *1178*, 248–255.
- (69) Suntornsuks, L. *Anal. Bioanal. Chem.* **2010**, *398*, 29–52.
- (70) Gahnon, Z.; Senapati, S.; Chang, H.-C. *Electrophoresis* **2010**, *31*, 666–671.
- (71) Vahey, M. D.; Voldman, J. *Anal. Chem.* **2009**, *81*, 2446–2455.
- (72) Ribeiro, C.; Arizaga, G. G. C.; Wyypych, F.; Sierakowski, M.-R. *Int. J. Pharm.* **2009**, *367*, 204–210.
- (73) Liu, Y.; Franzen, S. *Bioconjugate Chem.* **2008**, *19*, 1009–1016.
- (74) Saini, V.; Martyshkin, D. V.; Mirov, S. B.; Perez, A.; Perkins, G.; Ellismann, M. H.; Towner, V. D.; Wu, H.; Pereboeva, L.; Borovjagin, A.; Curiel, D. T.; Everts, M. *Small* **2008**, *2*, 262–269.
- (75) Bonaccorso, F.; Hasan, T.; Tan, P. H.; Sciascia, C.; Privitera, G.; Di Marco, G.; Guicciardi, P. G.; Ferrari, A. C. *J. Phys. Chem. C* **2010**, *114*, 17267–17285.
- (76) Jamison, J. A.; Krueger, K. M.; Yavuz, C. T.; Mayo, J. T.; LeCrone, D.; Redden, J. J.; Colvin, V. L. *ACS Nano* **2008**, *2*, 311–319.
- (77) Jamison, J. A.; Krueger, K. M.; Mayo, J. T.; Yavuz, C. T.; Redden, J. J.; Colvin, V. L. *Nanotechnology* **2009**, *20*, 355702.
- (78) Planken, K. L.; Cölfen, H. *Nanoscale* **2010**, *2*, 1849–1869.
- (79) Tiwari, D. K.; Tanaka, S.-I.; Inouye, Y.; Yashizawa, K.; Watanabe, T. M.; Jin, T. *Sensors* **2009**, *9*, 9332–9354.
- (80) Vannoy, C. H.; Xu, J.; Leblanc, R. M. *J. Phys. Chem. C* **2010**, *114*, 766–773.
- (81) Trefry, J. C.; Monahan, J. L.; Weaver, K. M.; Meyerhoefer, A. J.; Markopolous, M. M.; Arnold, Z. S.; Wooley, D. P.; Pavel, I. E. *J. Am. Chem. Soc.* **2010**, *132*, 10970–10972.
- (82) Gaborski, T. R.; Snyder, J. L.; Striemer, C. C.; Fang, D. Z.; Hoffman, M.; Fauchet, P. M.; McGrath, J. L. *ACS Nano* **2010**, *4*, 6973–6981.
- (83) Zhang, Y.; Schnoes, A. M.; Clapp, A. R. *Appl. Mater. Interfaces* **2010**, *2*, 3384–3395.
- (84) Scherer, C.; Noskov, S.; Utech, S.; Bantz, C.; Mueller, W.; Krohne, K.; Maskos. *J. Nanosci. Nanotechnol.* **2010**, *10*, 6834–6839.
- (85) Rameshwar, T.; Samal, S.; Lee, S.; Kim, S.; Chi, J.; Kim, I. S. *J. Nanosci. Nanotechnol.* **2006**, *6*, 2461–2467.
- (86) Schmidt, B.; Loeschner, K.; Hadrup, N.; Mortensen, A.; Sloth, J. J.; Koch, C. B.; Larsen, E. H. *Anal. Chem.* **2011**, *83*, 2461–2468.
- (87) Contado, C.; Dalpiaz, A.; Leo, E.; Zborowski, M.; Williams, P. S. *J. Chromatogr. A* **2007**, *1157*, 321–335.
- (88) Contado, C.; Argazzi, R. J. *J. Chromatogr. A* **2009**, *1216*, 9088–9098.
- (89) Park, S.; Sinha, N.; Hamad-Schifferli, K. *Langmuir* **2010**, *26*, 13071–13075.
- (90) Robertson, K. L.; Soto, C. M.; Archer, M. J.; Odoemene, O.; Liu, J. L. *Bioconjugate Chem.* **2011**, *22*, 595–604.
- (91) Langer, K.; Anhorn, M. G.; Steinhauser, I.; Dreis, S.; Celebi, D.; Schrickel, N.; Faust, S.; Vogel, V. *Int. J. Pharm.* **2008**, *347*, 109–117.
- (92) Calabretta, M.; Jamison, J. A.; Falkner, J. C.; Liu, Y.; Yuhas, B. D.; Mathews, K. S.; Colvin, V. L. *Nano Lett.* **2005**, *5*, 963–967.
- (93) Lees, E. M.; Gunzburg, M. J.; Nguyen, T. L.; Howlett, G. J.; Rothacker, J.; Nice, E. C.; Clayton, A. H. A.; Mulvaney, P. *Nano Lett.* **2008**, *8*, 2883–2890.
- (94) Lundqvist, M.; Sethson, I.; Jonsson, B.-H. *Langmuir* **2004**, *20*, 10639–10647.

- (95) Falabella, J. B.; Cho, T. J.; Ripple, D. C.; Hackley, V. A.; Tarlov, M. J. *Langmuir* **2010**, *26*, 12740–12747.
- (96) Pease, L. F., III; Feldblyum, J. I.; DePaoli Lacaerda, S. H.; Liu, Y.; Hight Walker, A. R.; Anumolu, R.; Yim, P. B.; Clarke, M. L.; Kang, H. G.; Hwang, J. *ACS Nano* **2010**, *4*, 6982–6988.
- (97) Takahashi, K.; Kato, H.; Saito, T.; Matsuyama, S.; Kinugasa, S. *Part. Part. Syst. Charact.* **2008**, *25*, 31–38.
- (98) Jans, H.; Liu, X.; Austin, L.; Maes, G.; Huo, Q. *Anal. Chem.* **2009**, *81*, 9425–9432.
- (99) Murdock, R. C.; Stole-Braydich, L.; Schrand, A. M.; Schlager, J. J.; Hussain, S. M. *Toxicol. Sci.* **2008**, *101*, 239–253.
- (100) Filipe, V.; Hawe, A.; Jiskoot, W. *Pharm. Res.* **2010**, *27*, 796–810.
- (101) Khlebtsov, N. G.; Bogatyrev, V. A.; Khlebtsov, B. N.; Dykman, L. A.; Englebienne, P. *Colloid J.* **2003**, *65*, 622–635.
- (102) Xing, Y.; So, M. K.; Koh, A. L.; Sinclair, R.; Rao, J. *Biochem. Biophys. Res. Commun.* **2008**, *372*, 388–394.
- (103) Ipe, B. I.; Shukla, A.; Lu, H.; Zou, B.; Rehage, H.; Niemeyer, C. M. *Chem. Phys. Chem.* **2006**, *7*, 1112–1118.
- (104) Wu, B.; Chen, Y.; Müller, J. D. *Biophys. J.* **2008**, *94*, 2800–2808.
- (105) Müller, C. B.; Loman, A.; Richtering, W.; Enderlein, J. *J. Phys. Chem. B* **2008**, *112*, 8236–8240.
- (106) Roy, S.; Dixit, C. K.; Woolley, R.; MacCraith, B. D.; O'Kennedy, R.; McDonagh, C. *Langmuir* **2010**, *26*, 18125–18134.
- (107) Rusu, L.; Gambhir, A.; McLaughlin, S.; Rädler, J. *Biophys. J.* **2004**, *87*, 1044–1053.
- (108) Ray, K.; Zhang, J.; Lakowicz, J. R. *Anal. Chem.* **2008**, *80*, 7313–7318.
- (109) Tang, L.; Dong, C.; Ren, J. *Talanta* **2010**, *81*, 1560–1567.
- (110) Ruan, Q.; Tetin, S. Y. *Anal. Biochem.* **2008**, *374*, 182–195.
- (111) Pons, T.; Medintz, I. L.; Wang, X.; English, D. S.; Mattooussi, H. *J. Am. Chem. Soc.* **2006**, *128*, 15324–15331.
- (112) Qiu, X.; Tang, L. C.; Dong, C. Q.; Ren, J. *C. Chin. Chem. Lett.* **2010**, *21*, 1227–1230.
- (113) Bergman, L.; Rosenholm, J.; Öst, A.-B.; Duchanoy, A.; Kankaanpää, P.; Heino, J.; Lindén, M. *J. Nanomater.* **2008**, *2008*, 712514.
- (114) Gomes, I.; Santos, N. C.; Oliveira, M. A.; Quintas, A.; Eaton, P.; Pereira, E.; Franco, R. *J. Phys. Chem. C* **2008**, *112*, 16340–16347.
- (115) Liu, Z.; Li, X.; Tabakman, S. M.; Jiang, K.; Fan, S.; Dai, H. *J. Am. Chem. Soc.* **2008**, *130*, 13540–13541.
- (116) Yang, Q.; Shuai, L.; Zhou, J.; Lu, F.; Pan, X. *J. Phys. Chem. B* **2008**, *112*, 12934–12939.
- (117) Mannelli, I.; Marco, M.-P. *Anal. Bioanal. Chem.* **2010**, *398*, 2451–2469.
- (118) Kneipp, J.; Kneipp, H.; Wittig, B.; Kneipp, K. *Nanomed. Nanotechnol., Biol. Med.* **2010**, *6*, 214–226.
- (119) Tom, R. T.; Samal, A. K.; Sreeprasad, T. S.; Pradeep, T. *Langmuir* **2007**, *23*, 1320–1325.
- (120) Zhang, D.; Neumann, O.; Wang, H.; Yuwono, V. M.; Barhoumi, A.; Perham, M.; Hartgerink, J. D.; Wittung-Stafshede, P.; Halas, N. J. *Nano Lett.* **2009**, *9*, 666–671.
- (121) Fu, A.; Zhou, N.; Huang, W.; Wang, D.; Zhang, L.; Li, H. *J. Biomed. Mater. Res., Part A* **2005**, *74A*, 156–163.
- (122) Brunner, T. J.; Bohner, M.; Dora, C.; Gerber, C.; Stark, W. J. *J. Biomed. Mater. Res., Part B: Appl. Biomater.* **2008**, *84B*, 350–362.
- (123) Tyner, K. M.; Roberson, M. S.; Berghorn, K. A.; Li, L.; Gilmour, R. F., Jr.; Batt, C. A.; Giannelis, E. P. *J. Controlled Release* **2004**, *100*, 399–409.
- (124) Wang, X.; Du, Y.; Luo, J. *Nanotechnology* **2008**, *19*, 065707.
- (125) Tyner, K. M.; Schiffman, S. R.; Giannelis, E. P. *J. Controlled Release* **2004**, *95*, 501–514.
- (126) Choy, J. H.; Kwak, S. Y.; Jeong, Y. J.; Park, J. S. *Angew. Chem., Int. Ed.* **2000**, *39*, 4041–4045.
- (127) Jenning, V.; Schafer-Korting, M.; Gohla, S. *J. Controlled Release* **2000**, *66*, 115–126.
- (128) Castelletto, V.; Newby, G. E.; Zhu, Z.; Hamley, I. W. *Langmuir* **2010**, *26*, 9986–9996.
- (129) Lipfert, J.; Doniach, S. *Annu. Rev. Biophys. Biomol. Struct.* **2007**, *36*, 307–237.
- (130) Hammouda, B. *Polymer Rev.* **2010**, *50*, 14–39.
- (131) Park, S. Y.; Lytton-Jean, A. K. R.; Lee, B.; Weigand, S.; Schatz, G. C.; Mirkin, C. A. *Nature* **2008**, *451*, 553–556.
- (132) Chen, M.-C.; Wong, H.-S.; Lin, K.-J.; Chen, H.-L.; Wey, S.-P.; Sonaje, K.; Lin, Y.-H.; Chu, C.-Y.; Sung, H.-W. *Biomaterials* **2009**, *30*, 6629–6637.
- (133) Bhattacharyya, M. S.; Hiwale, P.; Piras, M.; Medda, L.; Steri, D.; Piludu, M.; Salis, A.; Monduzzi, M. *J. Phys. Chem. C* **2010**, *114*, 19928–19934.
- (134) McKenzie, L. C.; Haben, P. M.; Kevan, S. D.; Hutchison, J. E. *J. Phys. Chem. C* **2010**, *114*, 22055–22063.
- (135) Serefoglu, E.; Oberdisse, J.; Staikos, G. *Biomacromolecules* **2007**, *8*, 1195–1199.
- (136) Paul, A.; Vicent, M. J.; Duncan, R. *Biomacromolecules* **2007**, *8*, 1573–1579.
- (137) Jin, S.-E.; Bae, J. W.; Hong, S. *Microsc. Res. Tech.* **2010**, *73*, 813–823.
- (138) Midgley, P. A.; Durkan, C. *Mater. Today* **2008**, *11*, 8–11.
- (139) Dedecker, P.; Hofkens, J.; Hotta, J. *Mater. Today* **2008**, *11*, 12–21.
- (140) Hell, S. W. *Nat. Methods* **2009**, *6*, 24–32.
- (141) Wenger, J.; Rigneault, H. *Int. J. Mol. Sci.* **2010**, *11*, 206–221.
- (142) Wang, Z.; Guo, W.; Li, L.; Luk'yanchuk, B.; Khan, A.; Liu, Z.; Chen, Z.; Hong, M. *Nat. Commun.* **2011**, *2*, 218.
- (143) Pons, T.; Mattooussi, H. *Ann. Biomed. Eng.* **2009**, *37*, 1934–1959.
- (144) Zhang, J.; Fu, Y.; Chowdhury, M. H.; Lakowicz, J. R. *J. Phys. Chem. C* **2008**, *112*, 18–26.
- (145) Casanova, D.; Gaiume, D.; Moreau, M.; Martin, J.-L.; Gacoin, T.; Boilot, J.-P.; Alexandrou, A. *J. Am. Chem. Soc.* **2007**, *129*, 12592–12593.
- (146) Delport, F.; Deres, A.; Hotta, J.; Pollet, J.; Verbruggen, B.; Sels, B.; Hofkens, J.; Lammertyn, J. *Langmuir* **2010**, *26*, 1594–1597.
- (147) Cobley, C. M.; Skrabalak, S. E.; Campbell, D. J.; Xia, Y. *Plasmonics* **2009**, *4*, 171–179.
- (148) Chorny, M.; Fishbein, I.; Alferiev, I. S.; Nyanguile, O.; Gaster, R.; Levy, R. *J. Mol. Ther.* **2006**, *14*, 382–391.
- (149) Jensen, G. C.; Yu, X.; Gong, J. D.; Munge, B.; Bhirde, A.; Kim, S. N.; Papadimitrakopoulos, F.; Rusling, J. F. *J. Nanosci. Nanotechnol.* **2009**, *9*, 249–255.
- (150) Thobhani, S.; Attree, S.; Boyd, R.; Kumarswami, N.; Noble, J.; Szymanski, M.; Porter, R. *A. J. Immunol. Methods* **2010**, *356*, 60–69.
- (151) Steinmetz, N. F.; Hong, V.; Spoerke, E. D.; Lu, P.; Breitenkamp, K.; Finn, M. G.; Manchester, M. *J. Am. Chem. Soc.* **2009**, *131*, 17093–17095.
- (152) Douglas, S. M.; Dietz, H.; Liedl, T.; Höglberg, B.; Graf, F.; Shih, W. M. *Nature* **2009**, *459*, 414–418.
- (153) De Jonge, N.; Peckys, D. B.; Kremer, G. J.; Piston, D. W. *Proc. Natl. Acad. Sci. U.S.A.* **2009**, *106*, 2159–2164.
- (154) Smith, J. E.; Wang, L.; Tan, W. *Trends Anal. Chem.* **2006**, *25*, 848–855.
- (155) Rayavarapu, R. G.; Petersen, W.; Ungureanu, C.; Post, J. N.; van Leeuwen, T. G.; Manohar, S. *Int. J. Biomed. Imaging* **2007**, *2007*, 29817.
- (156) Skrabalak, S. E.; Chen, J.; Sun, Y.; Lu, X.; Au, L.; Colbey, C. M.; Xia, Y. *Acc. Chem. Res.* **2008**, *41*, 1587–1595.
- (157) Wang, Y.; Shen, Y.; Xie, A.; Li, S.; Wang, X.; Cai, Y. *J. Phys. Chem. C* **2010**, *114*, 4297–4301.
- (158) Sastry, T. P.; Sundaraseelan, J.; Swarnalatha, K.; Liji Sobhana, S. S.; Uma Makheswari, M.; Sekar, S.; Mandal, A. B. *Nanotechnology* **2008**, *19*, 245604.
- (159) Thibierge, S.; Zik, O.; Moses, E. *Rev. Sci. Instrum.* **2004**, *75*, 2280–2289.
- (160) Gatti, A. M.; Kirkpatrick, J.; Gambarelli, A.; Capitani, F.; Hansen, T.; Eloy, R.; Clermont, G. *J. Mater. Sci. Mater. Med.* **2008**, *19*, 1515–1522.
- (161) Gaczynska, M.; Osmulski, P. A. *Curr. Opin. Colloid Interface Sci.* **2008**, *13*, 351–367.
- (162) Cohen, S. R.; Bitler, A. *Curr. Opin. Colloid Interface Sci.* **2008**, *13*, 316–325.

- (163) Sitterberg, J.; Ozcetin, A.; Ehrhardt, C.; Bakowsky, U. *Eur. J. Pharm. Biopharm.* **2010**, *74*, 2–13.
- (164) Campbell, J. F.; Tessmer, I.; Thorp, H. H.; Erie, D. A. *J. Am. Chem. Soc.* **2008**, *130*, 10648–10655.
- (165) Irrgang, J.; Kscienczyk, J.; Lapiene, V.; Niemeyer, C. M. *Chem. Phys. Chem.* **2009**, *10*, 1483–1491.
- (166) Wang, H.; Tessmer, I.; Croteau, D. L.; Erie, D. A.; Van Houten, B. *Nano Lett.* **2008**, *8*, 1631–1637.
- (167) Kuzuya, A.; Komiyama, M. *Nanoscale* **2010**, *2*, 310–322.
- (168) Rothmund, P. W. K. *Nature* **2006**, *440*, 297–302.
- (169) Gu, H.; Chao, J.; Xiao, S.-J.; Seeman, N. C. *Nat. Nanotechnol.* **2009**, *4*, 245–248.
- (170) Park, H. K.; Lim, Y. T.; Kim, J. K.; Park, H. G.; Chung, B. H. *Ultramicroscopy* **2008**, *108*, 1115–1119.
- (171) Zeng, G.; Chen, J.; Zhong, L.; Wang, R.; Jiang, L.; Cai, J.; Yan, L.; Huang, D.; Chen, C. Y.; Chen, Z. W. *Proteomics* **2009**, *9*, 1538–1547.
- (172) Pavia, D. L.; Lampman, G. M.; Kriz, G. S.; Vyvyan, J. A. *Introduction to Spectroscopy*, 4th ed.; Brooks/Cole: Belmont, CA, 2008.
- (173) Biju, V.; Mundayoor, S.; Omkumar, R. V.; Anas, A.; Ishikawa, M. *Biotechnol. Adv.* **2010**, *28*, 199–213.
- (174) Ohmori, S.; Saito, T.; Tange, M.; Shukla, B.; Okazaki, T.; Yumura, M.; Iijima, S. *J. Phys. Chem. C* **2010**, *114*, 10077–10081.
- (175) Schwartzberg, A. M.; Zhang, J. Z. *J. Phys. Chem. C* **2008**, *112*, 10323–10337.
- (176) Amendola, V.; Meneghetti, M. *J. Phys. Chem. C* **2009**, *113*, 4277–4285.
- (177) Deka, J.; Paul, A.; Chattopadhyay, A. *J. Phys. Chem. C* **2009**, *113*, 6936–6947.
- (178) Hall, W. P.; Ngatia, S. N.; Van Duyne, R. P. *J. Phys. Chem. C* **2011**, *115*, 1410–1414.
- (179) Jiang, X.; Jiang, J.; Jin, Y.; Wang, E.; Dong, S. *Biomacromolecules* **2005**, *6*, 46–53.
- (180) Perevedentseva, E.; Cai, P.-J.; Chiu, Y.-C.; Cheng, C.-L. *Langmuir* **2011**, *27*, 1085–1091.
- (181) Kandori, K.; Kuroda, T.; Togashi, S.; Katayama, E. *J. Phys. Chem. B* **2011**, *115*, 653–659.
- (182) Wu, X.; Narsimhan, G. *Langmuir* **2008**, *24*, 4989–4998.
- (183) Olson, B. J. S. C.; Markwell, J. *Curr. Protoc. Protein Sci.* **2007**, *3.4*, 3.4.1–3.4.29.
- (184) Zhang, H.; Meyerhoff, M. E. *Anal. Chem.* **2006**, *78*, 609–616.
- (185) Ranjbar, B.; Gill, P. *Chem. Biol. Drug Des.* **2009**, *74*, 101–120.
- (186) Shang, L.; Wang, Y.; Jiang, J.; Dong, S. *Langmuir* **2007**, *23*, 2714–2721.
- (187) Asuri, P.; Bale, S. S.; Pangule, R. C.; Shah, D. A.; Kane, R. S.; Dordick, J. S. *Langmuir* **2007**, *23*, 12318–12321.
- (188) Mahmoudi, M.; Shokrgozar, M. A.; Sardari, S.; Moghadam, M. K.; Vali, H.; Laurent, S.; Stroeven, P. *Nanoscale* **2011**, *3*, 1127–1138.
- (189) Mamedova, N. N.; Kotov, N. A.; Rogach, A. L.; Studer, J. *Nano Lett.* **2001**, *1*, 281–286.
- (190) Shanmugam, G.; Polavarapu, P. L.; Kendall, A.; Stubbs, G. *J. Gen. Virol.* **2005**, *86*, 2371–2377.
- (191) Lakowicz, J. R. *Principles of Fluorescence Spectroscopy*, 3rd ed.; Springer: New York, 2006.
- (192) Haugland, R. P. *The Handbook: A Guide to Fluorescent Probes and Labeling Technologies*, 10th ed.; Invitrogen Corp.: California, 2005.
- (193) Nielson, L. J.; Eyley, S.; Thielemans, W.; Aylott, J. W. *Chem. Commun.* **2010**, *46*, 8929–8931.
- (194) Manokaran, S.; Zhang, X.; Chen, W.; Srivastavam, D. K. *Biochim. Biophys. Acta* **2010**, *1804*, 1376–1384.
- (195) Reulen, S. W. A.; Brusselaars, W. W. T.; Langereis, S.; Mulder, W. J. M.; Breurken, M.; Merkx, M. *Bioconjugate Chem.* **2007**, *16*, 590–596.
- (196) Hurst, S. J.; Lytton-Jean, A. K. R.; Mirkin, C. A. *Anal. Chem.* **2006**, *78*, 8313–8318.
- (197) Lockney, D. M.; Guenther, R. N.; Loo, L.; Overton, W.; Antonelli, R.; Clark, J.; Hu, M.; Luft, C.; Lommel, S. A.; Franzen, S. *Bioconjugate Chem.* **2011**, *22*, 67–73.
- (198) Mittal, R.; Bruchez, M. P. *Bioconjugate Chem.* **2011**, *22*, 362–368.
- (199) Nakamura, M.; Ishimura, K. *Langmuir* **2008**, *24*, 12228–12234.
- (200) Chen, H.; Gao, J.; Lu, Y.; Kou, G.; Zhang, H.; Fan, L.; Sun, Z.; Guo, Y.; Zhong, Y. *J. Controlled Release* **2008**, *128*, 209–216.
- (201) Sapsford, K. E.; Berti, L.; Medintz, I. L. *Angew. Chem., Int. Ed.* **2006**, *45*, 4562–4588.
- (202) Medintz, I. L.; Mattoussi, H. *Phys. Chem. Chem. Phys.* **2009**, *11*, 17–45.
- (203) Medintz, I. L.; Konnert, J. H.; Clapp, A. R.; Stanish, I.; Twigg, M. E.; Mattoussi, H.; Mauro, J. M.; Deschamps, J. R. *Proc. Natl. Acad. Sci. U.S.A.* **2004**, *101*, 9612–9617.
- (204) Boeneman, K.; Deschamps, J. R.; Buckhout-White, S.; Prasuhn, D. E.; Blanco-Canosa, J. B.; Dawson, P. E.; Stewart, M. H.; Susumu, K.; Goldman, E. R.; Ancona, M.; Medintz, I. L. *ACS Nano* **2010**, *4*, 7253–7266.
- (205) Prasuhn, D. E.; Felta, A.; Bianco-Canosa, J. B.; Susumu, K.; Stewart, M. H.; Mei, B. C.; Yakovlev, A. V.; Loukov, C.; Mallet, J. M.; Oheim, M.; Dawson, P. E.; Medintz, I. L. *ACS Nano* **2010**, *4*, 5487–5497.
- (206) Algar, W. R.; Tavares, A. J.; Krull, U. J. *Anal. Chim. Acta* **2010**, *673*, 1–25.
- (207) Morgner, F.; Geissler, D.; Stufler, S.; Butlin, N. G.; Löhmannsröben, H.-G.; Hilderbrandt, N. *Angew. Chem., Int. Ed.* **2010**, *49*, 7570–7574.
- (208) Pons, T.; Medintz, I. L.; Sapsford, K. E.; Higashiyama, S.; Grimes, A. F.; English, D. S.; Mattoussi, H. *Nano Lett.* **2007**, *7*, 3157–3164.
- (209) Sen, T.; Haldar, K. K.; Patra, A. *J. Phys. Chem. C* **2008**, *112*, 17945–17951.
- (210) Kong, J.; Yu, S. *Acta Biochem. Biophys. Sin.* **2007**, *38*, 549–559.
- (211) Krpetić, Ž.; Nativo, P.; Porta, F.; Brust, M. A. *Bioconjugate Chem.* **2009**, *20*, 619–624.
- (212) Liang, Y.-Y.; Zhang, L.-M. *Biomacromolecules* **2007**, *8*, 1480–1486.
- (213) Susumu, K.; Uyeda, H. T.; Medintz, I. L.; Pons, T.; Delehanty, J. B.; Mattoussi, H. *J. Am. Chem. Soc.* **2007**, *129*, 13987–13996.
- (214) Lundqvist, M.; Sethson, I.; Jonsson, B.-H. *Biochemistry* **2005**, *44*, 10093–10099.
- (215) Li, K.; Chen, Y.; Li, S.; Nguyen, G.; Niu, Z.; You, S.; Mello, C. M.; Lu, X.; Wang, Q. *Bioconjugate Chem.* **2010**, *21*, 1369–1377.
- (216) Bruckman, M. A.; Kaur, G.; Lee, L. A.; Xie, F.; Sepulveda, J.; Breitenkamp, R.; Zhang, X.; Joralemon, M.; Russell, T. P.; Emrick, T.; Wang, Q. *ChemBioChem* **2009**, *9*, 519–523.
- (217) Endres, P. J.; Paunesku, T.; Vogt, S.; Meade, T. J.; Woloschak, G. E. *J. Am. Chem. Soc.* **2007**, *129*, 15760–15761.
- (218) Chiang, C. K.; Chen, W. T.; Chang, H. T. *Chem. Soc. Rev.* **2011**, *40*, 1269–1281.
- (219) Shon, Y. S.; Choi, D.; Dare, J.; Dinh, T. *Langmuir* **2008**, *24*, 6924–6931.
- (220) Gibson, J. D.; Khanal, B. P.; Zubarev, E. R. *J. Am. Chem. Soc.* **2007**, *129*, 11653–11661.
- (221) Park, C.; Youn, H.; Kim, H.; Noh, T.; Kook, Y. H.; Oh, E. T.; Park, H. J.; Kim, C. J. *Mater. Chem.* **2009**, *19*, 2310–2315.
- (222) Bothun, G. D. *J. Nanobiotechnol.* **2008**, *6*, 13.
- (223) Sant, S.; Thommes, M.; Hildgen, P. *Langmuir* **2008**, *24*, 280–287.
- (224) Liu, J.; Gong, T.; Wang, C.; Zhong, Z.; Zhang, Z. *Int. J. Pharm.* **2007**, *340*, 153–162.
- (225) Yuan, W.; Wu, F.; Geng, Y.; Xu, S.; Jin, T. *Nanotechnology* **2007**, *18*, 145601.
- (226) Cedervall, T.; Lynch, I.; Berggard, T.; Thulin, E.; Nilsson, H.; Dawson, K. A.; Linse, S. *Proc. Natl. Acad. Sci. U.S.A.* **2007**, *104*, 2050–2055.
- (227) Duhr, S.; Braun, D. *Proc. Natl. Acad. Sci. U.S.A.* **2006**, *103*, 19678–19682.
- (228) Piazza, R.; Parola, A. *J. Phys.: Condens. Matter* **2008**, *20*, 153102.
- (229) Blundell, T. L.; Sibanda, B. L.; Sternberg, M. J.; Thornton, J. M. *Nature* **1987**, *326*, 347–352.
- (230) Greer, J. *Proteins* **1990**, *7*, 317–334.
- (231) Sali, A.; Blundell, T. L. *J. Mol. Biol.* **1993**, *234*, 779–815.
- (232) Sanchez, R.; Sali, A. *Methods Mol. Biol.* **2000**, *143*, 97–129.

- (233) Chothia, C.; Lesk, A. M. *EMBO J.* **1986**, *5*, 823–826.
(234) Saunders, S. R.; Eden, M. R.; Roberts, C. B. *J. Phys. Chem. C* **2011**, *115*, 4603–4610.
(235) Kim, Y.; Klutz, A. M.; Hechler, B.; Gao, Z.-G.; Gachet, C.; Jacobson, K. A. *Purinergic Signalling* **2009**, *5*, 39–50.
(236) Mukherjee, A. K.; Kumar, T. S.; Rai, S. K.; Roy, J. K. *Biotechnol. Bioprocess Eng.* **2010**, *15*, 984–992.
(237) Medintz, I. L.; Deschamps, J. R. *Curr. Opin. Biotechnol.* **2006**, *17*, 17–27.
(238) Prasuhn, D. E.; Deschamps, J. R.; Susumu, K.; Boeneman, K.; Blanco-Canosa, J. B.; Dawson, P. E.; Medintz, I. L. *Small* **2010**, *6*, 555–564.
(239) Boeneman, K.; Mei, B. C.; Dennis, A. M.; Bao, G.; Deschamps, J. R.; Matoussi, H.; Medintz, I. L. *J. Am. Chem. Soc.* **2009**, *131*, 3828–3829.
(240) Hutter, E.; Boridy, S.; Labrecque, S.; Lalancette-Hebert, M.; Kriz, J.; Winnik, F. M.; Maysinger, D. *ACS Nano* **2010**, *4*, 2595–2606.
(241) Fairhurst, D. <http://www.xigonanotools.com/applications/applications.asp> (accessed March 24, 2011).
(242) Ferreira, G. N. M.; da-Silva, A.-C.; Tomé, B. *Trends Biotechnol.* **2009**, *27*, 689–697.
(243) Cheng, Z.-G.; Tang, D.-Y. *Bioprocess Biosyst. Eng.* **2007**, *30*, 243–249.
(244) Amstad, E.; Zurcher, S.; Mashagi, A.; Wong, J. Y.; Textor, M.; Reimhult, E. *Small* **2009**, *5*, 1334–1342.
(245) Burg, T. P.; Godin, M.; Knudsen, S. M.; Shen, W.; Carlson, G.; Foster, J. S.; Babcock, K.; Manalis, S. R. *Nature* **2007**, *446*, 1066–1069.
(246) Montes-Burgos, I.; Walczyk, D.; Hole, P.; Smith, J.; Lynch, I.; Dawson, K. J. *Nanopart. Res.* **2010**, *12*, 47–53.
(247) Braeckmans, K.; Buyens, K.; Bouquet, W.; Vervaet, C.; Joye, P.; De Vos, F.; Plawinski, L.; Doeuvre, L.; Angles-Cano, E.; Sanders, N. N.; Demeester, J.; De Smedt, S. C. *Nano Lett.* **2010**, *10*, 4435–4442.
(248) Fraikin, J.-L.; Teesalu, T.; McKenney, C. M.; Ruoslahti, E.; Cleland, A. N. *Nat. Nanotechnol.* **2011**, DOI: 10.1038/nnano.2011.24.
(249) Willmott, G. R.; Vogel, R.; Yu, S. S. C.; Groenewegen, L. G.; Roberts, G. S.; Kozak, D.; Anderson, W.; Trau, M. *J. Phys.: Condens. Matter* **2010**, *22*, 454116.
(250) Roberts, G. S.; Kozak, D.; Anderson, W.; Broom, M. F.; Vogel, R.; Trau, M. *Small* **2010**, *6*, 2653–2658.
(251) Monopoli, M. P.; Walczyk, D.; Campbell, A.; Elia, G.; Lynch, I.; Bombelli, F. B.; Dawson, K. A. *J. Am. Chem. Soc.* **2011**, *133*, 2525–2534.
(252) Marnett, L. *J. Chem. Res. Toxicol.* **2009**, *22*, 1491.
(253) Sahu, S. C.; Casciano, D. A. *Nanotoxicity: From in Vivo and in Vitro Models to Health Risks*; Wiley: New York, 2009.
(254) Landsiedel, R.; Kapp, M. D.; Schulz, M.; Wiench, K.; Oesch, F. *Mutat. Res.* **2009**, *681*, 241–258.
(255) Monteiro-Riviere, N. A.; Inman, A. O.; Zhang, L. W. *Toxicol. Appl. Pharmacol.* **2009**, *234*, 222–235.
(256) Dobrovolskaia, M. A.; Germolec, D. R.; Waever, J. L. *Nat. Nanotechnol.* **2009**, *4*, 411–414.
(257) Franca, A.; Pelaz, B.; Moros, M.; Sanchez-Espinel, C.; Hernandez, A.; Fernandez-Lopez, C.; Grazu, V.; de la Fuente, J.; Pastoriza-Santos, I.; Liz-Marzan, L. M.; Gonzalez-Fernandez, A. *Small* **2010**, *6*, 89–95.
(258) Bellucci, S.; Chiaretti, M.; Onorato, P.; Rossella, F.; Grandi, M. S.; Galinetto, P.; Sacco, I.; Micciulla, F. *Nanomedicine* **2010**, *5*, 209–215.
(259) Ianaro, A.; Tersigni, M.; D'Acquisto, F. *Mini-Rev. Med. Chem.* **2009**, *9*, 306–317.
(260) Vallhov, H.; Qin, J.; Johansson, S. M.; Ahlorg, N.; Muhammed, M. A.; Scheynius, A.; Gabrielsson, S. *Nano Lett.* **2006**, *6*, 1382–1386.
(261) Esch, R. K.; Han, L.; Foarde, K. K.; Ensor, D. S. *Nanotoxicology* **2010**, *4*, 73–83.
(262) Dobrovolskaia, M. A.; Neun, B. W.; Clogston, J. D.; Ding, H.; Ljubimova, J.; McNeil, S. E. *Nanomedicine* **2010**, *5*, 555–562.